National Library of Canada
Bibliothèque nationale du Canada

Canadian Theses Service
Service des thèses canadiennes

Ottawa, Canada
K1A 0N4

## NOTICE

The quality of this microform is heavily dependent upon the quality of the original thesis submitted for microfilming. Every effort has been made to ensure the highest quality of reproduction possible.

If pages are missing, contact the university which granted the degree.

Some pages may have indistinct print especially if the original pages were typed with a poor typewriter ribbon or if the university sent us an inferior photocopy.

Reproduction in full or in part of this microform is governed by the Canadian Copyright Act, R.S.C. 1970, c. C-30, and subsequent amendments.

## AVIS

La qualité de cette microforme dépend grandement de la qualité de la thèse soumise au microfilmage. Nous avons tout fait pour assurer une qualité supérieure de reproduction.

S'il manque des pages, veuillez communiquer avec l'université qui a conféré le grade.

La qualité d'impression de certaines pages peut laisser à désirer, surtout si les pages originales ont été dactylographiées à l'aide d'un ruban usé ou si l'université nous a fait parvenir une photocopie de qualité inférieure.

La reproduction, même partielle, de cette microforme est soumise à la Loi canadienne sur le droit d'auteur, SRC 1970, c. C-30, et ses amendements subséquents.

NL-339 (r. 88/04) c

Canada

National Library of Canada
Bibliothèque nationale du Canada

Canadian Theses Service
Service des thèses canadiennes

Ottawa, Canada
K1A 0N4

The author has granted an irrevocable non-exclusive licence allowing the National Library of Canada to reproduce, loan, distribute or sell copies of his/her thesis by any means and in any form or format, making this thesis available to interested persons.

The author retains ownership of the copyright in his/her thesis. Neither the thesis nor substantial extracts from it may be printed or otherwise reproduced without his/her permission.

L'auteur a accordé une licence irrévocable et non exclusive permettant à la Bibliothèque nationale du Canada de reproduire, prêter, distribuer ou vendre des copies de sa thèse de quelque manière et sous quelque forme que ce soit pour mettre des exemplaires de cette thèse à la disposition des personnes intéressées.

L'auteur conserve la propriété du droit d'auteur qui protège sa thèse. Ni la thèse ni des extraits substantiels de celle-ci ne doivent être imprimés ou autrement reproduits sans son autorisation.

ISBN 0-315-55492-4

Canada

The University of Alberta

# Numerical Analysis of Orthodontic Appliances

by

Kosay El-Rayes

(C)

A thesis
submitted to the Faculty of Graduate Studies and Research
in partial fulfilment of the requirements for the degree of

Master of Science

Department of Mechanical Engineering

Edmonton, Alberta

Fall 1989

The University of Alberta

Release Form

| | |
|---|---|
| Name of Author: | **Kosay El-Rayes** |
| Title of Thesis: | **Numerical Analysis of Orthodontic Appliances** |
| Degree: | Master of Science |
| Year this degree granted: | Fall 1989 |

Permission is hereby granted to **The University of Alberta Library** to reproduce single copies of this thesis and to lend or sell such copies for private, scholarly, or scientific research purposes only.

The author reserves other publication rights, and neither the thesis nor extensive tracts from it may be printed or otherwise reproduced without the author's written consent.

.....Kosay El-Rayes.....

(Student's signature)

Kosay El-Rayes
472 Wanyandi Road
Edmonton, Alberta
T5T 4M6

Date : July 24, 1989

The University of Alberta

Faculty of Graduate Studies and Research

The undersigned certify that they have read, and recommend to the Faculty of Graduate Studies and Research for acceptance, a thesis entitled

**Numerical Analysis of Orthodontic Appliances**

submitted by

**Kosay El-Rayes**

in partial fulfilment of the requirements for the degree of

**Master of Science.**

Gary Faulkner

A.W. Liposett

(Supervisors)

Doug Hoberaak

Date: July 17, 1989

*dedicated to my parents*

# Abstract

Achieving efficient tooth movement is a major objective of orthodontic practice. This tooth motion is often required to close spaces in the dental arch created by the extraction of specific teeth. One of the space closure mechanisms is the segmental arch technique in which a retraction appliance, capable of delivering a system of moments and forces, is placed between the posterior (back) and anterior portions of the dental arch. Therefore, the determination of the magnitudes and ratios of these moments and forces is crucial for achieving efficient tooth movement. Several numerical and experimental techniques can be used for the analysis of the appliances which produce these force systems. The current numerical method, a segmental shooting technique, has proven to have several advantages over other techniques in terms of cost and analysis time. In this technique the solution of the nonlinear equations of the large elastic deformation is avoided by dividing the spring into a large number of small segments and then a linearized differential equation is solved for each segment. The total solution is achieved by solving a series of initial value problems, and the unknowns at the first node are determined using a shooting technique along with a modified Newton-Raphson numerical solver. This solution technique was incorporated in the development of a general computer code capable of analyzing complex spring geometries both symmetric or nonsymmetric with various force and geometric boundary conditions. After performing several comparative studies to verify the output of the segmental shooting technique, the computer code was used to perform various parametric studies on pre-activated T-springs as well as vertical loop springs. These studies evaluated the effect of changing certain geometric parameters, wire material, and wire cross section on the mechanical characteristics of these retraction appliances.

# Acknowledgments

I wish to express my sincere appreciation to Dr. M.G. Faulkner and Dr. A.W. Lipsett for their continuous guidance and support that enabled me to complete this present study. I would like also to thank Dr. D.L. Haberstock for his orthodontic experience input that made the results of the research clinically applicable.

I would like also to acknowledge Mr. Victor Tam and Mr. Steven McEvoy for their assistance in operating the force measurement device, and Mr. John Foy for helping me in operating the Instron Universal Testing machine. Funding for this research was provided by the Natural Sciences and Engineering Research Council of Canada (NSERC grant A7514).

# Contents

**Chapter 1**

**Introduction** 1

1.1 Orthodontic Background . . . . . 1

1.2 Analysis of Orthodontic Appliances . . . . . 10

1.3 Thesis Outline . . . . . 14

**Chapter 2**

**Solution Technique Development** 15

2.1 Basic Equations . . . . . 15

2.2 Segmental Technique . . . . . 24

2.3 Numerical Solver (Shooting Method) . . . . . 29

2.4 Computer Code Development . . . . . 32

2.4.1 Parameters and Geometry Input Routines . . . . . 32

2.4.2 Force and Boundary Input Routine . . . . . 33

2.4.3 Segmental Technique Routine . . . . . 37

2.4.4 Numerical Solver Routines . . . . . 38

2.5 Analytical Verification . . . . . 40

**Chapter 3**

**Comparative Studies** 46

3.1 T-Spring Comparative Study . . . . . 46

3.2 Pre-Activated T-Spring Comparative Study . . . . . 53

3.2.1 Experimental Testing of Pre-activated T-Spring . . . . . 54

3.2.2 Young's Modulus Determination . . . . . 58

3.2.3 Numerical Analysis of Pre-activated T-Spring . . . . . 59

**Chapter 4**

**Parametric Studies** 69

4.1 Pre-Activated T-Spring Parametric Studies . . . . . 69

4.1.1 Length $a$ Parametric Study . . . . . 73

4.1.2 Combined $a$ and $b$ Lengths Parametric Study . . . . . 82

4.1.3 Bracket Offset Parametric Study . . . . . 87

4.2 Vertical Loop Springs Parametric Studies . . . . . 92

4.2.1 Spring Wire Material and Cross Section Parametric Study . . 95

4.2.2 Height ($h$) Parametric Study . . . . . 98

4.2.3 Combined loop radius ($R$) and arm length ($a$) parametric study 102

4.2.4 Pre-Activation Angle Parametric Study (0.016" round stainless steel wire) . . . . . 106

4.2.5 Pre-Activation Angle Parametric Study (0.016" × 0.022" $TMA$ wire) . . . . . 114

4.2.6 Loop and Arm Helices Parametric Study . . . . . 120

Chapter 5

Conclusions 131

References 134

Appendix A

Segmental Shooting Technique Program Listing 138

Appendix B

False Position Numerical Solver for 3 Unkowns 178

Appendix C

Gauss-Quadrature Numerical Integration Routines 182

Appendix D

Comparative Studies Data 186

Appendix E

Stress Calculation Routine 190

# List of Tables


2.1 Analytical results of curved cantilever beam deflection . . . . . 45
2.2 Numerical results of curved cantilever beam deflection . . . . . 45

3.1 T-Spring sections data . . . . . 48
3.2 Pre-activated T-spring sections data . . . . . 61

4.1 Typical pre-activated T-spring moments and forces . . . . . 71
4.2 Moments and forces of pre-activated T-springs with different $a$ lengths 75
4.3 Moments and forces of pre-activated T-springs with different $a$ and $l$ . 79
4.4 Moments and forces of pre-activated T-springs with different $a$ and $b$ 84
4.5 Moments and forces of pre-activated T-spring for different bracket offset 88
4.6 Moment and force values of the typical vertical loop spring . . . . . 93
4.7 Moments and forces for different wire sizes and materials . . . . . 96
4.8 Moments and forces of vertical loop springs with different $h$ . . . . . 100
4.9 Moments and forces of vertical springs with different $a$ and $R$ . . . . 104
4.10 Moments and forces of stainless steel pre-activated vertical springs . . 108
4.11 Moments and forces of 10° pre-activated vertical spring . . . . . 110
4.12 Moments and forces of 10° pre-activated spring by loop yielding . . . 113
4.13 Moments and forces of $TMA$ pre-activated vertical springs . . . . . 116
4.14 Moments and forces of $TMA$ 35° pre-activated vertical spring . . . . 118
4.15 Moments and forces for vertical spring with loop helix #25 . . . . . 122

4.16 Moments and forces for vertical spring with loop and arm helices #26 124
4.17 Moments and forces for 50° pre-activated spring with helices #27 . . 126
4.18 Moments and forces for 70° pre-activated spring with helices #28 . . 129

D.1 Koenig et al.[24] experimental and numerical data for T-loop . . . . . 186
D.2 Fuchshuber [20] experimental and numerical data for the T-loop . . . 187
D.3 Segmental shooting technique analysis of the T-loop . . . . . 187
D.4 Experimental data for the pre-activated T-spring . . . . . 188
D.5 Segmental shooting technique analysis of the pre-activated T-spring . 189
D.6 Young's modulus for different orthodontic wires . . . . . 189

# List of Figures


1.1 Orthodontic retraction springs . . . . . 3
1.2 Segmented arch technique schematic . . . . . 4
1.3 Center of resistance and equivalent force system of an incisor . . . . . 7
1.4 Schematic of tooth movement for different $M/F$ values . . . . . 9

2.1 Free and deformed rod shapes . . . . . 16
2.2 Infinitesimal element of the deformed rod . . . . . 18
2.3 Local coordinate system of a segment . . . . . 20
2.4 Assembling of successive segments . . . . . 25
2.5 Flow chart of the input routines . . . . . 34
2.6 Forces and boundary input routine schematic . . . . . 36
2.7 Program flow chart . . . . . 39
2.8 Deflection of curved cantilever beam under horizontal load . . . . . 41

3.1 Orthodontic T-spring geometry . . . . . 47
3.2 T-Spring initial and deformed shape (segmental technique output) . . 49
3.3 Comparison of numerical and experimental results of T-loop moment 51
3.4 Comparison of numerical and experimental results of T-loop force . . 52
3.5 Pre-activated T-spring . . . . . 53
3.6 Force/displacement measurement system schematic . . . . . 55
3.7 Force/moment measurement apparatus . . . . . 56

3.8 Pre-activated T-spring sectioning . . . . . 60
3.9 Pre-activated T-spring deformed geometries . . . . . 63
3.10 Pre-activated T-spring left moment (experimental and numerical) . . 66
3.11 Pre-activated T-spring right moment (experimental and numerical) . 67
3.12 Pre-activated T-spring tension (experimental and numerical) . . . . . 68

4.1 Typical pre-activated T-spring geometry . . . . . 70
4.2 Typical pre-activated T-spring $M/F$ as a function of activation . . . 72
4.3 Pre-activated T-springs with different length $a$ . . . . . 74
4.4 $M/M_o$ for pre-activated T-springs with different $a$ length . . . . . 76
4.5 $T/T_o$ for pre-activated T-springs with different $a$ length . . . . . 77
4.6 $M/F$ value for pre-activated T-springs with different $a$ Length . . . . 77
4.7 Pre-activated T-springs with different lengths $a$ and $l$ . . . . . 78
4.8 $M/M_o$ for pre-activated T-springs with different lengths $a$ and $l$ . . . 80
4.9 $T/T_o$ for pre-activated T-springs with different lengths $a$ and $l$ . . . . 81
4.10 $M/F$ for pre-activated T-springs with different lengths $a$ and $l$ . . . . 81
4.11 Pre-activated T-springs with different lengths $a$ and $b$ . . . . . 83
4.12 $M/M_o$ for pre-activated T-springs with different lengths $a$ and $b$ . . . 85
4.13 $T/T_o$ for pre-activated T-springs with different lengths $a$ and $b$ . . . . 86
4.14 $M/F$ for pre-activated T-springs with different lengths $a$ and $b$ . . . . 86
4.15 Deformed geometry of pre-activated T-spring with bracket offset . . . 87
4.16 $M/M_o$ of pre-activated T-spring for different bracket offset #1 . . . . 90
4.17 $M/M_o$ of pre-activated T-spring for different bracket offset #2 . . . . 90
4.18 Shear of pre-activated T-spring for different bracket offset . . . . . 91
4.19 Tension of pre-activated T-spring for different bracket offset . . . . . 91
4.20 Typical vertical loop spring geometry . . . . . 92
4.21 Moment to force ratio of the typical vertical loop spring . . . . . 94
4.22 Vertical loop springs with different height $h$. . . . . 99

4.23 $M/M_o$ and $F/F_o$ for vertical springs with different $h$. . . . . 101
4.24 $M/F$ values for vertical loop springs with different $h$. . . . . 101
4.25 Vertical loop springs with different $R$ and $a$ . . . . . 103
4.26 $M/M_o$ and $F/F_o$ for vertical springs with different $R$ and $a$ . . . . . 105
4.27 $M/F$ values for vertical loop springs with different $R$ and $a$ . . . . . 105
4.28 Vertical loop springs with different pre-activation angles . . . . . 107
4.29 $M/M_o$ and $F/F_o$ for stainless steel pre-activated vertical springs . . . 109
4.30 $M/F$ value for stainless steel pre-activated vertical springs . . . . . 109
4.31 $M/F$ values of 10° pre-activated vertical loop spring . . . . . 111
4.32 Yielded typical vertical loop spring initial geometry . . . . . 112
4.33 $TMA$ Vertical loop springs with different pre-activation angles . . . . 115
4.34 $M/M_o$ and $F/F_o$ for $TMA$ pre-activated vertical springs . . . . . 117
4.35 $M/F$ value for $TMA$ pre-activated vertical springs . . . . . 117
4.36 $M/F$ values of 35° $TMA$ pre-activated vertical spring . . . . . 119
4.37 Vertical springs with loop and arm helices geometries . . . . . 121
4.38 $M/F$ values for the vertical loop spring with loop helix . . . . . 123
4.39 $M/F$ values for the vertical spring with loop and arm helices . . . . . 125
4.40 $M/F$ values for 50° pre-activated vertical spring with helices . . . . . 127
4.41 $M/F$ values for 70° pre-activated vertical spring with helices . . . . . 130

E.1 Mohr's circle for an orthodontic spring element . . . . . 192

# Glossary

**activation:** The difference in the horizontal length between the the free and deformed shapes of the orthodontic spring.

**alveolar bone:** The bone the surrounds and supports the teeth.

**alveolar crest:** A fiber layer that constitute the border between the tooth cementum and the gum.

**anterior:** The front of a structure.

**apex of tooth root:** The tip of the tooth root.

**arch wire:** A wire fastened to two or more teeth through fixed attachments. It is used to guide tooth movement.

**bicuspid:** Premolar tooth which is one of the two teeth between the molars and the canines of the upper and lower jaws. It has two cusps.

**center of resistance:** Forces applied at this point on the tooth result in a translational movement in the direction of the force.

**cross-bite tooth:** Any of the back teeth that allow the cusps of the upper teeth to fit in the central groves of the lower teeth.

**dental arch:** The curve formed by the grouping of a normal set of teeth.

**furcation:** The part of a tooth where the roots divide.

**incisal edge:** The cutting edge of the tooth.

**incisor:** One of the eight front teeth, four in each dental arch.

**inter-bracket distance:** The horizontal distance between the two brackets on which the two ends of the orthodontic spring are mounted.

**malocclusion:** Abnormal contact of the teeth of the upper jaw with the teeth of the lower jaw.

**mandible:** Lower jaw (mandibular (*adj.*)).

**maxilla:** Upper jaw (maxillary (*adj.*)).

**M/F:** The ratio of the moment to the force at the two ends of the orthodontic spring.

**mucosae:** Mucous membranes.

**neutral position:** The deformed configuration of a pre-activated spring where the ends have zero slope and the axial forces are zero. The activation of the pre-activated springs is measured from this position.

**occlusion:** The contact between the biting or chewing surfaces of the upper and lower teeth.

**periodontal ligament:** (PDL) The fiber-like tissue that joins the teeth to the sockets (alveoli). It is made up of many bundles of connective tissue in groups and linked up with blood vessels, lymph vessels and nerves. The periodontal ligament holds and supports the teeth.

**posterior:** The back of a structure.

**pre-activation:** The initial bending of the orthodontic spring arms such that they form an angle with the horizontal. This allows higher moments to be generated by the spring.

**TMA:** Titanium molybdenum alloy. A material used for orthodontic wires which is characterized by a low Young's modulus with a relatively high yield strength.

**tooth alignment:** The arrangement of the teeth in relation to their supporting bone, adjacent teeth, and opposing teeth.

**tooth root:** The part of the tooth that is firmly joined to supporting structures of the jaws.

# Chapter 1

# Introduction

## 1.1 Orthodontic Background

Orthodontic treatment is usually performed to improve occlusion, which is defined simply as "the relation of the maxillary and mandibular teeth when in functional contact during activity of the mandible" [1]. Excessive flaring of the maxillary anterior teeth, crossbites, and anterior crowding are examples of malocclusions [2]. The orthodontic treatment in most cases of malocclusion involves teeth movement, which is achieved by introducing force systems to the reposition of the teeth within the dental arch and, thus, improving the occlusion and esthetics. The teeth are often moved to close spaces in the dental arch which are created by the extraction of teeth. This tooth motion to close spaces has been traditionally accomplished by using either sliding or wire loop mechanics. In sliding mechanics the orthodontist uses elastomeric chains and sometimes wire coil springs to close the spaces by drawing the teeth together along the arch wire. However, the friction due to the bracket sliding along the arch wire can be very high so that the forces generated by the elastomers

are significantly reduced. This in turn results in lower force values acting upon the teeth to be moved. Furthermore, the force generated by the elastomers decays non-linearly with time due to the presence of moisture and heat in the oral environment. This, in addition to the friction which varies with the arch wire cross section, the surface finish and the bracket slot dimensions, makes the sliding mechanics technique unpredictable and difficult to control. On the other hand, wire loop mechanics uses an activated wire loop connected between the individual teeth or groups of teeth. The activation of the loop generates the necessary force needed to draw the teeth together and the space closure is achieved by the deactivation of this loop. As there is no sliding of the bracket along the arch wire, friction is not a problem with this space closure technique.

The wire loop appliances can be classified into either continuous or segmented arch types. In the continuous arch, the wire loop or spring is an integral part of the arch wire connecting the anterior and posterior segments and the loop is often positioned between the two teeth where the space exits. The fact that the loop is part of the arch wire restricts the applicability of this technique to small inter-bracket distances (the inter-bracket distance ,*I.B.D.*, is the distance between the two dental brackets on which the two ends of the orthodontic appliance are mounted). In the segmented arch technique, on the other hand, separate segments of arch wire are used to group the anterior and posterior teeth. The two groups of teeth or segments are joined together using a wire loop or a retraction spring that is activated to generate the required forces for space closure. This segmentation of the arch wire allows for more flexibility in the space closure mechanisms and can be used for large inter-bracket distances. Examples of some common loop designs used by the segmented arch technique for space closure are shown in Figure 1.1. The first two springs from the left are identified as vertical loop springs while the third spring is a T-spring

Figure 1.1: Orthodontic retraction springs

and the fourth is a pre-activated T-spring. Relative to the vertical loop springs, the T-springs are characterized by a low load/deflection rate primarily because of their wider loop configuration. The T-spring geometry was designed to be used in the segmental arch technique and it is usually bend from flexible wire material, e.g. TMA (titanium molybdenum alloy). This is in contrast to the vertical loop springs which traditionally has been fabricated from stainless steel wire as part of a continuous arch. The low force levels produced by the T-springs makes it possible to incorporate large activations which is advantageous as fewer reactivations would be required. The lower load/deflection rate coupled with a relatively high yield strength also allow for the pre-activation or bending of the spring arms to form an initial angle with the horizontal. This pre-activation can produce a large increase in the moment to force ratio of the spring. This is an important parameter in determining the type of tooth movement and will be discussed below. One drawback of the relatively large sized T-spring is the irritation that can be experienced by the oral mucosae. Consequently, smaller springs such as the vertical loops are still being used by many orthodontists today.

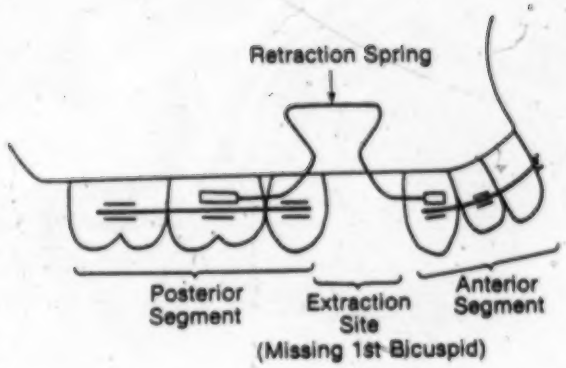


Figure 1.2: Segmented arch technique schematic

A schematic of the segmented arch technique is shown in Figure 1.2 [3] where a first bicuspid has been extracted to create space for the crowded incisors. The anterior segment groups the incisor and the cuspid (canine) teeth while the posterior segment incorporates the molar and the second bicuspid. The retraction spring shown in the figure (pre-activated T-spring) is attached to the bracket of the first molar and the cuspid and it applies a moment and a force to both segments. This force system enables the closure of the created space by drawing the anterior and posterior segments toward each other.

The way by which these different techniques discussed above achieve tooth movement is that the force applied on the crowns of the teeth generate directional stresses which are transferred by the periodontal ligament (PDL) to the alveolar bone. The periodontal ligament is a soft tissue (0.15 to 0.38 $mm$ wide [4]) that connects the tooth root to the alveolar bone. The functions of this ligament are basically to absorb the occlusal forces, provide neurosensory input and permit adaptive tooth

movements. The alveolar bone is what surrounds and supports the teeth and unlike other bone tissues the alveolar bone is more easily remodelled through continuous resorption and apposition processes in response to the stresses applied to it. This enables adaptive tooth movement to occur.

One question of concern for the orthodontists is what range of force values should be applied by the retraction appliances in order to achieve optimal tooth movement. These force values are different for different root lengths or tooth groupings, and may vary from one patient to another. For example, a multirooted tooth obviously would require higher force values to achieve movement than a single rooted tooth. There have been various attempts to determine an optimum range of force values that would achieve maximum rate of tooth movement. The most accepted hypothesis which has emerged from these attempts states that the rate of movement is linearly related to the stresses generated in the supporting structure of the tooth. However, beyond a certain point an increase in the stress value would not achieve a significant increase in the tooth movement rate. Therefore, the retraction appliance should be designed to to deliver forces within a certain range such that the generated stresses would achieve a maximum rate of tooth movement. For example, the range of forces required to retract a canine tooth efficiently is between 1 and 2 $N$ [5]. Moreover, it was realized that one way of reducing anchorage loss is to use an appliance that would generate relatively continuous stress values in the range 7 to 14 $KPa$. Higher stress values in the supporting structures result in an increase in the posterior teeth movement rate while the retraction of the anterior teeth would be reduced. This might be desirable occasionally, but usually this is not the intended goal of most orthodontic therapy. Furthermore, experimental evidence shows that appliances with a load/deflection rate such as TMA T-springs generate continuous stress values in the desired range and thus yield maximum rates of tooth movement. This is not the case for stainless steel

vertical loop springs which posses high load/deflection rates.

The magnitude of the forces and moments generated by the deformation of the retraction springs are important in orthodontics but so are the moment to force ratios. This is due to the fact that the forces of the retraction springs are not applied at the center of resistance of the tooth. The center of resistance is defined as that point of the tooth where if the line of action of the resultant applied force passes through then the result would be a pure tooth translation in the direction of the force. The center of resistance of a single rooted tooth is usually located along the long axis of the tooth, while for multirooted teeth the center of resistance lies between the roots near the furcation [6].

Earlier studies indicated that the center of resistance of the central incisor tooth is approximately one third of the distance from the alveolar crest to the apex of the tooth root [6]. This means that the distance between the bracket slot where the force is applied and the center of resistance would be approximately 10 $mm$. This value for the center of resistance was determined by modelling the root of the tooth as paraboloid of revolution and using an experimental holographic technique. A recent study by Tanne et al. [7], in which the force and moment applied on a tooth, periodontal ligament and alveolar bone assembly was analyzed using a three dimensional finite element mesh, suggested that the center of resistance for the central incisor is located at approximately one quarter of the distance from the alveolar crest to the apex of the root. The corresponding distance between the point of application of the force and the center of resistance would then be 8.39 $mm$. It should be noted, however, that the location of the center of resistance varies with the alveolar bone height, root length, PDL thickness and the biomechanical properties of the tissues. Also, the center of resistance for other than translation is affected by direction and the magnitudes of the applied forces and moments on the tooth. However, for the

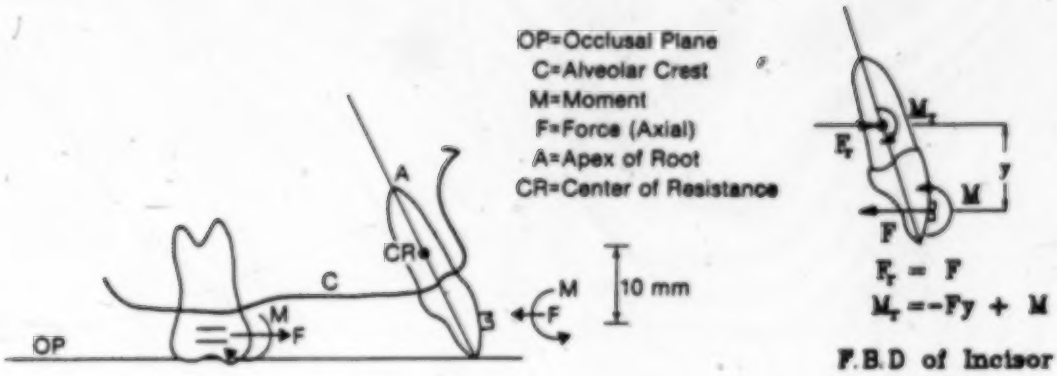


Figure 1.3: Center of resistance and equivalent force system of an incisor

simplicity of the later discussions, it is chosen to be approximately 10 *mm* from the bracket slot position.

Figure 1.3 shows the location of the center of resistance of the incisor with respect to the other points in the dental arch. In addition, a free body diagram of this tooth is drawn on the right side of the figure. The force and moment applied by the orthodontic spring are $F$ and $M$ respectively, while $F_r$ and $M_r$ represent the effective reactions applied on the tooth or the center of resistance by the surrounding PDL and alveolar bone assembly.

If the line of action of the equivalent forces delivered by the orthodontic spring does not pass through the center of resistance of the tooth then it would be expected that the tooth would have a combination of rotational and translational motion depending on the moment to force ratio provided. The absolute values of the moments and forces generated by the orthodontic springs would determine the rate of this movement. Since there are rotational movements then it is convenient to define a center of rotation

which is the point about which the tooth rotates. The location of this point can be at any position on or off the tooth depending on the $M/F$ value. For example, if only a force is applied at the bracket of the tooth which is located 10 $mm$ from the center of resistance then the applied moment to force ratio would be equal to zero. In this case the center of rotation would be some distance further from the brackets than to the center of resistance. This is shown in Figure 1.4(a) and the tooth motion is characterized as uncontrolled tipping. If both a moment and a force were applied at the bracket with the moment to force ratio less than 10 $mm$ then as the M/F value increases, the center of rotation will move further toward infinity producing a clockwise tipping motion. A special case of this situation is when the center of rotation would be located at the root apex producing what is called tipping around the apex or controlled tipping. This is believed to occur for M/F values in the 6.5 - 7.5 $mm$ range [7], and is shown in Figure 1.4(b). The third type of motion is translation. It occurs when the moment to force ratio is approximately 10 $mm$ and results in a zero moment at the center of resistance of the tooth. The center of rotation in this case is at infinity as shown in Figure 1.4(c). The fourth category of tooth motion is when the $M/F$ value is greater than 10 $mm$ and in this case the tooth would go through a counter-clockwise tipping and as the $M/F$ value increases the center of rotation would move closer to the center of resistance of the tooth. If the moment to force ratio value is around 11.5 $mm$ then the center of rotation would be located at the incisal edge of the tooth and the motion is characterized as root movement which is shown in Figure 1.4(d). The final type of motion is the pure rotation which is caused by applying only a moment at the bracket of the tooth. In this case the center of rotation would be located at the center of resistance as shown Figure 1.4(e).

The conclusion that can be drawn from the above discussion is that analyzing the force systems produced by the different orthodontic appliances is a major factor in

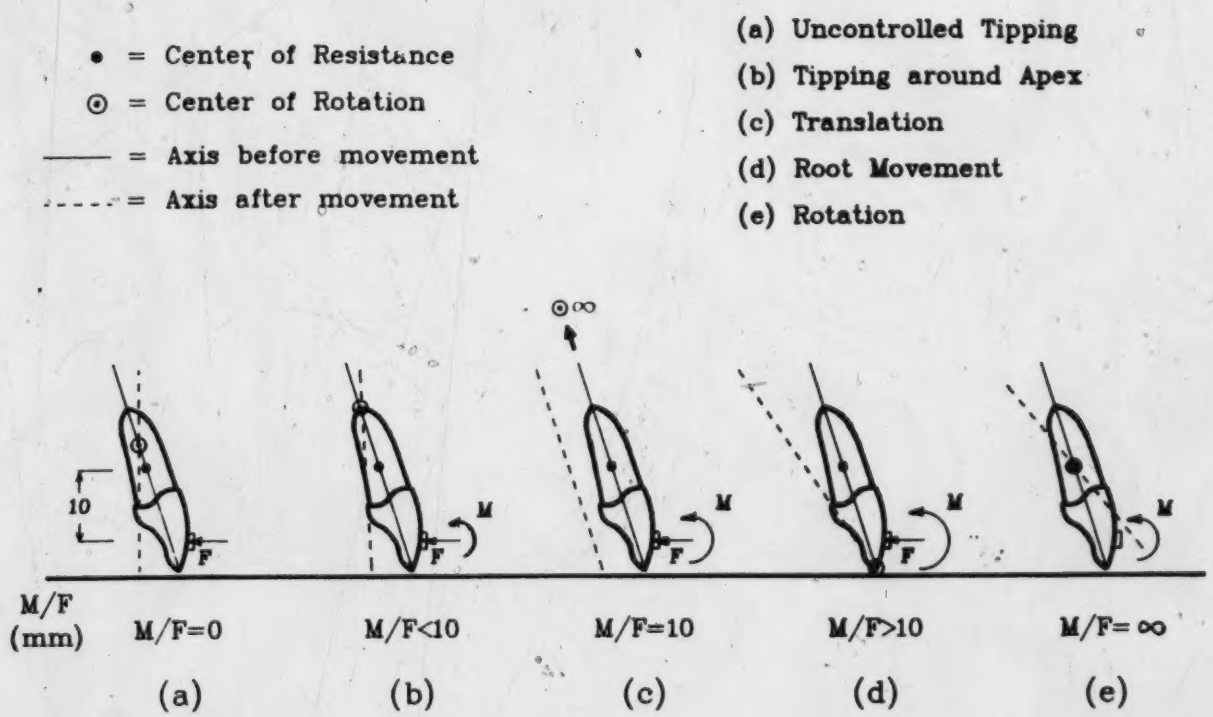


Figure 1.4: Schematic of tooth movement for different $M/F$ values

achieving proper tooth movement. A proper force system can reduce the time and the cost of orthodontic treatment. Moreover, such force analysis can play a major role in minimizing patient discomfort as well as enabling the selection of the proper appliances to generate predictable force values and moment to force ratios.

## 1.2 Analysis of Orthodontic Appliances

In order to understand the force systems produced by various orthodontic appliances, both experimental and analytical studies have been done. Initially, several devices were built to experimentally determine the values of the forces and moments of the orthodontic springs. Early devices were basically force balances that measured the amount of force required to deflect the orthodontic appliance a certain distance. The description of many of these early devices are given in [10]. The second generation of the force measurement devices employed strain gauges and electrical displacement transducers resulting in more accurate measurements. In the device developed by Solonche [11] the strain gauges were mounted on cantilever beams and torsion bars to measure both forces and moments. Alternatively, in a device developed by Paquien [12] the strain gauges were used to measure the forces of the orthodontic appliance by mounting it to a triangular base plate. This system has the ability to measure forces and moments in three directions. The most recent device was developed by Faulkner et al. [13] in which the orthodontic appliance is mounted to a cross resolver which is supported by six pairs of binocular load cells. A more detailed description of this device is given in chapter 3 as it is the same device used to verify the results of the numerical analysis technique introduced by this thesis.

As the force values of the orthodontic appliances are in the range of 0 - 3 $N$ and the moments values are in the range of 0 - 30 $N\ mm$, then the force measurement devices

must be capable of measuring low force levels. Consequently, these devices are difficult to build and researchers were prompted to look for numerical techniques that would provide a sound analysis of the forces systems generated by deforming the orthodontic appliances. One of the first attempts to analyze orthodontic springs was done by Waters et al. [14]. In his analysis the appliance was divided into a set of straight beams and each of these beams was analyzed using simple beam theory. The total solution was reached by applying force and geometric compatibility. The fact that the appliance is divided into a small number of straight beams means that the technique use would be limited to very simple geometries. Koenig and Burstone [15] used finite difference matrix techniques coupled with a Prohl method to solve the static portion of the generalized field equations for arbitrary curved and twisted beams and then used the developed code to analyze a lingual arch wire and a vertical loop spring for a small activation range (maximum spring activation was 0.681 $mm$). The vertical loop spring in this case was divided into 70 nodes. This finite difference method was modified later by DeFranco et al. [16] by introducing an incremental technique in the solution of the equations such that nonlinear load-deformation characteristics of orthodontic appliances can be determined, i.e. larger deformations could be analyzed. In this formulation the loads are applied in steps and the geometric parameters are computed for each step based on the geometrical values at the previous step. Using this technique they were able to analyze a 20° pre-activated vertical loop spring using 90 nodes.

Finite element techniques have also been used in the analysis of orthodontic springs. Yang and Baldwin [17] analyzed orthodontic springs using two node beam elements with stiffness matrices developed using Castigliano's theorem. While this technique is valid for small deflections, the nonlinear relation between the joint displacement and forces which is caused by the large deformations, was handled by

introducing a midpoint tangent incremental solution technique. In their analysis of a symmetric loop spring Yang and Baldwin used 14 elements for half of the spring and 10 incremental steps were required to calculate the force value for the maximum activation. Grief et al. [18], also used two node straight beam finite elements in the analysis of orthodontic appliances . However, the large displacement nonlinearities were handled using an algorithm which combines an incremental technique with a Newton-Raphson iterative procedure. The incremental procedure makes it possible to linearize the original nonlinear stiffness matrix producing an incremental linear stiffness matrix which is a function of the deformed shape. This means that the global stiffness matrix of the system is continuously updated for each load step. However, with such a technique the force equilibrium is not satisfied exactly, therefore, the Newton-Raphson iterative method is introduced which applies the load in a single step and then performs successive iterations until equilibrium is achieved. Using this method, a vertical loop spring was analyzed using 24 straight beam elements. The finite element method was also used by Miyakawa and Shiokawa [19] to analyze the behaviour of the assembly of the orthodontic appliance, teeth and their supporting structures. Finally, Fuchshuber [20] used the ADINA finite element package to analyze a T-spring and pre-activated T-spring. The analysis technique in this case is similar to the technique presented by Grief et al. [18], but instead of the updated Lagrangian formulation a total Lagrangian incremental formulation was used with a quasi-Newton iterative procedure. The finite element used in the analysis of the springs was an isoparametric beam element.

Most of the techniques discussed above try to accommodate the large deflections using small deflection analysis techniques by introducing incremental solutions. This fact requires that the loads and boundary conditions have to be applied in small increments so that the basic theory of small deflections is valid within each load step.

This means the computation time for many of the orthodontic springs is very high as the deformations are relatively large. This is especially true in the case of pre-activated springs. Moreover, computer memory limitations can hinder the analysis of complex spring geometries as a large number of elements, which result in a large global stiffness matrix, need to be used in finite element techniques . These two factors of time and memory size have resulted in the use of large mainframe computers, which have relatively high computational costs, in most of the previous numerical studies on the orthodontic appliances. However, the new trend is to use micro-computers for analysis as they are more convenient in terms of availability and cost. Therefore, the objective of this study was to develop a numerical technique that would allow the analysis of complex orthodontic appliances to be done using a simpler technique on a micro-computer. This meant that the technique should be able to perform the analysis in a small number of steps and without the need of large storage capacity.

A numerical method that was developed by Faulkner and Stredulinsky [21] for the analysis of large deflections of thin elastic rods appeared to offer a technique which could be used for similar analyses to be performed on the orthodontic springs. In both cases the large deformations are assumed to be within the elastic range and the rod or wire cross section is much smaller than the length. In this technique the solution of the nonlinear differential equation for the large deformation is avoided by dividing the rod into a large number of segments such that the strains and relative rotation of each segment would be small. This makes it possible to linearize the differential equation that describes the shape of the segment. The solution is achieved by solving a series of initial value problems coupled with a shooting technique that uses a Newton-Raphson false position solver. A detailed description of this technique will be presented in Chapter 2 including the modification of the equations required for the analysis of orthodontic springs.

## 1.3 Thesis Outline

The objective of this research is to develop a computer code that would be able to perform a detailed force analysis of the orthodontic appliances. The segmental shooting technique used for this analysis is presented in Chapter 2, showing how the linearized differential equation of the initially curved segment was derived and how the numerical solver works. Also, an analytical verification of the technique is presented in this chapter.

Chapter 3 includes two comparative studies that were performed to verify the output of the segmental shooting technique. A description of the force measurement device used in the pre-activated T-spring comparative study and the procedure used to determine Young's modulus of the orthodontic wire are also included in Chapter 3.

After the segmental shooting technique had been verified, the developed computer code was used to perform several parametric studies on the pre-activated T-spring and the vertical loop spring designs. These studies are presented in Chapter 4. Chapter 5 summarizes the conclusions of the study.

# Chapter 2

# Solution Technique Development

In this chapter the segmental technique of solution will be developed showing how it can be applied in the analysis of the forces and moments produced by the deformation of the orthodontic springs. The numerical shooting technique, as well as, the computer code development will be also presented. Finally, analytical verification of the solution technique will be discussed.

## 2.1 Basic Equations

The segmental technique for the analysis of large deflection of thin elastic rods was first introduced by Stredulinsky [22], and was used in determining the required supporting loads for laying offshore pipelines. In the development of the technique, the following assumptions were incorporated:

- The deflections and forces are two dimensional.
- The deflections are within the elastic range (i.e no plastic deformations).

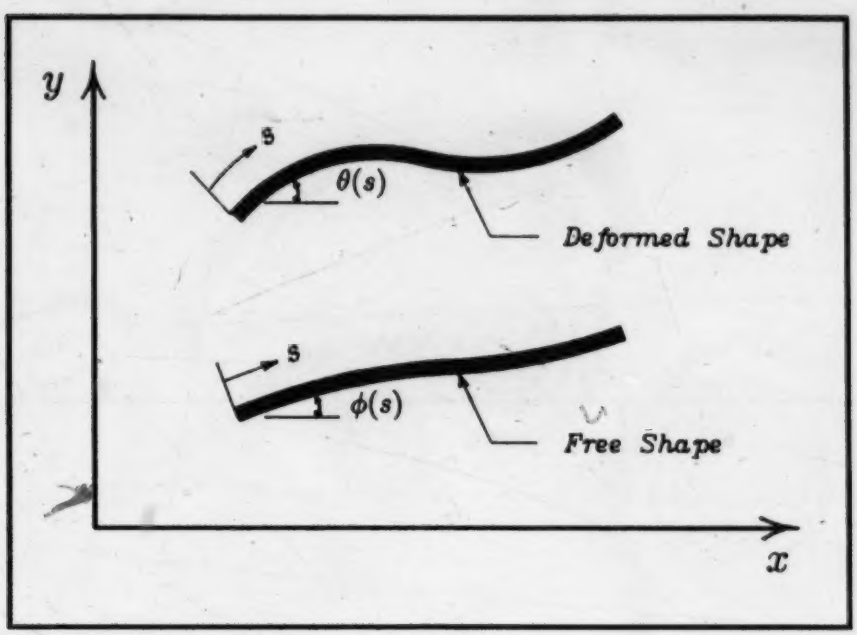


Figure 2.1: Free and deformed rod shapes

- The longitudinal strains are small (i.e. the rod is inextensible).

These assumptions are also valid for the deformation of orthodontic springs, hence the same analysis technique can be employed. However, the equations of the segmental technique were originally developed for the deflections of rods which are initially straight. Therefore, these equations had to be modified such that rods or sections of wire which are initially curved can also be analyzed. Moreover, in the case of orthodontic springs the distributed loads due the weight of the wire can be ignored. The development of the equations of the segmental technique in which the above modifications are incorporated is presented below.

Consider the rod element shown in Figure 2.1. The unstressed or free shape of the rod can be represented by a function $\phi(s)$, where $s$ is a length coordinate, while

$\phi$ is the angle of the tangent with the $x$ - axis. Similarly the deformed or deflected shape can be represented by another function $\theta(s)$ as shown in the figure. According to Bernoulli-Euler beam law, the bending moment at any point of the deflected shape is given by,

$$M = EI\left[\frac{d\theta}{ds} - \frac{d\phi}{ds}\right] , \tag{2.1}$$

where $E$ is the Young's modulus of the material, $I$ is the moment of inertia of the rod cross section, and

$$\frac{d\phi}{ds} = \frac{1}{R} , \tag{2.2}$$

where $R$ is the initial radius of curvature of any point along the rod ( $R = \infty$ for an initially straight rod element). Substitution of equation (2.2) in equation (2.1) yields,

$$M = EI\left[\frac{d\theta}{ds} - \frac{1}{R}\right] . \tag{2.3}$$

Consider an infinitesimal element of the deformed rod shown in Figure 2.2. Employing the equations of equilibrium along this element leads to the following equations,

$+\uparrow \sum F_y = 0 \Rightarrow$

$$V\cos\theta - (V+dV)\cos(\theta+d\theta) - T\sin\theta + (T+dT)\sin(\theta+d\theta) = 0 \tag{2.4}$$

$\pm\rightarrow \sum F_x = 0 \Rightarrow$

$$-T\cos\theta + (T+dT)\cos(\theta+d\theta) - V\sin\theta + (V+dV)\sin(\theta+d\theta) = 0 \tag{2.5}$$

$\circlearrowleft \sum M_c = 0 \Rightarrow$

$$M + dM - M - (V+dV)ds = 0 . \tag{2.6}$$

For this infinitesimal element, the relative rotation between the start and end points is very small. Therefore, the equilibrium equation in the $y$ direction can be reduced to

$$d(T\sin\theta) - d(V\cos\theta) = 0$$

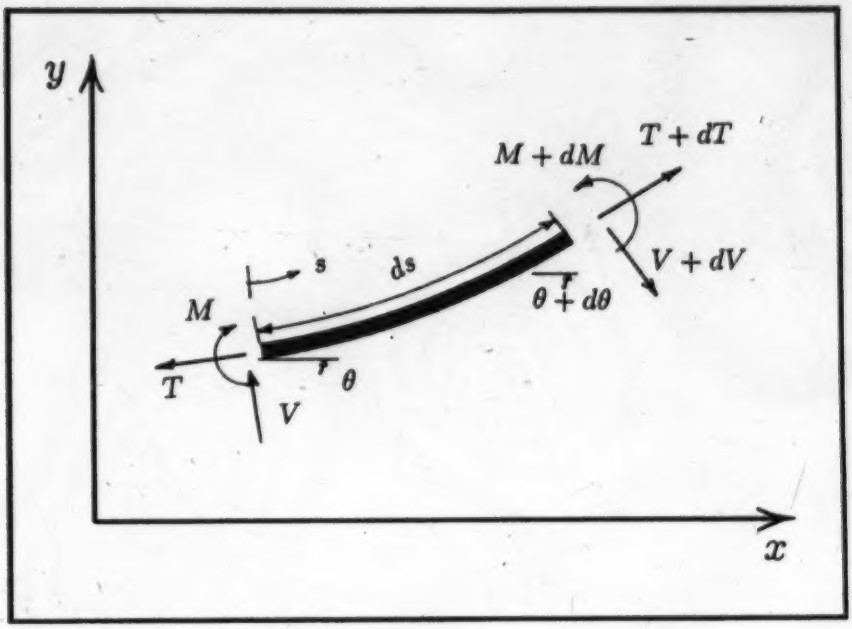


Figure 2.2: Infinitesimal element of the deformed rod

and dividing by $ds$ yields

$$\frac{d}{ds}(T\sin\theta) - \frac{d}{ds}(V\cos\theta) = 0\,. \tag{2.7}$$

Similarly for the force equilibrium in the $x$ direction becomes

$$\frac{d}{ds}(T\cos\theta) + \frac{d}{ds}(V\sin\theta) = 0\,, \tag{2.8}$$

while the moment equilibrium equation is

$$V = \frac{dM}{ds}\,. \tag{2.9}$$

Integrating equations (2.7) and (2.8) results in

$$(T\sin\theta) - (V\cos\theta) = C_1 \tag{2.10}$$

$$(T\cos\theta) + (V\sin\theta) = C_2 \tag{2.11}$$

and with the following boundary conditions at $s = 0$,

$$T = T_1 \quad , \quad V = V_1 \quad , \quad \theta = \beta \quad ,$$

yields,

$$C_1 = T_1 \sin\beta - V_1 \cos\beta \tag{2.12}$$

$$C_2 = T_1 \cos\beta + V_1 \sin\beta \, . \tag{2.13}$$

Multiplying equation (2.10) by $-\cos\theta$ and equation (2.11) by $\sin\theta$ and adding the resulting equations gives

$$V(\cos^2\theta + \sin^2\theta) = V = C_2 \sin\theta - C_1 \cos\theta \, . \tag{2.14}$$

Substituting equation (2.3) in equation (2.9) gives

$$V = \frac{dM}{ds} = \frac{d}{ds}\left[EI\left[\frac{d\theta}{ds} - \frac{1}{R}\right]\right] \, ,$$

therefore, equation (2.14) can be written as,

$$\frac{d}{ds}\left[EI\left[\frac{d\theta}{ds} - \frac{1}{R}\right]\right] = C_2 \sin\theta - C_1 \cos\theta \tag{2.15}$$

where $C_1$, and $C_2$ are given by equations (2.12) and (2.13).

For a given initial shape, the solution of this equation will yield the deformed shape $\theta(s)$ under specific boundary forces. In what follows, the rod is broken into segments, and for a given segment $E, I$, and $R$ are assumed constant, so that equation (2.15) reduces to

$$EI\,\frac{d^2\theta}{ds^2} = C_2 \sin\theta - C_1 \cos\theta \, , \tag{2.16}$$

which is a second order nonlinear differential equation describing the deformed shape of the segment. This differential equation can be linearized by selecting a local coordinate system for each segment of the rod, so that the value of $\theta$, referred to

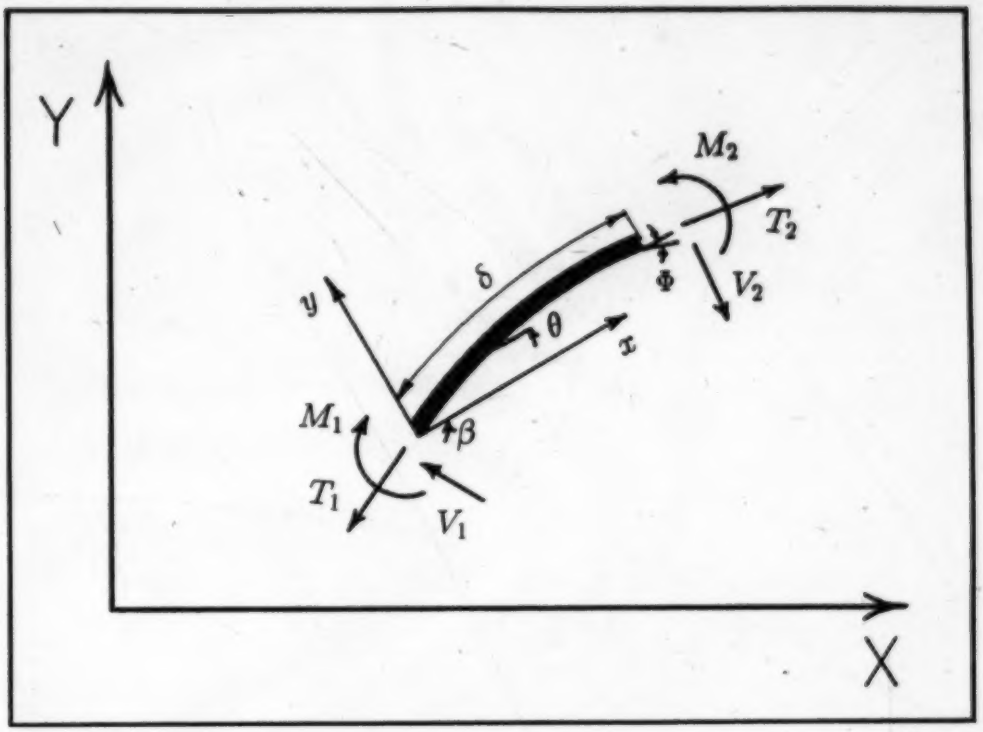


Figure 2.3: Local coordinate system of a segment

this local coordinate system, along the segment will be small. An example of such a local coordinate system, for a segment of length $\delta$, is shown in Figure 2.3.

In Figure 2.3 the origin of the local coordinate system is located at node 1 or the starting node of the segment. The angle between the tangent to node 1 and the local $x$-coordinate is given by $\beta$, while the corresponding angle at node 2 or the ending node of the segment is given by $\Phi$ i.e. $\theta = \beta$ at $s = 0$ , $\theta = \Phi$ at $s = \delta$.

Substituting the values of constants $C_1$ and $C_2$ in equation (2.16):

$$EI\,\frac{d^2\theta}{ds^2} = T_1\cos\beta\sin\theta + V_1\sin\beta\sin\theta - T_1\sin\beta\cos\theta + V_1\cos\beta\cos\theta\ ,$$

and for small angles, the above equation can be written as

$$EI\,\frac{d^2\theta}{ds^2} = T_1\theta + V_1\beta\theta - T_1\beta + V_1\ .$$

As both $\beta$ and $\theta$ are small, then the term $V_1\beta\theta$ can be ignored compared to the other terms. Therefore, the nonlinear differential equation (2.16) is simplified into the following equation

$$EI\,\frac{d^2\theta}{ds^2} - T_1\theta = V_1 - T_1\beta\ . \tag{2.17}$$

This is a second order linear differential equation which can be solved by standard techniques. Before solving the equation it can be non-dimensionalized by multiplying both sides by $\delta^2/EI$, so that

$$\delta^2\frac{d^2\theta}{ds^2} - \frac{\delta^2 T_1}{EI}\theta = \frac{\delta^2 V_1}{EI} - \frac{\delta^2 T_1}{EI}\beta\ .$$

Introducing the following dimensionless quantities,

$$\rho = \frac{s}{\delta}\ ,$$

$$\tau_1 = \frac{\delta^2 T_1}{EI}\ ,$$

$$\begin{aligned} \nu_1 &= \frac{\delta^2 V_1}{EI}, \\ \mu &= \frac{M\delta}{EI} = \frac{\delta}{EI}\left[EI\left[\frac{d\theta}{ds} - \frac{1}{R}\right]\right] \\ &= \left[\frac{d\theta}{d\rho} - \frac{\delta}{R}\right], \end{aligned}$$

yields the non-dimensional form of equation (2.17) as

$$\frac{d^2\theta}{d\rho^2} - \tau_1\theta = \nu_1 - \tau_1\beta . \tag{2.18}$$

The above equation can be solved by the standard way to give

$$\theta = Ae^{\sqrt{\tau_1}\rho} + Be^{-\sqrt{\tau_1}\rho} + C , \tag{2.19}$$

with the values of the constants A,B and C determined from the boundary conditions at $\rho = 0$.

As seen in equation (2.19), the power of the exponential is $\sqrt{\tau_1}\rho$. The presence of the square root can cause numerical problems from a programming point of view. Instead, the differential equation (2.18) can be solved using the following power series solution,

$$\theta = \sum_{k=0}^{\infty} \alpha_k \rho^k . \tag{2.20}$$

The boundary conditions used to determine the values of the series solution coefficients are

$$\theta\Big|_{\rho=0} = \beta \tag{2.21}$$

$$\frac{d\theta}{d\rho}\Big|_{\rho=0} = \mu_1 + \frac{\delta}{R} \tag{2.22}$$

$$\frac{d^2\theta}{d\rho^2}\Big|_{\rho=0} = \nu_1 \tag{2.23}$$

where $\tau_1$ , $\nu_1$ , and $\mu_1$ are respectively the nondimensional tension, shear, and bending moment at the first or starting node of the segment.

Expanding equation (2.20) yields

$$\begin{aligned}
\theta &= \alpha_o + \alpha_1\rho + \alpha_2\rho^2 + \sum_{k=3}^{\infty}\alpha_k\rho^k \quad \Rightarrow \quad \theta\Big|_{\rho=0} = \alpha_o \\
\frac{d\theta}{d\rho} &= \alpha_1 + 2\alpha_2\rho + \sum_{k=3}^{\infty}k\alpha_k\rho^{(k-1)} \quad \Rightarrow \quad \frac{d\theta}{d\rho}\Big|_{\rho=0} = \alpha_1 \\
\frac{d^2\theta}{d\rho^2} &= 2\alpha_2 + \sum_{k=3}^{\infty}k(k-1)\alpha_k\rho^{(k-2)} \quad \Rightarrow \quad \frac{d^2\theta}{d\rho^2}\Big|_{\rho=0} = 2\alpha_2 .
\end{aligned}$$

Substituting these equations in the differential equation (2.18), and using the boundary conditions, (2.21), (2.22) and (2.23), then the values of the series solution coefficients can be found to be as follows:

$$\alpha_o = \beta \tag{2.24}$$

$$\alpha_1 = \mu_1 + \frac{\delta}{R} \tag{2.25}$$

$$\alpha_2 = \frac{\nu_1}{2} \tag{2.26}$$

$$\alpha_k = \frac{\tau_1(\alpha_{(k-2)})}{k(k-1)} \quad for \quad k = 3, 4, 5, ..... \tag{2.27}$$

## 2.2 Segmental Technique

As mentioned earlier the solution of the nonlinear differential equation describing the large deformation can be avoided by considering a series of small segments and solving a linearized differential equation for each segment. The solution then proceeds from one segment to another in a manner similar to the transfer matrix method. Therefore, for a given segment $j$, starting with initial values for the global coordinates and slope, $X_1$, $Y_1$, and $\gamma_1$, as well as the initial values of the moment, shear force, and tension, $M_1$, $V_1$, and $T_1$, the series solution of the differential equation is used to compute the corresponding values at the ending node of the segment. These computed values are then used as the initial values for the following segment $j+1$ and so on until the end of the beam or the spring is reached. A schematic of this solution procedure is shown in Figure 2.4.

The solutions for values at the ending node of each segment are found as follows:

- [A] For each segment, six values at the starting node are given. They are:

  1. Global X-coordinate ($X_{i-1}$).
  2. Global Y-coordinate ($Y_{i-1}$).
  3. Angle of tangent with global X-axis ($\gamma_{i-1}$).
  4. Moment ($M_{1(j)}$).
  5. Tension force ($T_{1(j)}$).
  6. Shear force ($V_{1(j)}$).

  as well, the segment length $\delta$, segment stiffness $EI$, and $R$ the initial radius of curvature of the segment are specified. These allow the nondimensional moment, shear, and tension at the starting node of the segment to be computed as

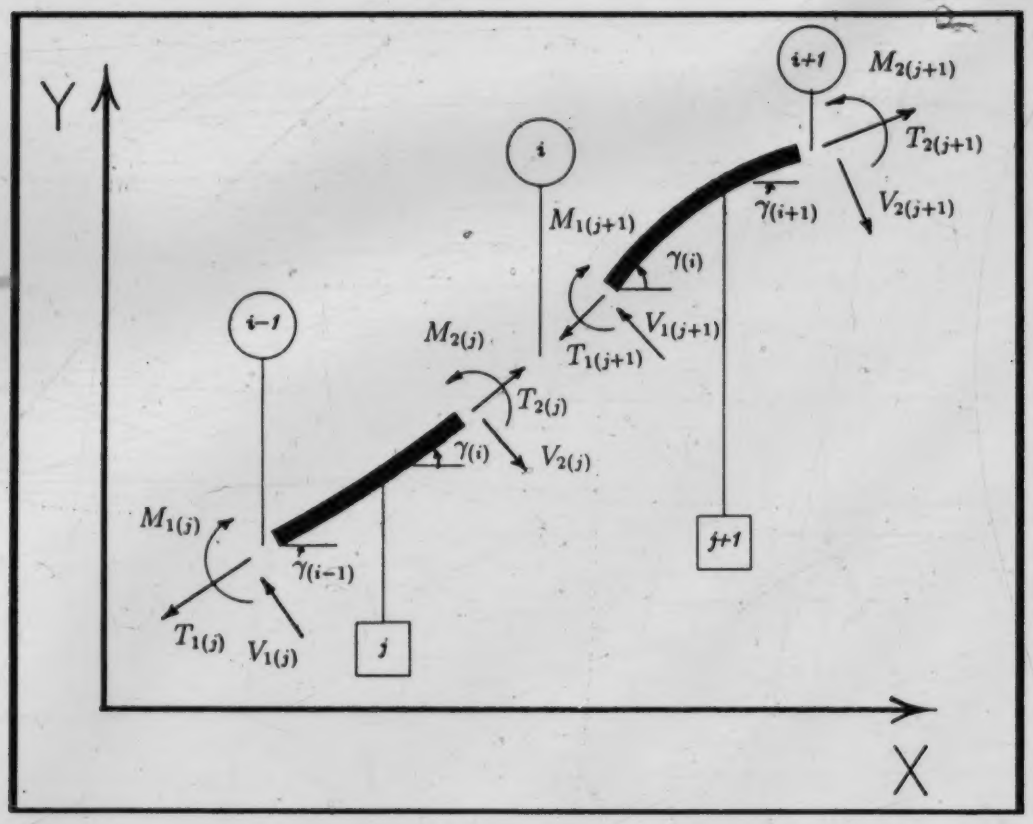


Figure 2.4: Assembling of successive segments

$$\mu_1 = M_1\delta/EI \tag{2.28}$$

$$\tau_1 = T_1\delta^2/EI \tag{2.29}$$

$$\nu_1 = V_1\delta^2/EI\,. \tag{2.30}$$

- [B] A local coordinate system is chosen with the origin located at the starting node of the segment. The angle between the tangent and the local $x$-coordinate is given by $\beta$ as shown in Figure 2.3. The value of $\beta$ is chosen so that the average value of $(\theta)^2$, which is ignored in the earlier derivations, is minimal. Therefore, if a linear curvature approximation of the deformed segment is adopted by considering the first three terms of the series solution:

$$\theta = \beta + \left(\mu_1 + \frac{\delta}{R}\right)\rho + \frac{\nu_1}{2}\rho^2\,,$$

then

$$\begin{aligned}(\theta^2)_{AVE} &= \int_0^1 \theta^2 d\rho \\ &= \beta^2 + \beta\left(\mu_1 + \frac{\delta}{R} + \frac{\nu_1}{3}\right) + \frac{1}{3}\left(\mu_1 + \frac{\delta}{R}\right)^2 + \frac{\nu_1^2}{20} + \frac{1}{4}\nu_1\left(\mu_1 + \frac{\delta}{R}\right)\,.\end{aligned}$$

Minimizing this expression with respect to $\beta$ gives

$$\beta_j = -\left(\frac{\mu_1}{2} + \frac{\delta}{2R} + \frac{\nu_1}{6}\right)\,. \tag{2.31}$$

The angle of the tangent at the end point of the segment with respect to local $x$-axis, $\Phi$ , is given by

$$\Phi = \theta\Big|_{\rho=1} = \left(\sum_{k=0}^{\infty}\alpha_k\rho^k\right)\Big|_{\rho=1} = \sum_{k=0}^{\infty}\alpha_k\,, \tag{2.32}$$

while the angle of the tangent at the end point of the segment with respect to the global X-axis will be

$$\gamma_i = \gamma_{i-1} - \beta_j + \Phi_j\,. \tag{2.33}$$

- [C] The local coordinates of the end node of the segment are found from

$$x = \int_0^s \cos\theta ds \simeq \int_0^s ds \simeq s$$
$$y = \int_0^s \sin\theta ds \simeq \int_0^s \theta ds ,$$

and in non-dimensional form

$$\frac{x}{\delta} = \rho , \quad \text{and} \quad \frac{y}{\delta} = \int_0^\rho \theta d\rho = \sum_{k=0}^{\infty} \frac{\alpha_k \rho^k}{k+1} .$$

Therefore, at the end node where $\rho = 1$

$$\frac{x_2}{\delta} = 1 , \quad \text{and} \quad \frac{y_2}{\delta} = \sum_{k=0}^{\infty} \frac{\alpha_k}{k+1} = h_j .$$

If the first three terms of the above series is considered, i.e

$$\frac{y_2}{\delta} \simeq \left(\beta + \frac{\mu_1}{2} + \frac{\delta}{2R} + \frac{\nu_1}{6}\right) ,$$

then the optimum choice of $\beta$ value given in equation (2.31), results in the local $x-$axis passing through both end points of the segment, as

$$\frac{y_2}{\delta} \simeq 0 .$$

The position of the ending node of the segment in terms of the global X and Y coordinates can be determined from geometrical relations to be

$$X_i = X_{i-1} + (x_2 \cos(\gamma_{i-1} - \beta)) - (y_2 \sin(\gamma_{i-1} - \beta))$$
$$Y_i = Y_{i-1} + (x_2 \sin(\gamma_{i-1} - \beta)) + (y_2 \cos(\gamma_{i-1} - \beta)) ,$$

which can be simplified as:

$$X_i = X_{i-1} + (\delta \cos(\gamma_{i-1} - \beta)) - (\delta h_j \sin(\gamma_{i-1} - \beta)) \qquad (2.34)$$
$$Y_i = Y_{i-1} + (\delta \sin(\gamma_{i-1} - \beta)) + (\delta h_j \cos(\gamma_{i-1} - \beta)) . \qquad (2.35)$$

- [D] The bending moment at the ending node is computed from

$$\mu = \left[ \frac{d\theta}{d\rho} - \frac{\delta}{R} \right] = \left[ \sum_{k=1}^{\infty} (k\alpha_k \rho^{(k-1)}) - \frac{\delta}{R} \right].$$

Therefore, at the end point or node 2 of the segment where $\rho = 1$ the nondimensional moment will be

$$\mu_2 = \sum_{k=1}^{\infty} (k\alpha_k) - \frac{\delta}{R} \tag{2.36}$$

with the moment value being

$$M_2 = \frac{\mu_2 EI}{\delta}. \tag{2.37}$$

- [E] The shear force is determined from

$$\nu = \frac{d}{d\rho} \left[ \frac{d\theta}{d\rho} - \frac{\delta}{R} \right] = \sum_{k=2}^{\infty} k(k-1)\alpha_k \rho^{(k-2)}.$$

Therefore, the nondimensional shear force at the end point is given by

$$\nu_2 = \sum_{k=2}^{\infty} k(k-1)\alpha_k \tag{2.38}$$

and the shear force will be

$$V_2 = \frac{\nu_2 EI}{\delta^2}. \tag{2.39}$$

- [F] The axial force or tension at the end point of the segment is computed by applying equilibrium along the local $x-$axis.

$$\pm \rightarrow \sum f_x = 0 \quad \Rightarrow \quad \tau_2 \cos\Phi + \nu_2 \sin\Phi - \tau_1 \cos\beta - \nu_1 \sin\beta = 0,$$

and using the small angle approximation, gives the nondimensional tension as

$$\tau_2 = \tau_1 + \nu_1\beta - \nu_2\Phi \tag{2.40}$$

and the tension will be

$$T_2 = \frac{\tau_2 EI}{\delta^2}. \tag{2.41}$$

The values of forces, slope and position of the last node of the segment have now been determined. These values will be the initial values for the following segment, and the sequence of computations outlined above will be repeated in turn for all segments of the rod or spring.

## 2.3 Numerical Solver (Shooting Method)

In order to start the segmental technique, six values at the initial node of the rod or the spring must be given. These values are X and Y position, slope, tension, shear, and bending moment. While some of these quantities are initially unknown, a corresponding number of these quantities are known at the last node of the rod or the spring. For example, in the case of a cantilever beam deflected by a given load at the free end, the slope at the free end is unknown while the slope at the fixed end is known to be zero. Another example is in the case of orthodontic springs. The values of the moment, shear and tension are unknown at both ends and the purpose of the analysis is to determine the values of these forces. On the other hand, the position and slope of both the first and last node of the deformed spring are usually known, as these are the positions and slopes of the two brackets between which the spring is mounted. Therefore, there is a need for a numerical solver that will make use of the specified boundary values at the last node to predict the unknown values at the first node of the rod or spring.

The numerical solver used is an iterative shooting method in which initial values for the unknowns at the first node are assumed and the segmental technique is used to compute the values at the last node. Then, the difference between the computed and specified values at the last node is calculated. This difference is used to improve or correct the initial values of the first node unknown by using a Newton-Raphson

false position routine.

This numerical solver can be described as follows for $N$ number of unknowns. Let $\underline{Z}$ represent a vector containing initial values for the unknowns at the first node, $\underline{Bs}$ is a vector containing the specified boundaries at the last node, and $\underline{B}$ is the vector containing the computed boundary values by the segmental technique.

$$\underline{Z}^{(k)} = \begin{pmatrix} Z_1^{(k)} \\ Z_2^{(k)} \\ \vdots \\ Z_N^{(k)} \end{pmatrix} \qquad \underline{Bs} = \begin{pmatrix} Bs_1 \\ Bs_2 \\ \vdots \\ Bs_N \end{pmatrix} \qquad \underline{B}^{(k)} = \begin{pmatrix} B_1^{(k)} \\ B_2^{(k)} \\ \vdots \\ B_N^{(k)} \end{pmatrix}$$

where $k$ is an iteration counter.

If we define a residual or an error vector by

$$\underline{F}^{(k)} = \underline{B}^{(k)} - \underline{Bs}\,, \tag{2.42}$$

where $\underline{F}^{(k)} \approx 0$ when the solution is reached, and since

$$\underline{B} = f(Z_1, Z_2, \ldots, Z_N)\,, \quad \text{then} \quad \underline{F} = f(Z_1, Z_2, \ldots, Z_N)$$

These error functions $F_1, F_2, \ldots, F_N$ are a system of nonlinear equations which can be solved using Newton-Raphson iterative method given by

$$\underline{Z}^{(k+1)} = \underline{Z}^{(k)} - \frac{\underline{F}^{(k)}}{\mathbf{J}^{(k)}} \tag{2.43}$$

where

$$\mathbf{J} = \begin{pmatrix} \frac{\partial F_1}{\partial Z_1} & \frac{\partial F_1}{\partial Z_2} & \cdots & \frac{\partial F_1}{\partial Z_N} \\ \frac{\partial F_2}{\partial Z_1} & \cdots & \ddots & \frac{\partial F_2}{\partial Z_N} \\ \vdots & \ddots & \ddots & \vdots \\ \frac{\partial F_N}{\partial Z_1} & \cdots & \cdots & \frac{\partial F_N}{\partial Z_N} \end{pmatrix}$$

$\underline{F}$ in this case is not given by an analytical function. Therefore, the partial derivatives, which are the elements of the Jacobian matrix J, are computed using a false position approach in which the following backward difference formulation is adopted,

$$\mathbf{J}_{lm}^{(k)} = \frac{\partial F_l^{(k)}}{\partial Z_m^{(k)}} = \frac{F_l(\underline{Z}^{(k)}) - F_l(Z_1^{(k)}, \ldots Z_m^{(k-1)}, \ldots Z_N^{(k)})}{Z_m^{(k)} - Z_m^{(k-1)}}$$

Therefore, two initial values for each unknown need to be assumed.

If one defines

$$\underline{D}^{(k)} = \underline{Z}^{(k+1)} - \underline{Z}^{(k)}, \tag{2.44}$$

then equation (2.43) can be written as

$$\underline{D}^{(k)} = -(\mathbf{J}^{(k)})^{-1}\, \underline{F}^{(k)} \quad \text{or} \quad \mathbf{J}^{(k)}\, \underline{D}^{(k)} = -\underline{F}^{(k)}. \tag{2.45}$$

Equation (2.45) has the form of $Ax = B$ system of linear equations which can be solved using a standard Gaussian elimination routine. Consequently, the vector $\underline{D}^{(k)}$ can be computed. Then, new or corrected initial values for the unknowns at the first node can be calculated using

$$\underline{Z}^{(k+1)} = \underline{Z}^{(k)} + \underline{D}^{(k)} \tag{2.46}$$

In some cases, especially for the case of three unknowns or higher, the degree of nonlinearity in the error functions is very high so the corrected values might overshoot causing either an overflow in the program, or at least the convergence rate becomes

very slow. In such cases, a relaxation factor vector ($w$) is introduced in equation (2.44). That is

$$Z^{(k+1)} = Z^{(k)} + w\, D^{(k)}$$

where $0 < w \leq 1$.

The details of the computation of the derivatives is the case of 3 unknowns is shown in Appendix B.

## 2.4 Computer Code Development

The routines of the computer code developed to analyze the deformation of orthodontic springs can be classified into four groups:

1. Parameters and geometry input routines
2. Boundary and force input routines
3. Segmental technique routines
4. Numerical solver routines

which are individually discussed below.

### 2.4.1 Parameters and Geometry Input Routines

The required data for each spring analyzed is the Young's modulus of the material, the moment of inertia of the cross section and the lengths and radii of curvature of the configuration.

The way in which the different spring geometries are input is to divide the spring into different parts such that each part has a constant initial radius of curvature. For example, the vertical loop spring shown in Figure 2.5 is divided into 7 different sections. Section 1 has a length of 4 $mm$ and an infinite radius of curvature (as it is initially straight). Section 2 has a radius of curvature of $+0.25$ $mm$ and a length equal to $R \times Arc\ Angle$ (Arc Angle = 90° or $\pi/2$ in this case). In this section, the radius has a positive value because the following convention was adopted; if the procession along the arc is in anti-clockwise direction, then the arc would have a positive value for the radius of curvature, while a negative value is assigned to the radius of curvature of arcs with clockwise direction. For this reason section 4 has a radius of curvature of $-1.0$ $mm$ while the arc angle is 180°. The same process is repeated until the entire spring is covered.

Figure 2.5 outlines the input of the above data to the program. First, the Young's modulus, moment of inertia, number of different sections, and the total number of segments are entered. Then, for the straight sections, the length and the number of segments within each section is required. In the case of curved sections the radius of curvature, arc angle, as well as the number of segments are required. Also, it should be noted that, in the case of initially curved sections, a larger number of segments is needed, so the assumption of a small $\theta$ within each segment is valid.

### 2.4.2 Force and Boundary Input Routine

To start the segmental technique solution the position and the forces of the first node of the spring or rod must be given. If some of these quantities are unknown, then, after specifying that they are unknowns, two initial values will be required for each one of them (usually, only one value is assumed and another value, close to it,

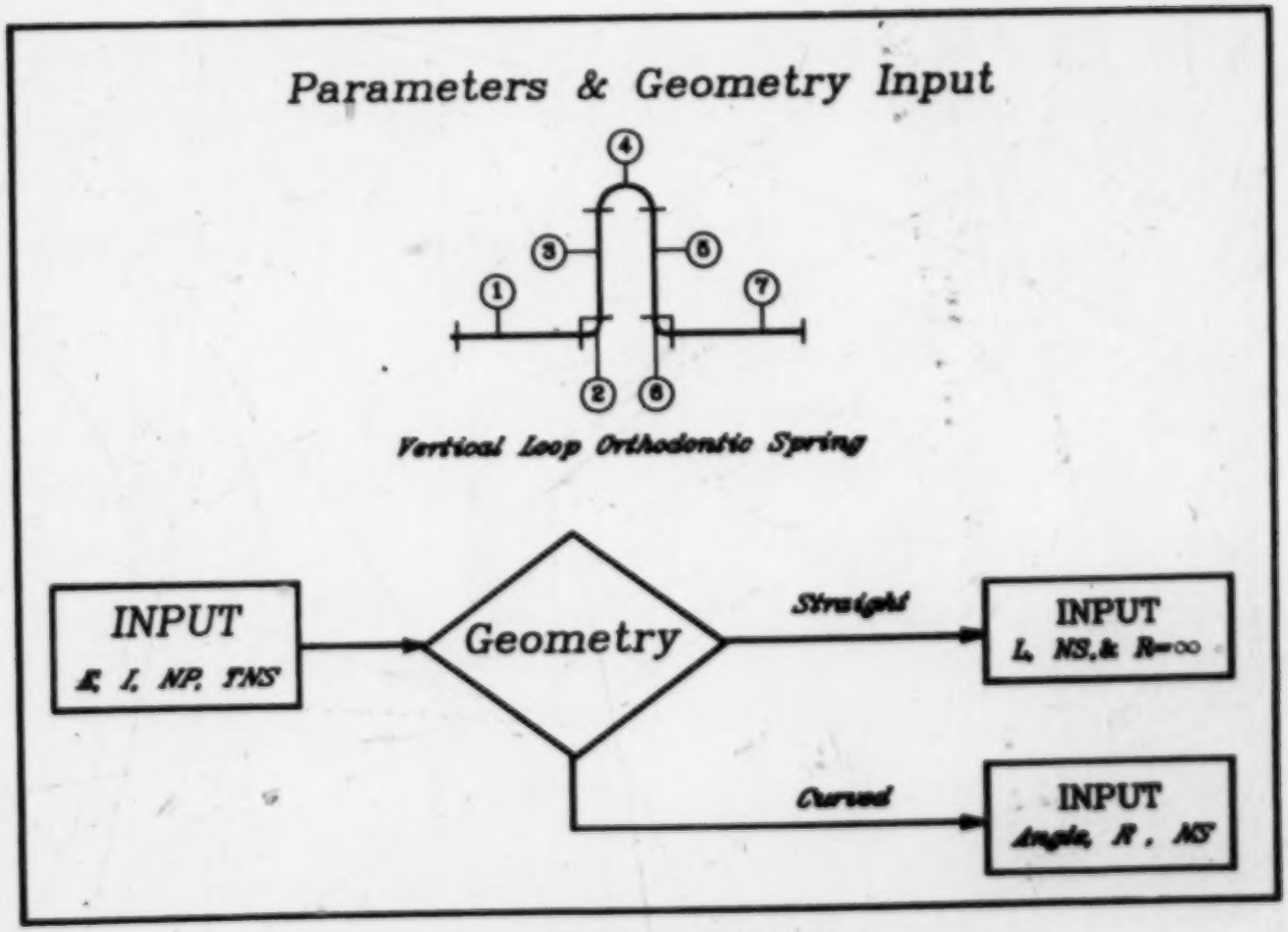


Figure 2.5: Flow chart of the input routines

is generated by the program). These initial values will be assigned to the shooting technique dependent variables, $Z_1^{(0)}$, $Z_1^{(1)}$, $Z_2^{(0)}$, $Z_2^{(1)}$, ..., $Z_N^{(0)}$, $Z_N^{(1)}$, where $N$ is the number of unknowns. After the first node data are entered, the routine will ask for $N$ known quantities at the last node of the spring or rod to be specified and their values to be entered. These values will be assigned to the shooting technique constants, $Bs_1$, $Bs_2$, ..., $Bs_N$.

Examples of how these boundary values are specified are shown in Figure 2.6. In Figure 2.6(a) there is a vertical loop spring mounted between two brackets that have $X_f$ horizontal distance and $Y_f$ vertical offset between them. In this case the $X$, and $Y$ position as well as the slope of the first node are known (usually $X_o, Y_o$ are set to be zero as the first node is chosen to be the origin of the global coordinate system). However, the values of the forces and moment are unknown, so initial values must be assumed. On the other hand, the $X$, and $Y$ position and the slope of the last node are known, so they will be specified as the boundary known values.

Figure 2.6(b) represents a simpler case than the one discussed above, as in this case the spring is symmetric and there is no vertical offset between the two brackets. In such a case only half of the spring need to considered (which means half the total number of segments). In addition, the shear force at the first and last nodes will be zero as a result of the symmetric deformation along the center line of the spring. Therefore, there are only two unknowns, the tension and the moment, at the first node. Correspondingly, only two boundary values at the last node are required. These are the $X$ position (half the distance between the two brackets) and the slope (which is zero).

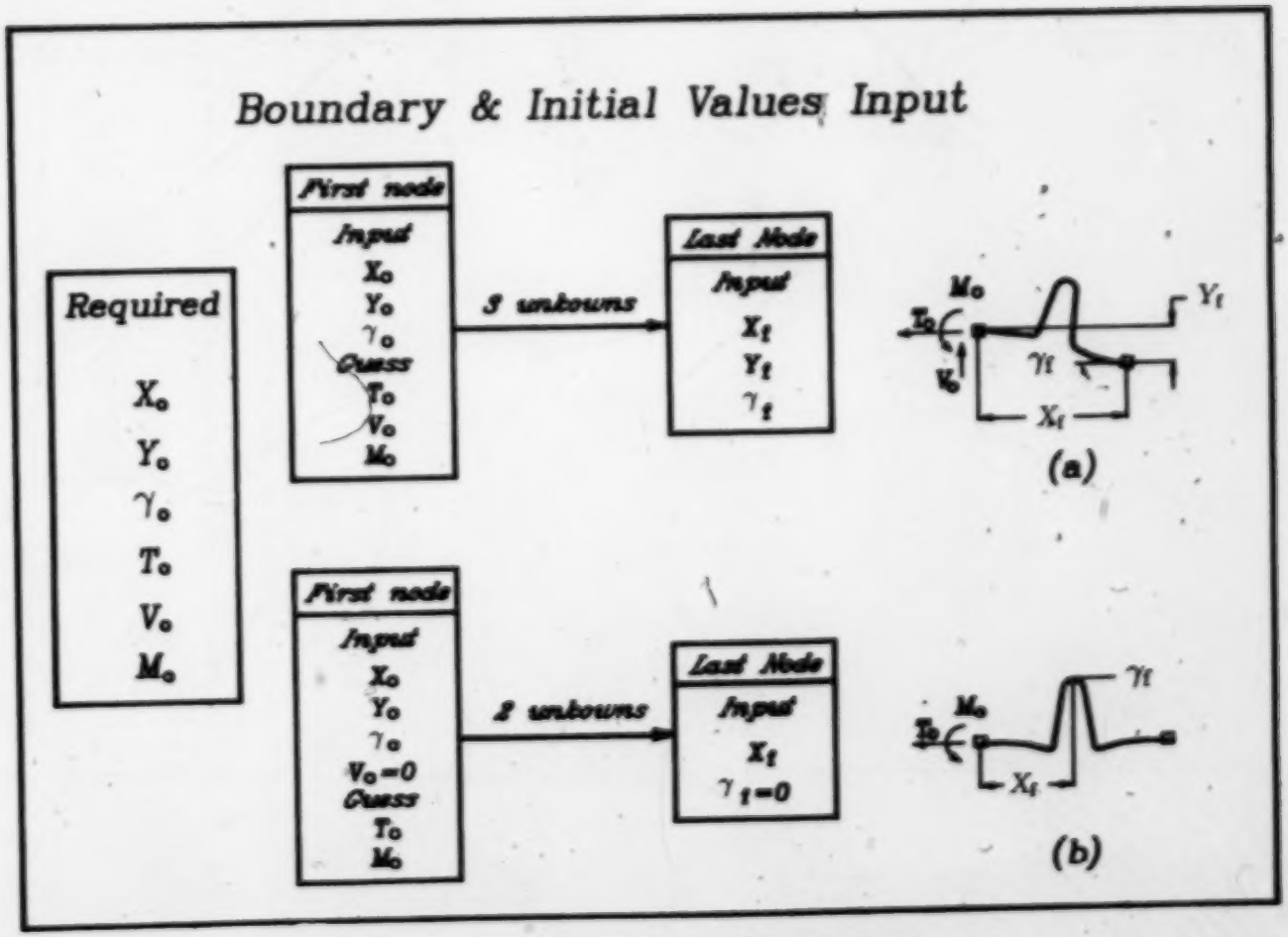


Figure 2.6: Forces and boundary input routine schematic

### 2.4.3 Segmental Technique Routine

This routine computes the values of forces and moments, as well as, the $X$, and $Y$ position and the slope of every node along the length of the spring or the rod. It is mainly a loop that contains the equations of the segmental technique outlined in section 2.2 .The starting values of the loop are the specified values at the first node, while the final values computed by the routine are the values at the last node.

The sequence of computations within the loop are as follows:

1. Input $\delta_{(j)}, R_{(j)}, X_{i-1}, Y_{i-1}, \gamma_{i-1}, T_{1(j)}, V_{1(j)}, M_{1(j)}$ .
2. Non-dimensionalize $M_{1(j)}, T_{1(j)}, V_{1(j)}$ using equations (2.28,2.29,2.30).
3. Compute the value of $\beta$ using equation (2.31) .
4. Compute the values of the series solution coefficients as given in equations (2.24,2.25,2.26,2.27).
5. Compute the value of $\Phi$ using equation (2.32) .
6. Compute the value of $\gamma_i$ using equation (2.33) .
7. Compute the values of $X_i$ & $Y_i$ using equations (2.34,2.35) .
8. Compute the value of $\mu_2$ using equation (2.36).
9. Compute the value of $\nu_2$ using equation (2.38).
10. Compute the value of $\tau_2$ using equation (2.40).
11. Compute the values of $T_{2(j)}, V_{2(j)}, M_{2(j)}$ using equations (2.37,2.39,2.41) .
12. Set $T_{1(j+1)} = T_{2(j)}$ , $V_{1(j+1)} = V_{2(j)}$ , $M_{1(j+1)} = M_{2(j)}$

13. Increment $i$ and $j$.

These 13 steps are repeated until the forces and position of all the segments have been calculated.

### 2.4.4 Numerical Solver Routines

This section of the program is composed mainly of 3 different shooting method subroutines, one is used if there is only one unknown, another for solving problems with 2 unknowns, and the third is for the more general case of 3 unknowns. A fourth subroutine is the Gaussian elimination procedure. Each of these three subroutines consists of a Newton-Raphson iterative loop from which the segmental technique routine is called a number of times depending on the number of the unknowns to be determined. For example, the segmental technique routine is called once every iteration loop if there is only one unknown, while in the case of two unknowns, it is called three times every iteration loop. This will facilitate the computation of the different partial derivatives, which are the elements of the Jacobian matrix. A detailed explanation of the 3 unknown shooting method is given in Appendix B.

Figure 2.7 represent a macro flow-chart of the developed computer code . It shows the interaction of the different parts of the program.

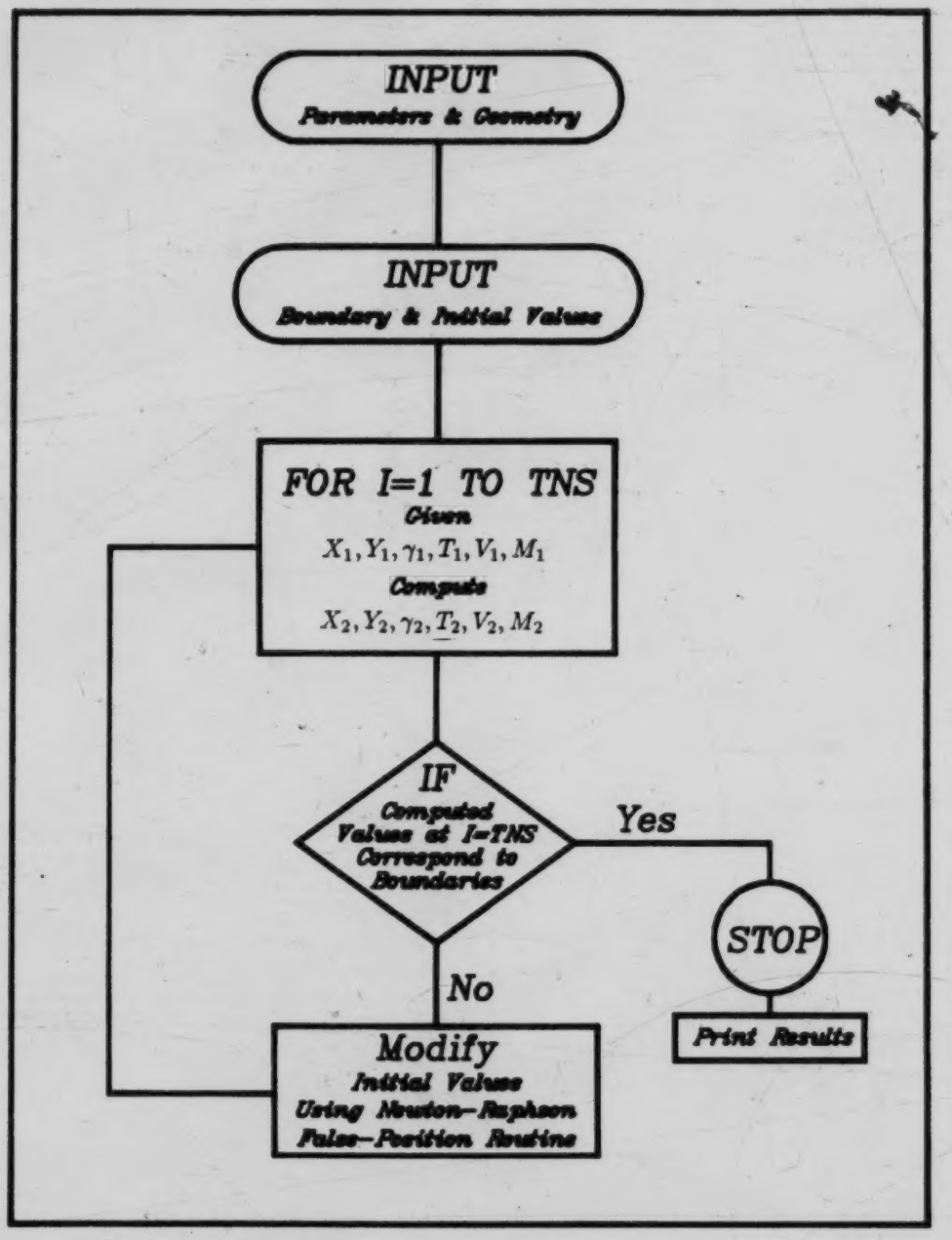


Figure 2.7: Program flow chart

## 2.5 Analytical Verification

When the segmental solution technique was first introduced, the equations were developed for initially straight rods only, and an analytical verification for such a case was given in [22]. However, in the case of orthodontic springs there is a combination of initially straight and initially curved rod elements. The equations were, therefore, modified to accommodate the more general case of rod elements that have an initial radius of curvature $R$ ($R = \infty$ for initially straight elements). Consequently, there was a need to analytically verify the modified equations of the segmental technique.

Frisch-Fay [23] has introduced an analytical solution for the large deformation of an initially curved (with a constant radius of curvature) cantilever bar under a horizontal load $P$ as shown in Figure 2.8.

According to [23] the differential equation expressing the bending moment in this case is

$$EI\frac{d^2\theta}{ds^2} - P\cos\theta = 0\,, \tag{2.47}$$

By defining

$$k = \sqrt{\frac{P}{EI}}\,,$$

then equation (2.47) can be rearranged to be

$$\frac{d^2\theta}{ds^2} = -k^2\sin\theta\,, \tag{2.48}$$

which is a special case of equation (2.16). Integrating equation (2.48) yields

$$\frac{1}{2}\frac{d\theta}{ds} = k^2\cos\theta + C\,. \tag{2.49}$$

The solution of the equation (2.49) can be simplified to standard elliptic forms by introducing the substitution

$$1 - \cos\theta = 2p^2\sin^2\varphi\,.$$

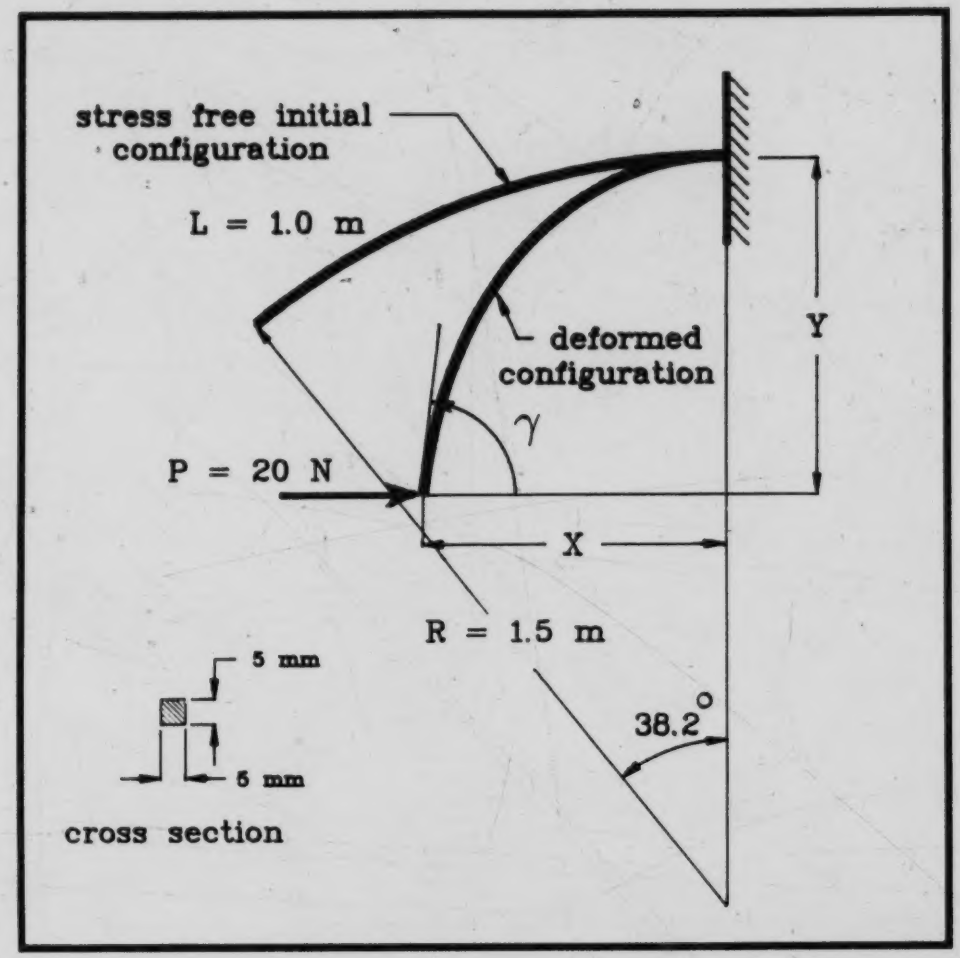


Figure 2.8: Deflection of curved cantilever beam under horizontal load

This will yield the following elliptic integral equations that describe the deformed shape of the cantilever bar. The length of the bar is given by

$$L = \frac{1}{k}\int_0^{\varphi_1} \frac{d\varphi}{(1-p^2\sin^2\varphi)^{\frac{1}{2}}} = F(p,\varphi_1)/k \ , \tag{2.50}$$

where $p$ is an integration parameter, and

$$\varphi_1 = \cos^{-1}\left(\frac{1}{2pkR}\right) ,$$

with $R$ being the initial radius of curvature. As the bar is assumed to be inextensible, i.e. the length of the bar after deformation is equal to the initial length, then equation (2.50) can be used to determine the value of the integration parameter $p$. The horizontal distance between the free and fixed ends is given by

$$X = [2E(p,\varphi_1) - F(p,\varphi_1)]/k \tag{2.51}$$

where $E$, and $F$ are elliptic integrals of the first and second kind defined as

$$E(p,\varphi_1) = \int_0^{\varphi_1} (1-p^2\sin^2\varphi)^{\frac{1}{2}} d\varphi \quad \text{and}$$
$$F(p,\varphi_1) = \int_0^{\varphi_1} \frac{d\varphi}{(1-p^2\sin^2\varphi)^{\frac{1}{2}}} .$$

The angle of the tangent at the free end, $\gamma$, is obtained from

$$\cos\gamma = 1 - 2p^2 + \frac{1}{2k^2R^2} , \tag{2.52}$$

while the vertical distance between the free and fixed ends, $Y$, is determined by solving the quadratic equation:

$$Y^2\frac{1}{R^2} + Y\frac{2}{k^2R^3} - \frac{2}{k^2R^2}(1-\cos\gamma) = 0 . \tag{2.53}$$

Consider the curved cantilever beam shown in Figure 2.8 with the following specifications:

$$I = 52.083\ mm^4 \ , \quad E = 207\ GPa \ , \quad L = 1.0\ m$$

$$R = 1.5\,m \quad , \quad P = 20\,N$$

$$\text{then} \quad k = \sqrt{\frac{P}{EI}} = 1.362\,m^{-1} \ .$$

Equation (2.50) was used to determine the elliptic integral parameter $p$ by applying a bisection method along with a Gauss-Quadrature numerical integration routine (see Appendix C). This yielded

$$p = 0.7056020770 \ , \quad \text{and} \quad \varphi_1 = 1.2165885727 \ .$$

Solving equation (2.51) using another Gauss-Quadrature routine (Appendix C) gives

$$X = 0.6089913525\,m \ ,$$

and using equation (2.51)

$$\gamma = 1.4464329173 \ .$$

The vertical distance was evaluated using equation (2.53) and found to be

$$Y = 0.6767434489\,m \ .$$

The same problem was solved using the segmental technique with various number of segments considered. The origin of the global coordinate system is chosen to be the free end of the bar, and the first node input data were

$$X_o = 0 \quad , \quad Y_o = 0 \quad , \quad \gamma_o = \textit{unknown}$$

$$M_o = 0 \quad , \quad T_o = -P\cos\gamma_o \quad , \quad V_o = -P\sin\gamma_o$$

In this case there is only one unknown and, therefore, only one boundary condition is required at the last node. In this case it is the slope at the fixed end which is equal to zero i.e. $\gamma_f = 0$ . The results of the numerical technique are listed in Table 2.2.

Comparing the values listed in Tables 2.1 and 2.2, it can be concluded that the segmental technique agrees well with the analytical solution. The agreement between the two methods gets better as the number of segments is increased. Moreover, these results give a guideline to the number of segments required for the curved portions of the orthodontic springs. For example, as the initial included angle of the curved cantilever is 38.2°, then error value of less than 0.2 % is achieved, if 3 segments per degree of angle are used. This was deduced by comparing the output of the segmental technique with 130 segments and the analytical results.

Table 2.1: Analytical results of curved cantilever beam deflection

| $X(m)$ | $Y(m)$ | $\gamma(rad.)$ |
|---|---|---|
| 0.608991 | 0.676743 | 1.446433 |

Table 2.2: Numerical results of curved cantilever beam deflection

| # of seg. | $X(m)$ | $Y(m)$ | $\gamma(rad.)$ |
|---|---|---|---|
| 1000 | 0.608854 | 0.676833 | 1.446667 |
| 750 | 0.608808 | 0.676862 | 1.446744 |
| 500 | 0.608716 | 0.676922 | 1.446900 |
| 250 | 0.608442 | 0.677100 | 1.447367 |
| 130 | 0.607936 | 0.677431 | 1.448230 |
| 70 | 0.607036 | 0.678025 | 1.449770 |
| 40 | 0.605584 | 0.678999 | 1.452272 |
| 10 | 0.595865 | 0.686095 | 1.469652 |
| 1 | 0.572868 | 0.819653 | 1.605943 |

# Chapter 3

# Comparative Studies

In this chapter the results of two comparative studies, which were performed to verify the solutions obtained by the segmental shooting technique, are given. The first study compares the numerical and experimental results obtained by previous investigators, for a T-loop spring, with those found using the current technique. The second study analyzes a pre-activated T-spring. In this case the output of the numerical segmental technique will be compared to values of moments and forces determined experimentally through the use of a three dimensional force measurement device.

## 3.1 T-Spring Comparative Study

The T-spring shown in Figure 3.1 was analyzed experimentally and numerically by Koenig et al. [24] and Fuchshuber [20]. Koenig et al. used a finite difference mesh to analyze the spring numerically, while Fuchshuber used the ADINA finite element package in his numerical analysis along with a 3-D force platform (described later)

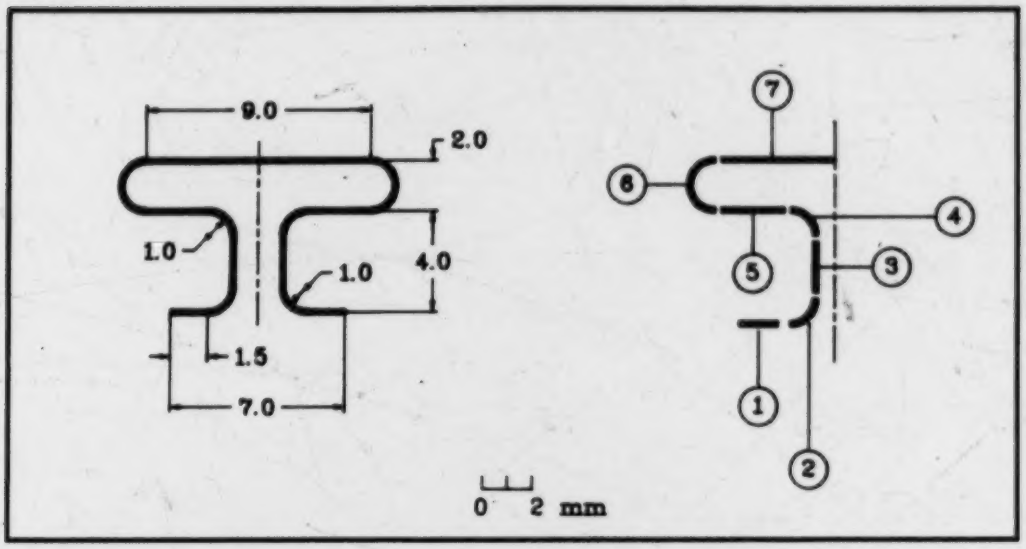


Figure 3.1: Orthodontic T-spring geometry

for the experimental test. The results obtained by the these techniques are listed in Appendix D in Tables D-1 and D-2.

The same spring was analyzed using the segmental technique in which only half of the spring is considered due to the geometric and boundary symmetry. As shown in Figure 3.1(b), one half of the spring is divided into 7 different sections. The data entered for each section is listed in Table 3.1. The material of the spring was stainless steel with 0.254 $\times$ 0.559 $mm$ (0.010" $\times$ 0.020") rectangular cross section, and the Young's modulus value used was 177 $GPa$. These are the same cross section and modulus values used by Fuchshuber [20]. A total of 2000 segments were used in this

Table 3.1: T-Spring sections data

| Sec.# | #of Seg. | Length($mm$) | Angle($Deg$) | Rad.($mm$) |
|---|---|---|---|---|
| 1 | 100 | 1.50 | - | - |
| 2 | 300 | - | 90.0 | 1.00 |
| 3 | 150 | 2.00 | - | - |
| 4 | 300 | - | 90.0 | 1.00 |
| 5 | 200 | 2.50 | - | - |
| 6 | 600 | - | 180.0 | -1.00 |
| 7 | 350 | 4.50 | - | - |

case, distributed over the different sections as shown in Table 3.1. The boundary conditions in this case are

- First Node :

$$X_o = 0\ ,\quad Y_o = 0\ ,\quad \gamma_o = 0\ ,\quad M_o = unknown\ ,\quad T_o = unknown\ ,\quad V_o = 0$$

- Last Node :

$$X_f = 3.5 + \frac{Activation}{2}\ ,\qquad \gamma_f = 0$$

The program of the segmental shooting technique took about 1 minute to perform the analysis for each activation value on an IBM 386/387 personal computer . This was the time which the solver required to reach the specified tolerance value of $1 \times 10^{-12}$, by going through 7 iteration loops. The computation time will, however, vary depending on the initial values of the unknowns as well as on the specified tolerance value of the solver.

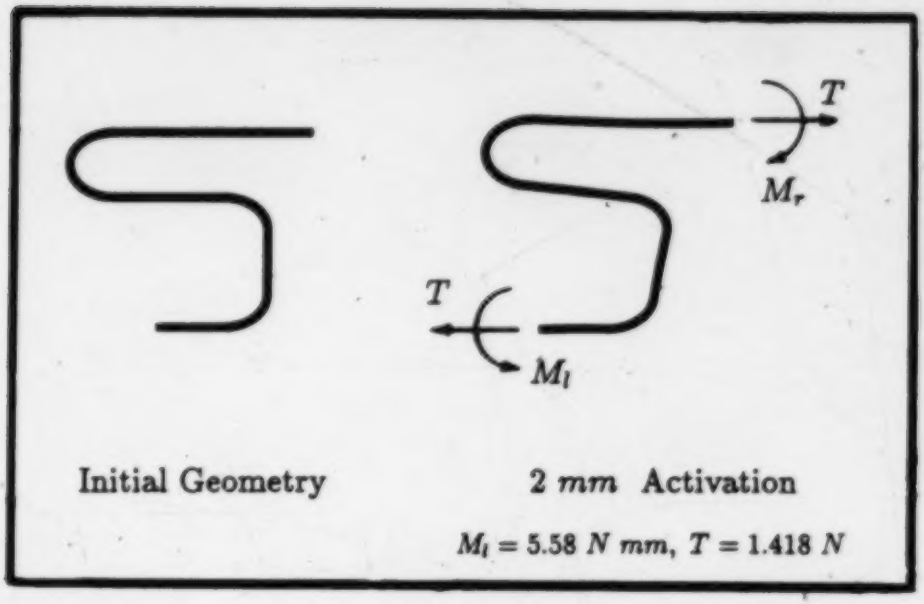


Figure 3.2: T-Spring initial and deformed shape (segmental technique output)

The forces and moments generated by the deformation of the spring were determined for a $0 - 2\ mm$ range of activations with increments of $0.25\ mm$. These values are tabulated in Appendix D (Table D-3), while the geometrical output of the program for the case of $2\ mm$ activation is shown in Figure 3.2. For this activation, the values of the moment, $M_l$, and force, $T$, at the first node, were found to be $5.587\ N\ mm$ and $1.418\ N$ respectively, while the corresponding values at the last node, $M_r$ and $T$, are $3.236\ N\ mm$ and $1.429\ N$. The $Y$ position of the last node was found to be $6.2\ mm$. If equilibrium is checked using the above values, then it can be shown that there is $0.011\ N$ (0.7%) out of balance in the forces, and $0.044\ N\ mm$ (0.7%) out of balance in the moments. These out of balance values are due to the linear approximation of the segment deformation which can be reduced by increasing the number of segments.

In order to compare the different methods of solution, the values of the moment

obtained by the 5 different techniques were plotted as shown in Figure 3.3, while the plot of the different tension or axial force values is shown in Figure 3.4. Looking at these two figures one can deduce that the segmental technique output is very close to the solution obtained by the nonlinear finite element analysis done by Fuchshuber [20], which in turn is close to his experimental results (10% maximum error). On the other hand, the discrepancy in the results obtained by Koenig et al. can be attributed to differences in the wire cross sections as well as the heat treatment and the alloying materials of the stainless steel wire. These later variations have an effect on the Young's modulus of the wire material.

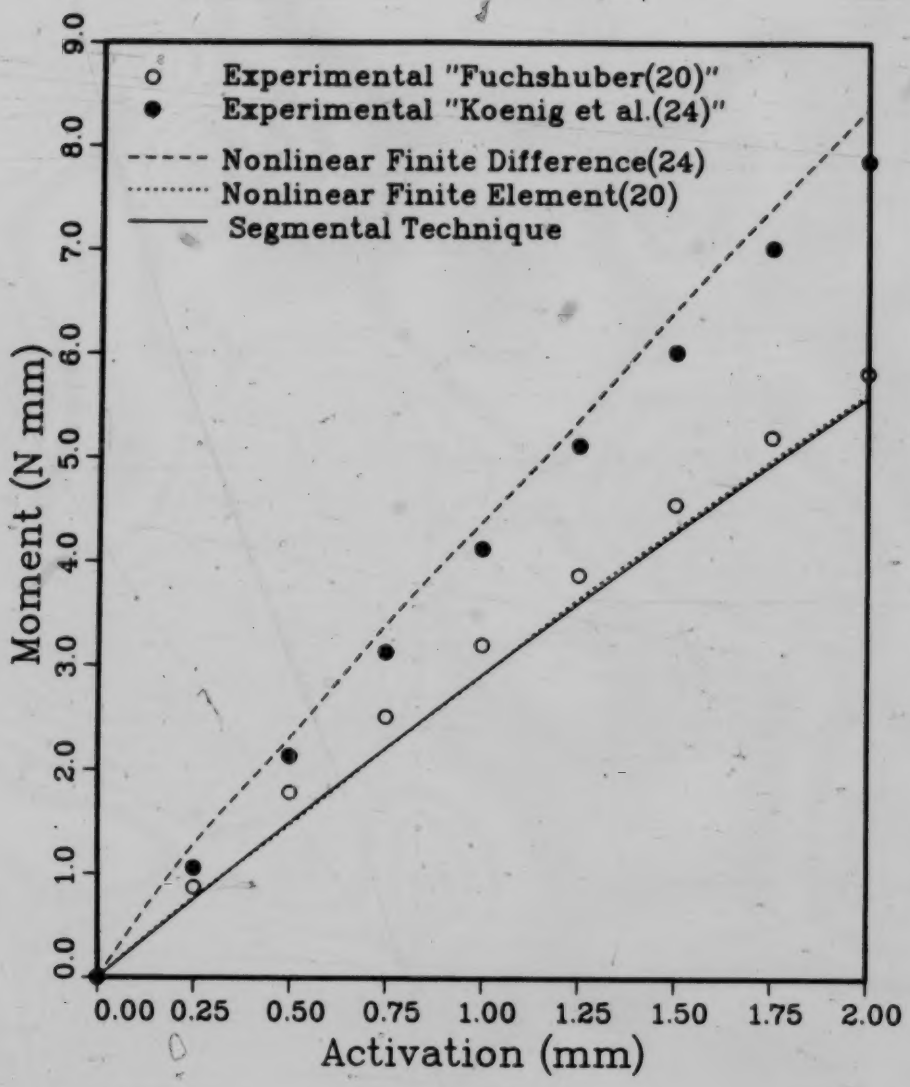


Figure 3.3: Comparison of numerical and experimental results of T-loop moment

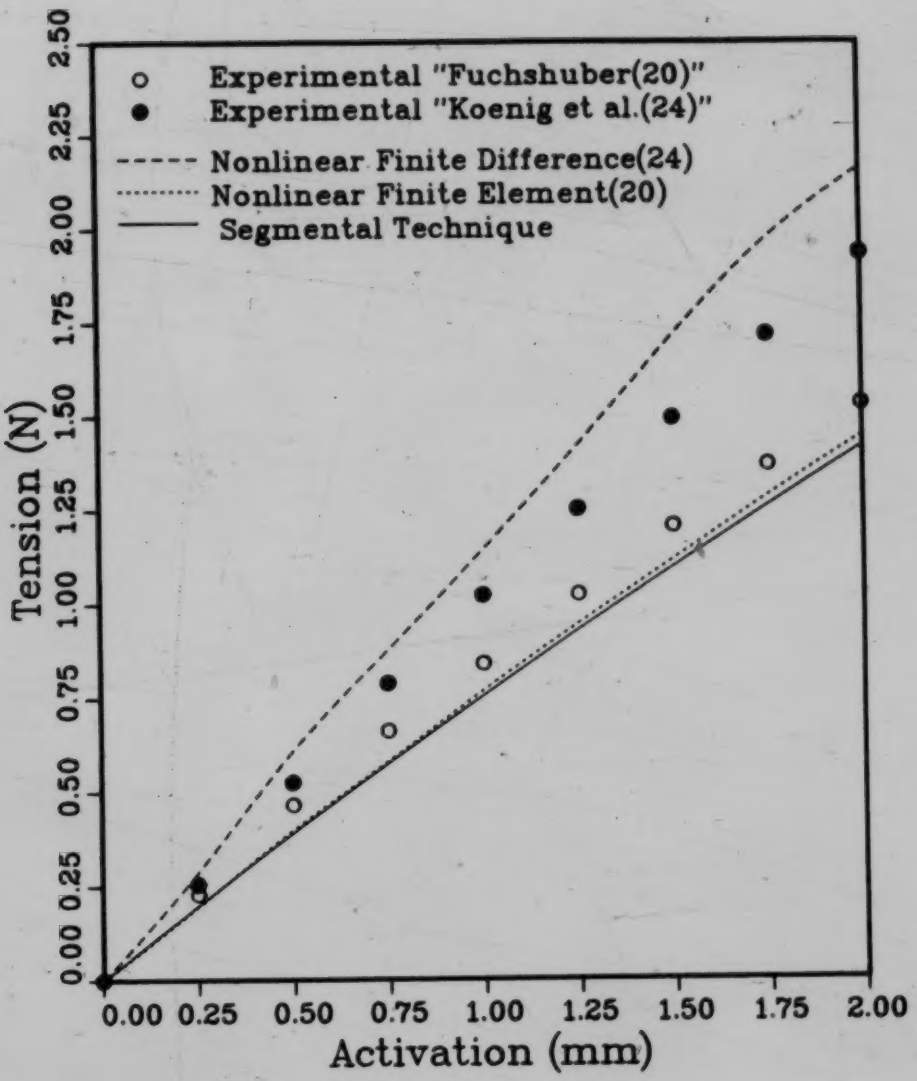
Experimental "Fuchshuber(20)"
Experimental "Koenig et al.(24)"
Nonlinear Finite Difference(24)
Nonlinear Finite Element(20)
Segmental Technique
Tension (N)
0.00 0.25 0.50 0.75 1.00 1.25 1.50 1.75 2.00 2.25 2.50
Activation (mm)
0.00 0.25 0.50 0.75 1.00 1.25 1.50 1.75 2.00

Figure 3.4: Comparison of numerical and experimental results of T-loop force

Figure 3.5: Pre-activated T-spring

## 3.2 Pre-Activated T-Spring Comparative Study

The pre-activated T-spring shown in Figure 3.5 was analyzed both experimentally using the force analysis apparatus described below and numerically using the segmental shooting technique. This spring design was chosen to be tested because there has not been any earlier attempts to numerically analyze the full asymmetric spring. Fuchshuber [20] analyzed a symmetric pre-activated T-spring using nonlinear finite element analysis, but due to large deformation in this case, the loads had to be applied in 160 increments which caused the computation time to increase drastically ($2\frac{1}{4}$ hours on the AMDAHL main frame computer). Finite difference techniques would suffer from the same limitations. This is not the case for the segmental technique, as the nonlinear or large deformation relations are incorporated in the development of the technique. This allows the solver to shoot for the final deformed shape in one step without going through several steps of linear deflections. Furthermore, this comparative study was done in order to check the results of the

experimental parametric studies [20] that were performed earlier on the pre-activated T-spring.

### 3.2.1 Experimental Testing of Pre-activated T-Spring

The force/moment measurement apparatus used to experimentally test the pre-activated T-spring was developed through different design stages at the Department of Mechanical Engineering, University of Alberta, and a detailed description of the apparatus and its specification is given in Faulkner et al.[13] and Fuchshuber [20]. The design of this apparatus employed a cross resolver attached to six pairs of binocular beams by a fine braided wire as shown in Figure 3.6 [20]. Strain gauges are mounted on the thin sections created by the binocular cut. Consequently, the strain gauges will undergo high strains, while the overall beam deflections are relatively low. The system is designed in such a way that the forces and moments are measured at one end of the spring, which is mounted to the cross resolver, while the activation or the deformation of the spring is done by mounting the other end to a movable stage which is positioned by means of 3 fine set screws. These screws allow the stage to be displaced in the X, Y, and Z directions. The resulting displacements are measured using 3 Mitutoyo digital micrometers each with 0.01 *mm* resolution. The total assembly of the device is shown in Figure 3.7.

The strain gauges load cells are connected to a Vishay/Ellis 20 Indicator/Scanner, which translate the electrical output of the strain gauges to the corresponding strain values . These values are transferred to an interactive program in an IBM PC via a data acquisition system. Also, the output of the digital micrometers is fed to the program through a multiplexer. This program, which contains the calibration data of the apparatus, will compute the moment and force values at the spring end that

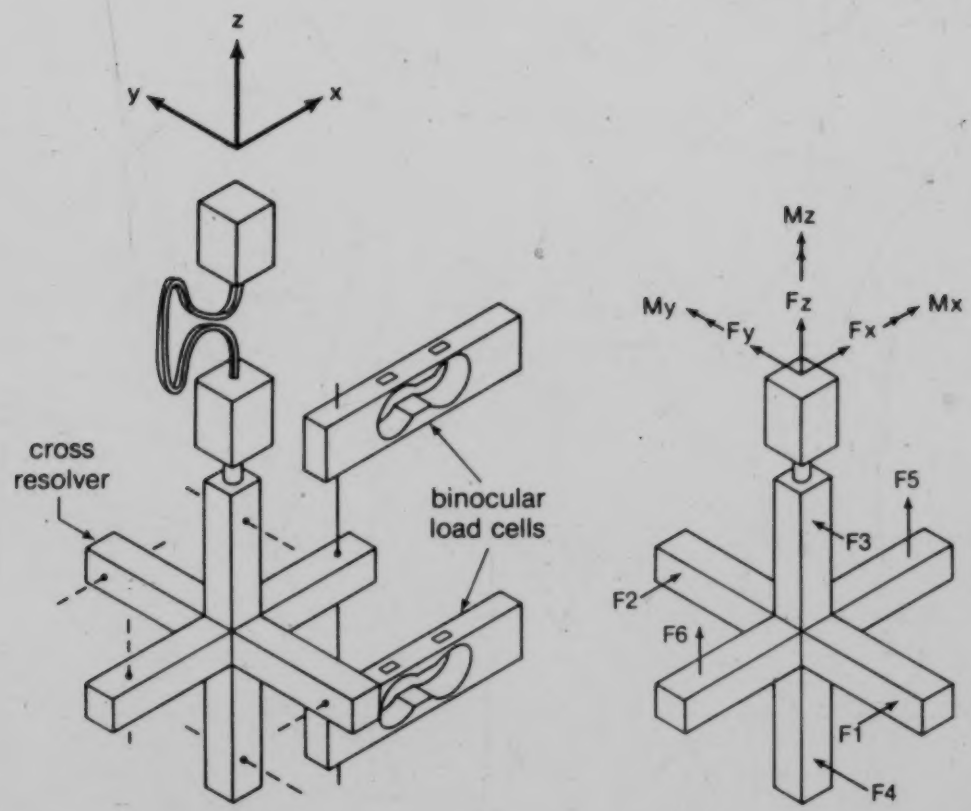


Figure 3.6: Force/displacement measurement system schematic

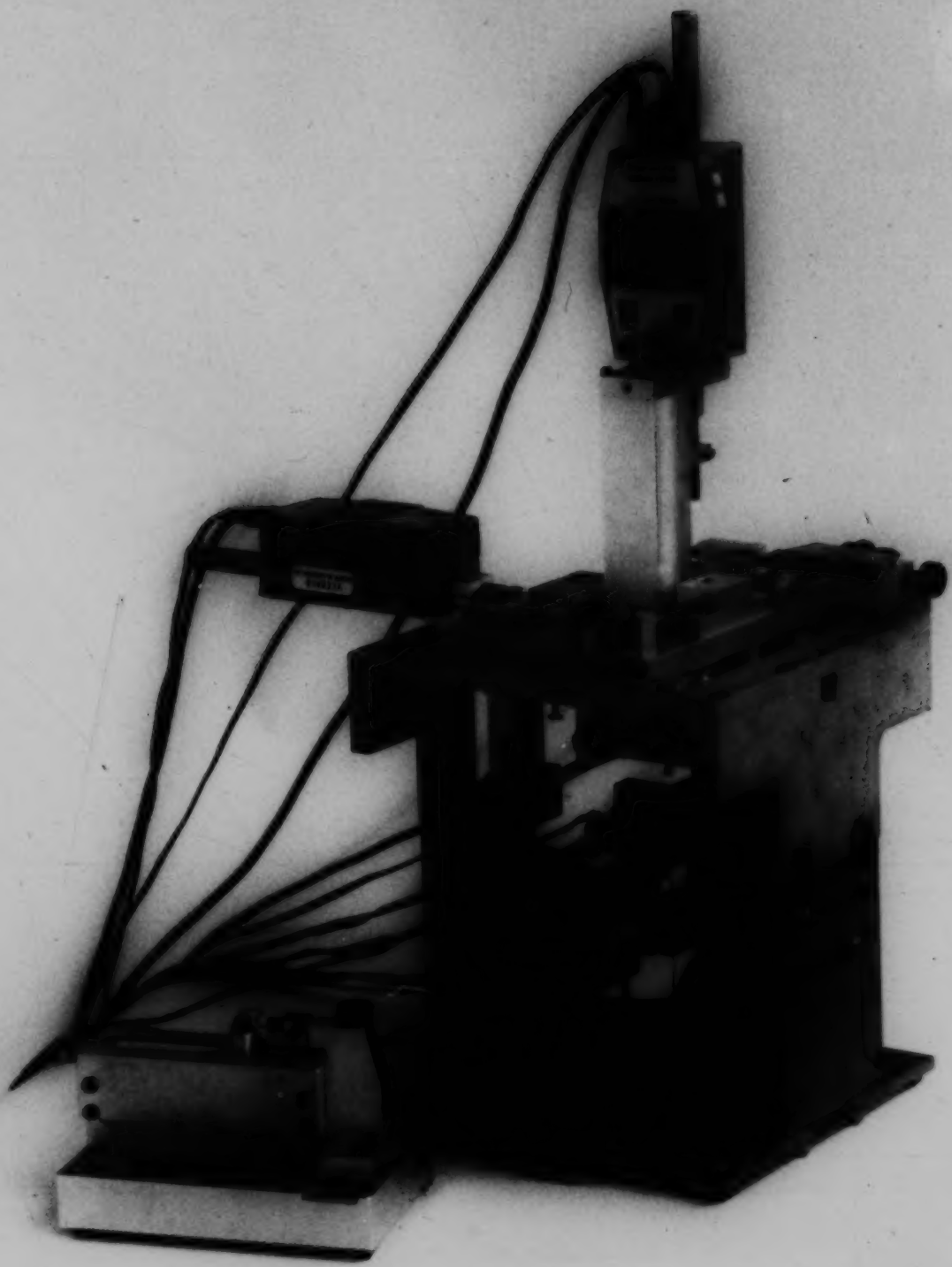

Figure 3.7: Force/moment measurement apparatus

caused the measured strains in the different binocular beams.

The apparatus can measure forces up to 5 $N$ with an accuracy of 3.6%, and moments up to 40 $N\ mm$ with an accuracy of 4.5%. The resolutions in the $z$ and $x$ directions are 0.003 $N$ for forces and 0.06 $Nmm$ for the moments, while in the $y$ direction the corresponding resolutions are 0.005 $N$ and 0.1 $Nmm$ [20].

The pre-activated T-spring shown in Figure 3.5, which was bent from TMA wire with $0.432 \times 0.635\ mm$ ($0.017" \times 0.025"$) cross section, was tested using the apparatus described above. Due to the fact that there is certain degree of non-symmetry in the spring geometry, it was expected that the moment values will be slightly different at the two ends of the spring. Therefore, the spring was tested with one orientation, reversed and tested again. This was done as the apparatus can only measure the values of moments and forces at the end connected to the cross resolver.

The test was done as follows. First, the spring was mounted to orthodontic brackets which are attached to small blocks. This makes it easier to mount the spring to the measuring apparatus. Then the device shown in bottom left of Figure 3.7 is used to determine the neutral position of the pre-activated spring. This is the position where the ends of the spring have zero slope and the axial force or tension is zero. It is from this position the activation of the spring is measured (the geometries of the spring at the neutral position and at 3 mm activation are shown in Figure 3.9). The horizontal distance between the ends of the spring at the neutral position was measured and found to be 23.25 $mm$. Then, the spring with the blocks was mounted on the apparatus and the values of moments and forces were determined for 5 different activations ($0 - 5\ mm$ i.e. until the inter-bracket distance reached 28.25 $mm$). The same process was repeated for the reversed orientation of the spring. For each orientation the test was repeated 7 times, and the average values of the different test results are listed in Appendix D Table D-4.

### 3.2.2 Young's Modulus Determination

One of the parameters needed in the analysis of elastic deformations is the Young's modulus, since using an incorrect value for it results in significant errors in the results obtained by the numerical techniques. While there are tabulated values of Young's modulus for the different materials, in the case of orthodontic wires, values measured were found to be up to 20% lower than the tabulated values [25]. This is due to the method of manufacturing these wires, in which they undergo severe cold drawing processes. Consequently, tension tests were performed on the different orthodontic wires materials (stainless steel and titanium molybdenum alloy, TMA) and cross sections used in this study, so accurate values of Young's modulus could be determined. This allowed a better comparison between the experimental and numerical results. These tests were done using an Instron Universal Testing machine along with MTS extensometer with 25.4 $mm$ (1") gauge-length.

The Young's modulus values obtained from the tension tests for stainless steel and TMA different wire cross sections are listed in Appendix D Table D-6. The average value for the stainless steel was found to be 174.4 $GPa$ with a standard deviation of $\pm 3.39$ $GPa$, while for the TMA, the average value is $71.7 \pm 2.92$ $GPa$. These values will be used in the different parametric studies discussed later.

For the pre-activated T-spring tested, the actual Young's modulus of the wire was found to be 73.9 $GPa$. This value will be used in the segmental technique analysis of the spring.

### 3.2.3 Numerical Analysis of Pre-activated T-Spring

The spring shown in Figure 3.8(a) was analyzed using the segmental technique. As mentioned earlier, there is a slight non-symmetry in the spring, therefore, the full spring geometry was considered in the analysis. This was done as follows,

1. The spring was divided into 17 different sections as shown in Figure 3.8(b).

2. The following parameters were entered

$$E = 73.9\ GPa \quad , \quad I = 0.00426\ mm^4$$

$$Number\ of\ sections = 17\ ,\ Total\ number\ of\ segments = 4000$$

3. The data for each section was entered as listed in Table 3.2.

4. In the case of pre-activated springs, the activation is measured form the neutral position, which means that this position has to be determined first by the program. This was done by specifying the following boundary conditions,

   - First Node:

$$X_o = 0\ ,\ Y_o = 0\ ,\ \gamma_o = 0\ ,\ T_o = 0\ ,\ M_o = unknown\ ,\ V_o = unknown$$

   - Last Node:

$$Y_f = 0 \quad , \quad \gamma_f = 0$$

   and it was determined that $X_f = 23.7676\ mm$. This can be compared to 23.25 $mm$ measured experimentally.

5. The moments and forces associated with the different activations were determined by specifying the following boundary values,

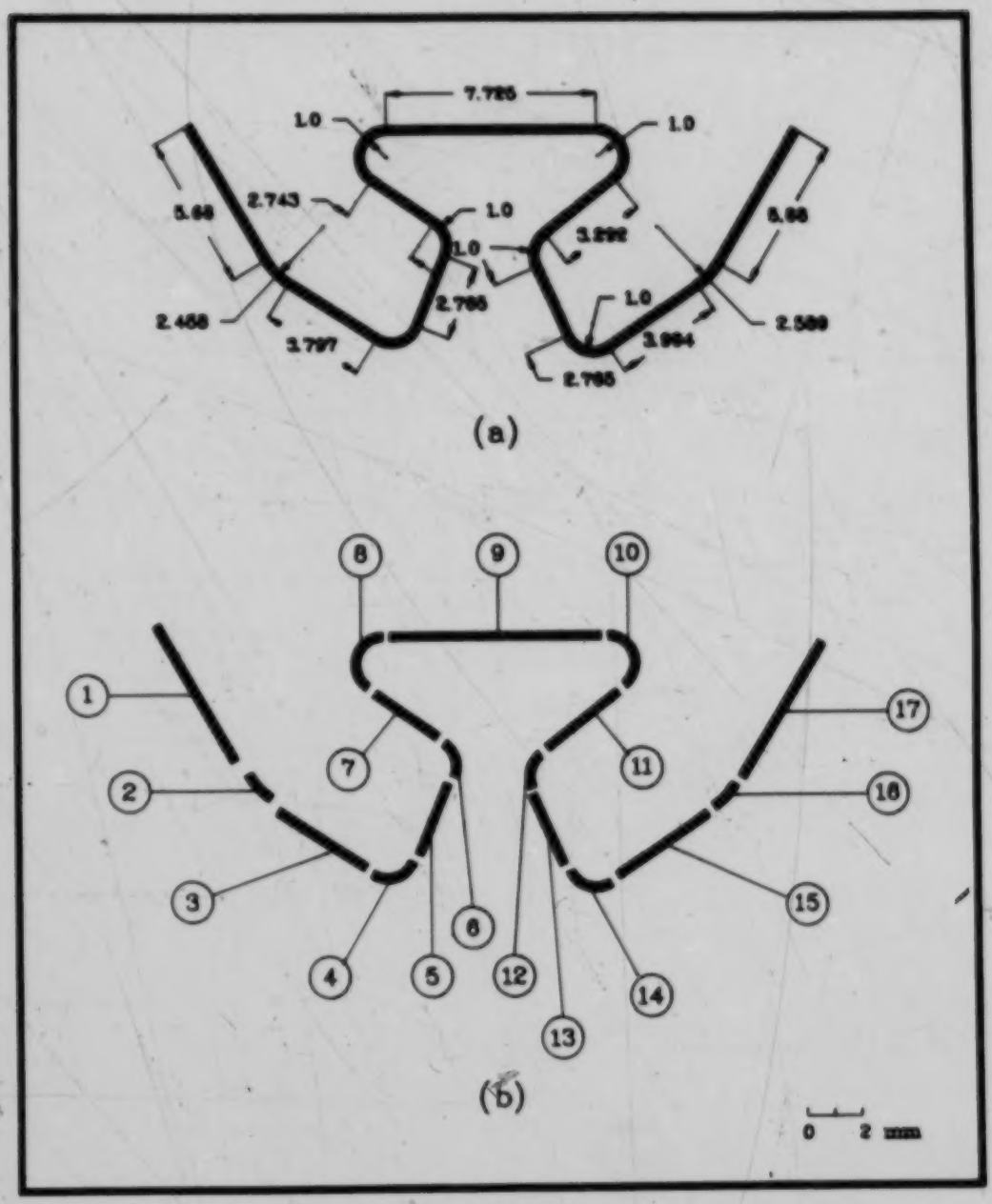


Figure 3.8: Pre-activated T-spring sectioning

Table 3.2: Pre-activated T-spring sections data

| Sec.# | #of Seg. | Length($mm$) | Angle($Deg$) | Rad.($mm$) |
|---|---|---|---|---|
| 1 | 250 | 5.680 | - | - |
| 2 | 100 | - | 27.50 | 2.458 |
| 3 | 200 | 3.797 | - | - |
| 4 | 300 | - | 100.00 | 1.000 |
| 5 | 150 | 2.765 | - | - |
| 6 | 250 | - | 78.00 | 1.000 |
| 7 | 150 | 2.743 | - | - |
| 8 | 450 | - | 144.50 | -1.000 |
| 9 | 300 | 7.725 | - | - |
| 10 | 450 | - | 142.00 | -1.000 |
| 11 | 150 | 3.292 | - | - |
| 12 | 250 | - | 76.00 | 1.000 |
| 13 | 150 | 2.765 | - | - |
| 14 | 300 | - | 100.00 | 1.000 |
| 15 | 200 | 3.994 | - | - |
| 16 | 100 | - | 25.00 | 2.589 |
| 17 | 250 | 5.680 | - | - |

- First Node:

$$X_o = 0\ ,\ Y_o = 0\ ,\ \gamma_o = 0\ ,\ T_o = unknown\ ,\ M_o = unknown\ ,\ V_o = unknown$$

- Last Node:

$$Y_f = 0\ \ ,\ \ \gamma_f = 0\ \ ,\ \ X_f = 23.7676 + activation$$

It took the program about 5 minutes on an IBM 386/387 PC to determine the forces and moments for each activation value. The analysis time in this case is about 5 times the time required for the case of the simple T-spring discussed earlier. This is due to several factors. One factor for the increased computation time is total number of segments used, 4000 in this case compared to 2000 in the case of the symmetric T-spring. Another factor is the number of unknowns which is 3 in the case of the asymmetric spring, while there were only two unknowns is the case of the symmetric spring. A higher number of unknowns implies that more partial derivatives need to be computed within each iteration loop. Also, it should be noted that in the case of 3 unknowns, the computation time is highly influenced by the choice of the relaxation factors of the numerical solver, as well as the selected initial values of the unknowns.

The values of the moments and forces determined by the segmental technique are listed in Appendix D, Table D-5, while the geometrical output of the neutral position and 3 *mm* activation is shown in Figure 3.9. The force out of balance in this case was found to be 0.032 *N* (1.8%), while the moment out of balance value is 0.106 *N mm* (0.6%).

The experimental and numerical results of the pre-activated T-spring are plotted in Figures 3.10, 3.11, and 3.12. The error bars in the figures represent $\pm 2s$, where $s$ is the standard deviation of the experimentally determined force or moment of each activation. The maximum error between the average experimental value and

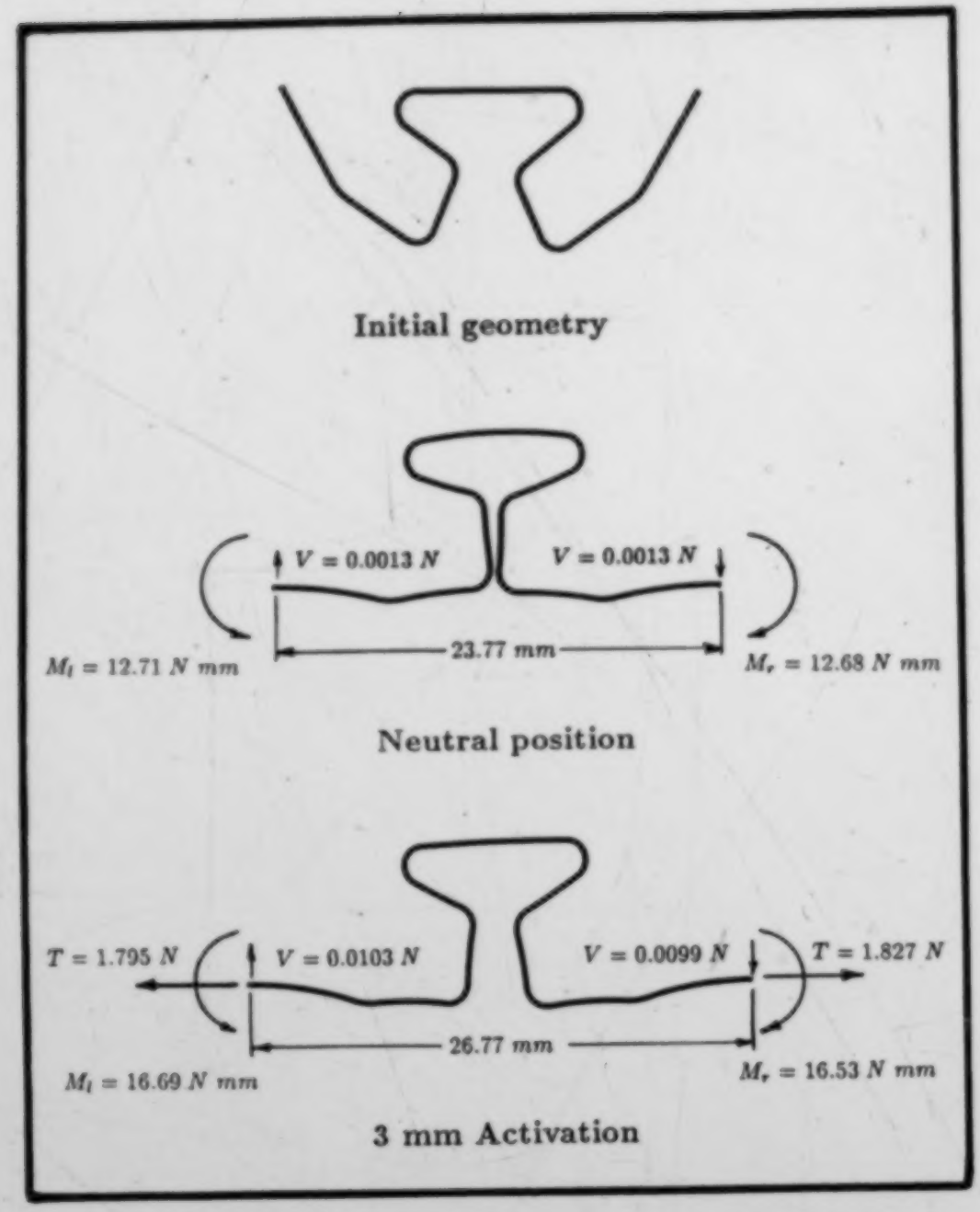


Figure 3.9: Pre-activated T-spring deformed geometries

(*segmental technique output*)

the numerical result for the left moment was 1.9% at the neutral position (zero activation), while maximum error in right moment value was 6.3% at 5 *mm* activation. For the tension, the maximum error was found to be 10.5% at 5 *mm* activation. The numerically determined shear values increased with the increase in the spring activation, with the shear value being 0.0013 *N* at the neutral position and 0.0165 *N* at 5 *mm* activation. Such small force values are in the order of the measurement device force resolution, therefore, the experimental results of the shear showed poor repeatability. Consequently, a comparison between the experimental and numerical results of the shear force was not done.

A comparison of the figures indicates that the segmental shooting technique results show relatively good agreement with the experimental tests, especially in view of the errors inherent in the experimental apparatus as well as the uncertainty of Young's modulus and second moment of area $I$. The effect of uncertainty in these values can be shown by the following error analysis:

Assume the force is given by

$$F = a\,EI \quad \text{where } a \text{ is a constant .}$$

For a rectangular cross section $I = bh^3/12$, with $b$ and $h$ being the width and height of the wire cross section respectively. This yields

$$F = a\,E\,\frac{bh^3}{12} .$$

The error analysis of the above equation is given by

$$\left(\frac{\varepsilon_F}{F}\right)^2 = \left(\frac{\varepsilon_E}{E}\right)^2 + \left(\frac{\varepsilon_b}{b}\right)^2 + 9\left(\frac{\varepsilon_h}{h}\right)^2 .$$

For the pre-activated T-spring tested the expected error values in the wire cross section height and width are 3% and 2% respectively, while the estimated error in the

Young's modulus value is about 4%. Substituting these values in the above equation results in a probable error in the force values of about 10%. A similar error value would be expected for the moment values.

Since the segmental shooting technique output has shown very good agreement with both experimental results and other analytical and numerical solutions, it will be utilized in parametric studies of several orthodontic springs designs. The fact that pre-activated springs can be analyzed with relative ease allows more variations to be considered than if experimental measurements had to be done for each case.

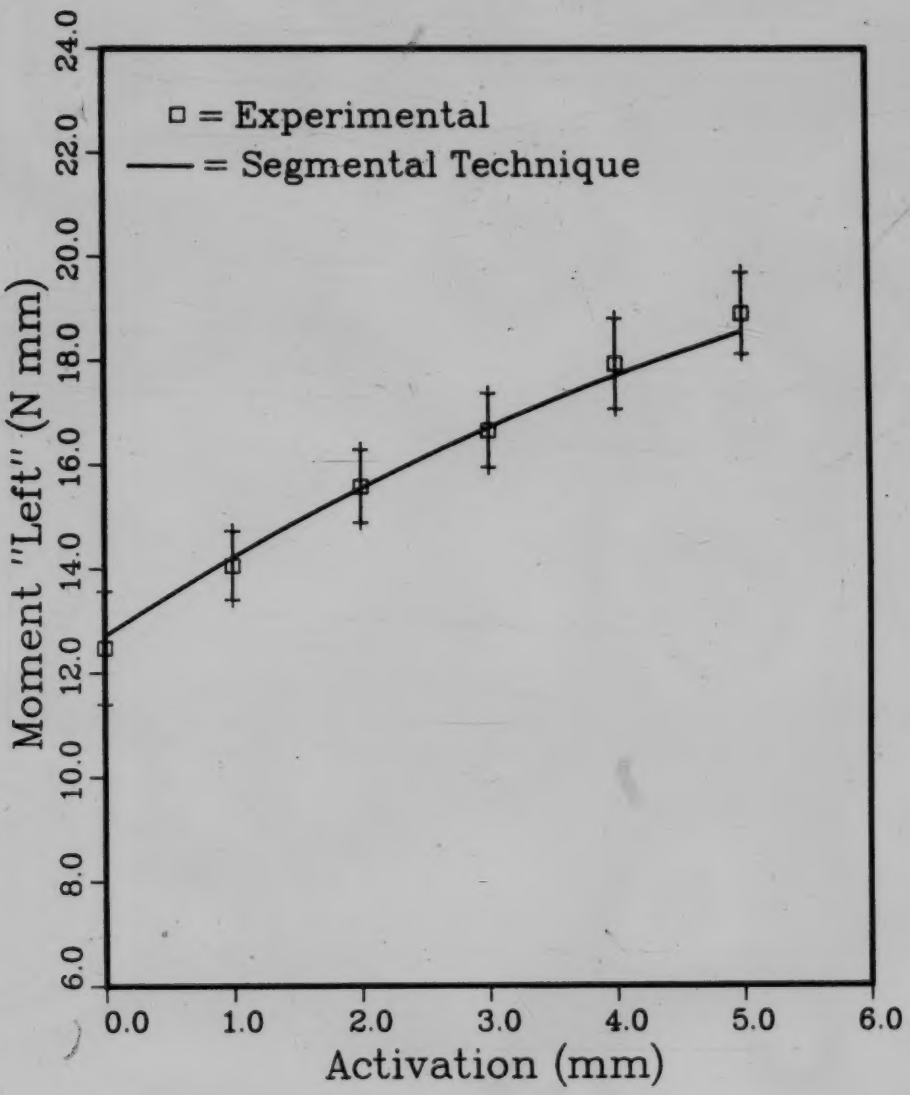


Figure 3.10: Pre-activated T-spring left moment (experimental and numerical)

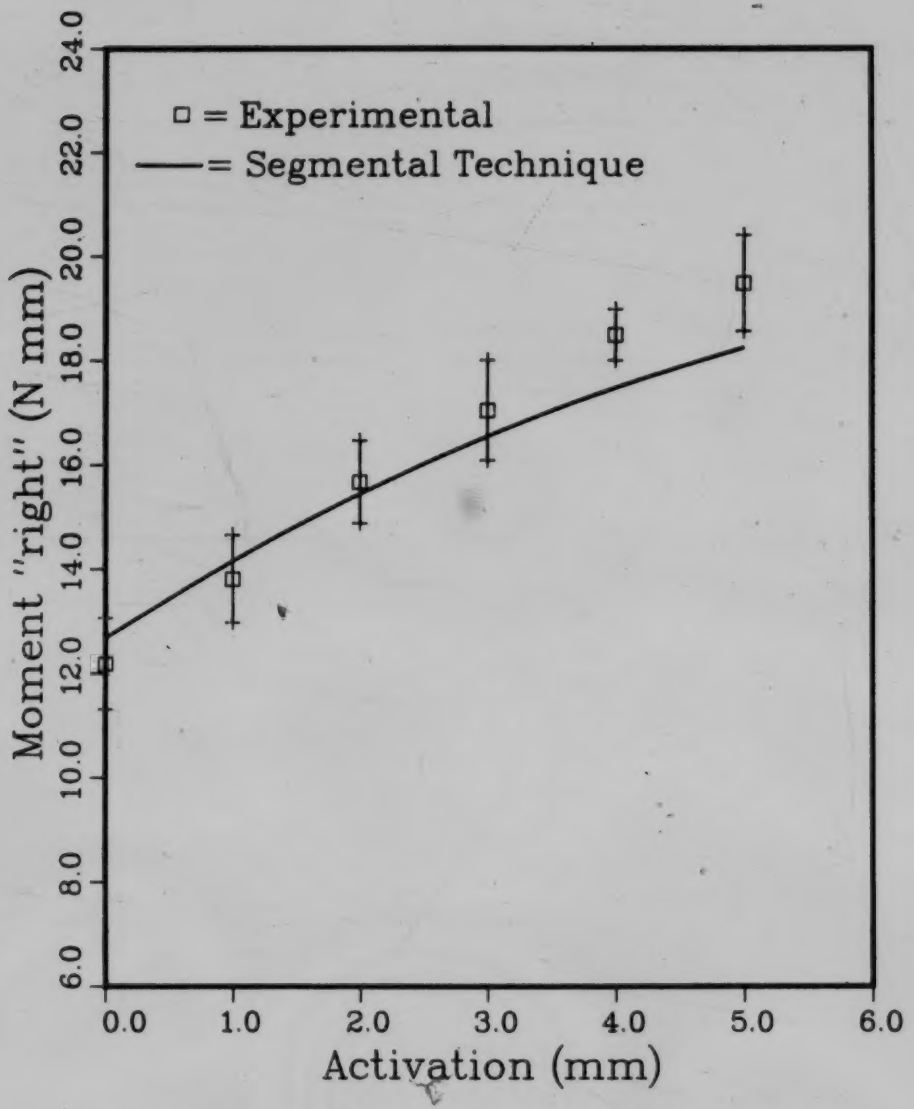


Figure 3.11: Pre-activated T-spring right moment (experimental and numerical)

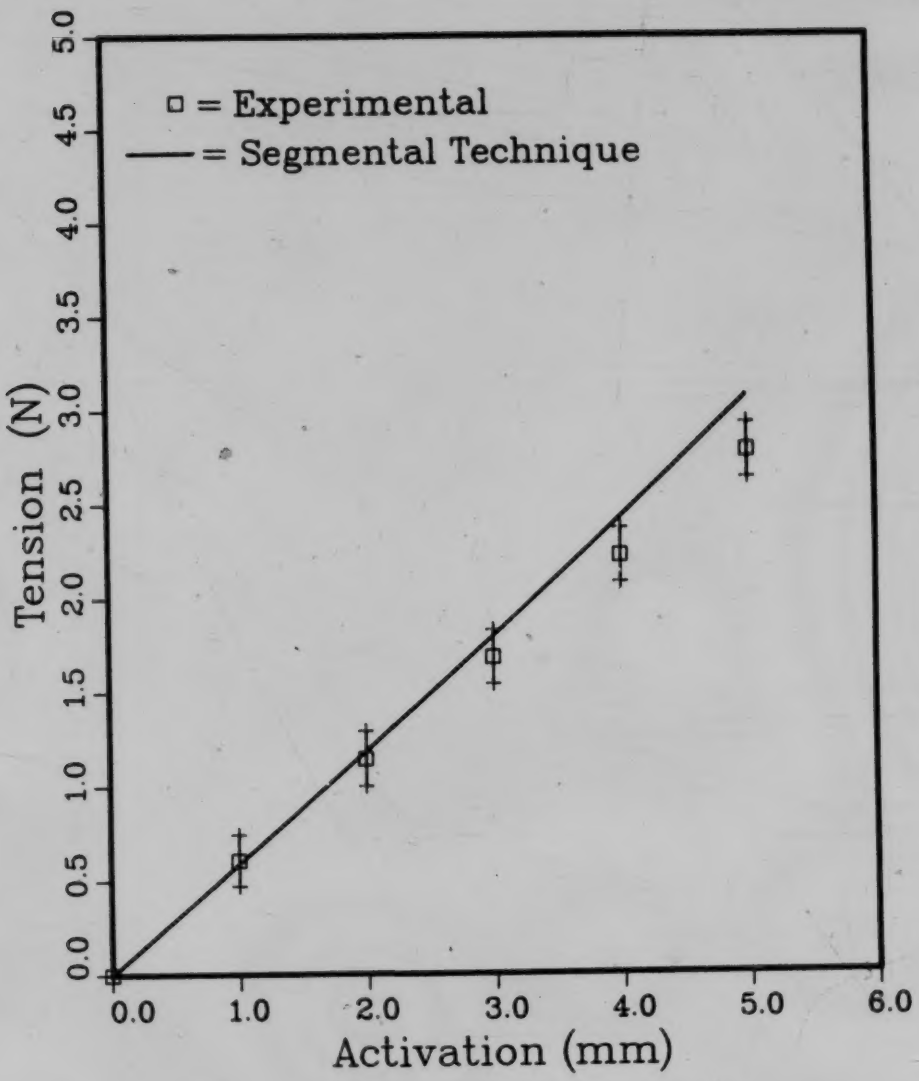


Figure 3.12: Pre-activated T-spring tension (experimental and numerical)

# Chapter 4

# Parametric Studies

In this chapter the results of the different parametric studies performed on the pre-activated T-spring as well as the vertical loop springs will be presented. These studies were performed using the segmental shooting technique.

## 4.1 Pre-Activated T-Spring Parametric Studies

The geometry and dimensions of a typical pre-activated symmetric T-spring are shown in Figure 4.1. As shown in the figure, the spring can be broken down into nine different sections, five initially straight sections with the lengths $a$, $b$, $c$, $d$, $l$, and four initially curved sections with radii of curvature $R$ and arc angles $\Theta$. Also, indicated are typical values for these variables and this spring will serve as the base case for all pre-activated T-spring parametric studies. The wire material of this type of springs is, usually, TMA. TMA wire is available in different cross sections such as 0.018" $\times$ 0.018" (0.457 $\times$ 0.457 $mm$), 0.016" $\times$ 0.022" (0.406 $\times$ 0.559 $mm$), and 0.017" $\times$ 0.025" (0.432 $\times$ 0.635 $mm$), with the last used in the parametric studies of

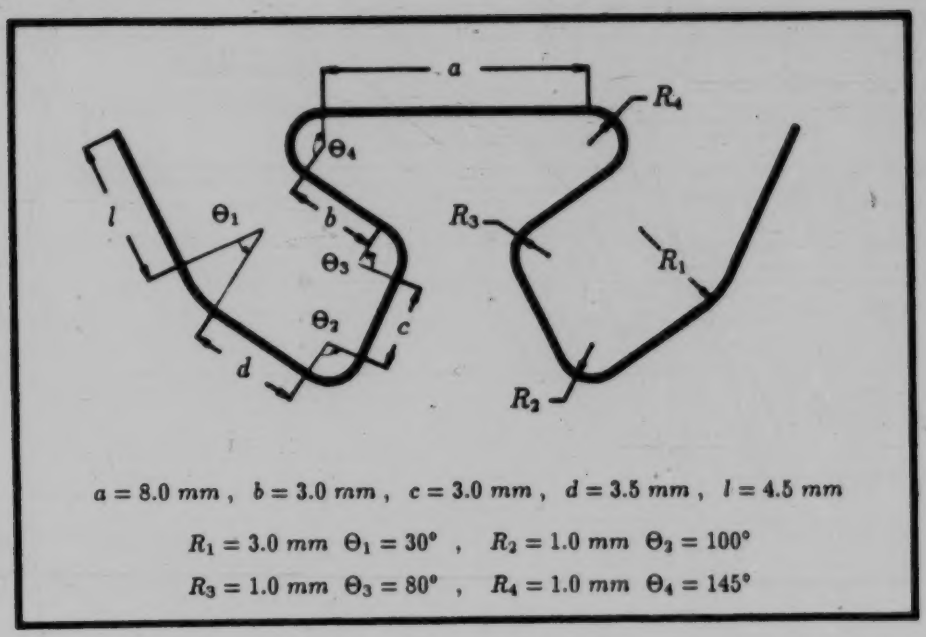
a
$R_4$
$\Theta_4$
l
$\Theta_1$
b
$R_3$
$R_1$
$\Theta_3$
$\Theta_2$
c
d
$R_2$
$a = 8.0\ mm$ , $b = 3.0\ mm$ , $c = 3.0\ mm$ , $d = 3.5\ mm$ , $l = 4.5\ mm$
$R_1 = 3.0\ mm$ $\Theta_1 = 30°$ , $R_2 = 1.0\ mm$ $\Theta_2 = 100°$
$R_3 = 1.0\ mm$ $\Theta_3 = 80°$ , $R_4 = 1.0\ mm$ $\Theta_4 = 145°$

Figure 4.1: Typical pre-activated T-spring geometry

the pre-activated T-Spring. The cross section dimensions of the orthodontic wires will be given in inches throughout this chapter as the wire available commercially is usually specified by inches. The Young's modulus value of the standard TMA wire is 73 $GPa$, while the yield strength was assumed to be 1240 $MPa$ [26]. This yield value was compared with the values of the stresses generated by the spring deformation to approximately determine the maximum activation of the spring beyond which it would yield. The stress values at the different points of the deformed spring were computed using a stress calculation routine incorporated into the segmental shooting technique program. The description of this routine as well as the assumptions involved in this stress analysis are given in Appendix E.

The values of moments and forces associated with the different horizontal activations of the above spring are listed in Table 4.1. In this table $I.B.D.$ stands for inter-bracket distance, which is the horizontal distance between the mid points of the

Table 4.1: Typical pre-activated T-spring moments and forces

| *ACT.(mm)* | *M (Nmm)* | *F (N)* | *I.B.D.(mm)* |
|---|---|---|---|
| 0.0 | 13.977 | 0.0 | 20.765 |
| 0.5 | 14.850 | 0.271 | 21.265 |
| 1.0 | 15.683 | 0.543 | 21.765 |
| 1.5 | 16.476 | 0.815 | 22.265 |
| 2.0 | 17.231 | 1.088 | 22.765 |
| 2.5 | 17.950 | 1.363 | 23.265 |
| 3.0 | 18.631 | 1.639 | 23.765 |
| 3.5 | 19.278 | 1.918 | 24.265 |
| 4.0 | 19.890 | 2.200 | 24.765 |
| 4.5 | 20.468 | 2.483 | 25.265 |
| 5.0 | 21.014 | 2.771 | 25.765 |
| 5.5 | * | * | 26.265 |

* *Spring Yielded*

two brackets where the ends of the spring are mounted. It is equal to the horizontal distance between the two ends of the spring after deformation. Note the non-zero value of the moment at zero activation. This is the moment required to deform the spring to the neutral position, where the ends of the spring have zero slope and the axial force is equal to zero, as previously mentioned. Also, it is noted in the table that the spring is expected to yield if the activation exceeds 5 *mm*. Yield of this spring design usually occurs at the bend with $R_2$ radius .

The moment to force ratio of this spring is plotted in Figure 4.2 as a function of activation . This curve shows that the moment to force ratio of pre-activated T-spring *decreases* as the activation of spring *increases*, and this is attributed to the fact that the spring activation is measured from the neutral position where the value of the

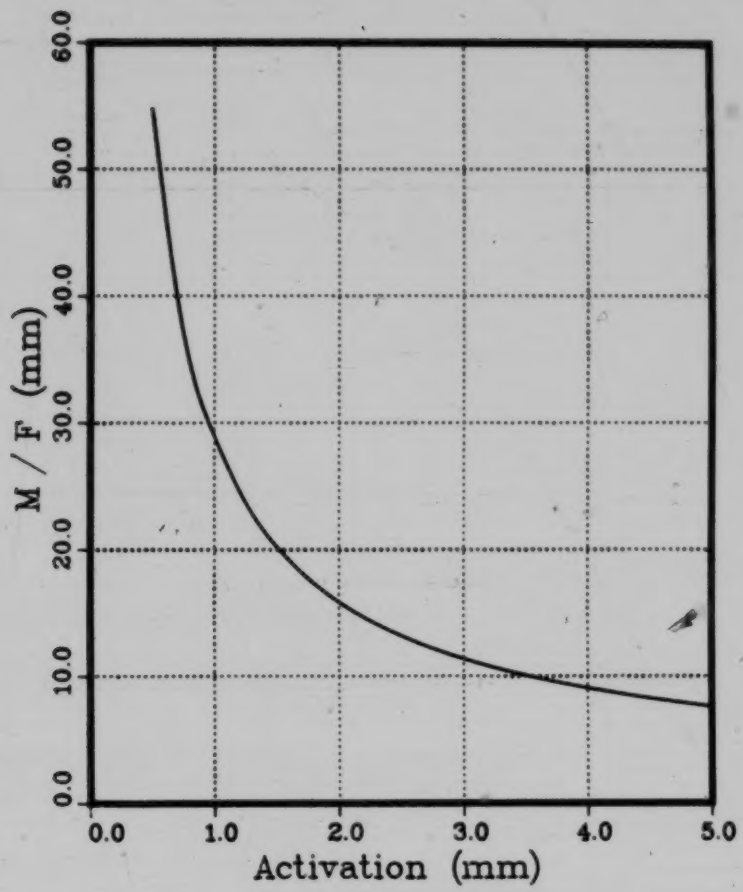


Figure 4.2: Typical pre-activated T-spring $M/F$ as a function of activation

force is equal to zero, which means that the value of $M/F$ for zero activation is equal to $\infty$. Moreover, as this spring design is pre-activated, the end points initially have 65° slope angles with the horizontal, requiring a large moment to be initially applied in order to deform the spring to the neutral position. The value of this moment is about 60% of the moment value when the spring is fully activated. Therefore, the rate of *increase* of the moment value with the *increase* in activation is much smaller than the rate of *increase* of the force value, as can be seen by looking at the data in Table 4.1, especially in 0 to 2 activation range. This explains why the $M/F$ curve is very steep in this range. Furthermore, this curve demonstrates that a 10 $mm$ moment to force ratio, required for the tooth translation without tipping as mentioned in Chapter 1, is achieved within the 3 to 5 $mm$ activation range. Consequently, the spring will be able to perform its function over a wide range of activations, reducing the need for frequent adjustments. However, one disadvantage of this design is that the width and height of the loop can cause some irritation to the soft tissue of patients. Therefore, several parametric studies were performed to study the effects of reducing the loop size on the mechanical characteristics of the spring. These studies will be presented in the following sections.

### 4.1.1 Length $a$ Parametric Study

One way of reducing the width of the loop is to *decrease* length $a$ of the spring (see Figure 4.1). This was investigated in two ways. The first *decreased* length $a$ from 8 $mm$ to 3.0 $mm$, in decrements of 1 $mm$, while keeping all the other dimensions the same. The second study considered a *decrease* in length $a$ with a corresponding *increase* in length $l$, such that the horizontal distance between the two ends of the spring at the neutral position was the same for each spring.

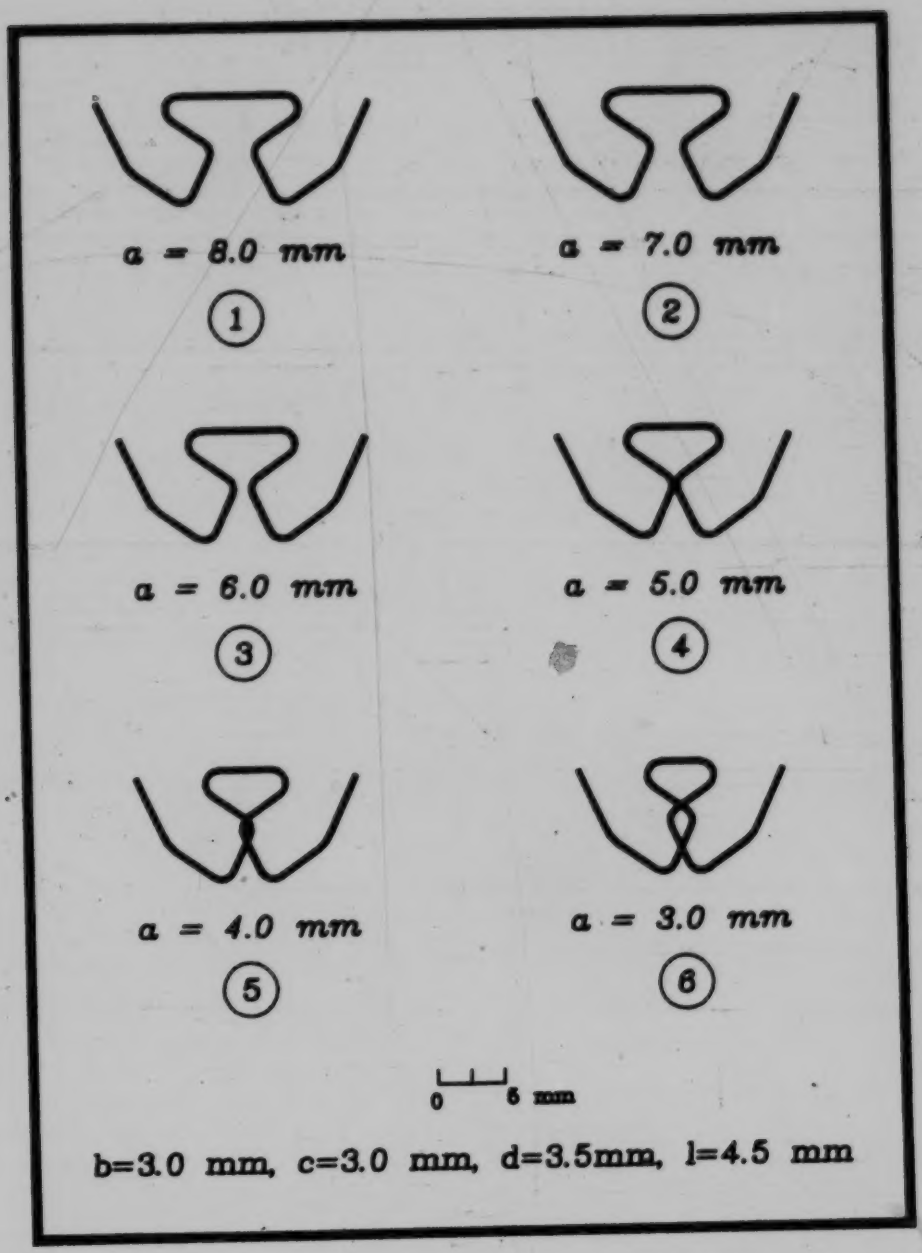


Figure 4.3: Pre-activated T-springs with different length $a$

Table 4.2: Moments and forces of pre-activated T-springs with different $a$ lengths ($0.017" \times 0.025"$ TMA wire)

| Spring | Length | Neutral Position | | 3 $mm$ Activation | | |
|---|---|---|---|---|---|---|
| # | $a$ ($mm$) | $M$ ($N$ $mm$) | $X$ ($mm$) | $M$ ($N$ $mm$) | $T$ ($N$) | $I.B.D.$($mm$) |
| 6 | 3.0 | 15.500 | 16.994 | 20.117 | 2.172 | 19.995 |
| 5 | 4.0 | 15.178 | 17.731 | 19.802 | 2.030 | 20.731 |
| 4 | 5.0 | 14.860 | 18.477 | 19.497 | 1.911 | 21.477 |
| 3 | 6.0 | 14.552 | 19.231 | 19.199 | 1.808 | 22.231 |
| 2 | 7.0 | 14.258 | 19.994 | 18.911 | 1.719 | 22.994 |
| 1 | 8.0 | 13.975 | 20.760 | 18.630 | 1.639 | 23.760 |

The different spring geometries of the first part of this parametric study are shown in Figure 4.3. The base case, spring # 1, has been analyzed in the preceding section and it will be considered the standard for this parametric study and for the subsequent parametric studies performed on the pre-activated T-spring. The values of the moments and forces, at the neutral position as well as 3 $mm$ activation, for the different springs are listed in Table 4.2. The horizontal distance between the two ends of the spring ($X$) is, also, given. This distance is the same as the inter-bracket distance, $I.B.D.$, for the activated spring.

The effects of reducing length $a$ on the moment, force, and moment to force ratio ($M/F$) are shown in Figures 4.4, 4.5, and 4.6 respectively. The values of the moments and forces obtained are plotted as a ratio of $M_o$ and $T_o$, which are the values of the moment and the force of the typical pre-activated T-spring (spring # 1).

The plots of $M/M_o$ and $T/T_o$ show that both the moment and the force values *increase* as length $a$ *decreases*, with the percentage *increase* in the moment less than

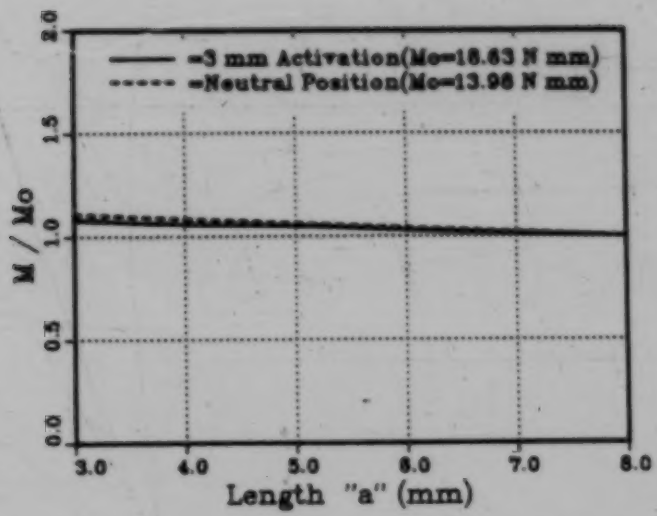


Figure 4.4: $M/M_o$ for pre-activated T-springs with different $a$ length ($0.017" \times 0.025"$ $TMA$ $wire$)

the percentage *increase* in the value of the force (note that the length $a$ *decreases* in the figure from right to left). Therefore, the moment to force ratio *decreases*, as shown in Figure 4.6, as length $a$ *decreases*. However, the moment to force ratio at 3 $mm$ activation of springs #3 and #4 ($a = 5.0\ mm$, $a = 4.0\ mm$) is still close to the desired 10 mm value required for tooth translation. In conclusion, reducing the size of the pre-activated T-spring loop by decreasing length $a$ from 8 to 3 $mm$ causes a small increase in the load/deflection rate of this spring, while the moment to force ratio is not significantly altered by this geometric modification.

The springs analyzed above do not have the same $I.B.D.$ for a given activation, and this makes it difficult to compare them for clinical purposes. Therefore, another investigation was performed in which length $a$ was *decreased* and length $l$ was *increased* (see Figure 4.1), so that all the springs would have the same horizontal distance at

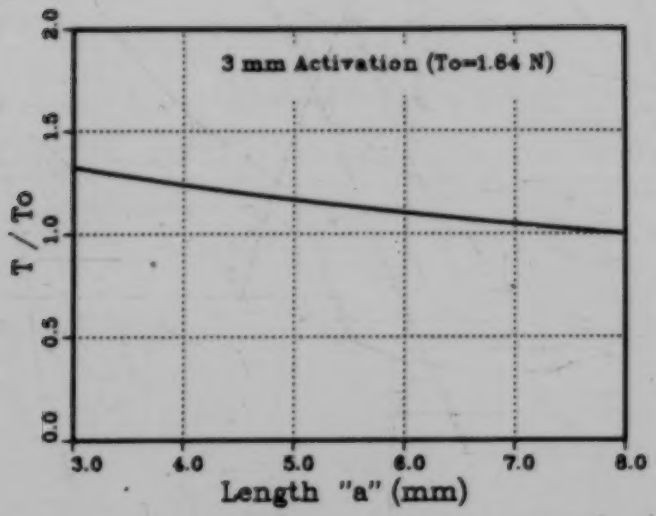


Figure 4.5: $T/T_o$ for pre-activated T-springs with different $a$ length ($0.017" \times 0.025"$ *TMA wire*)

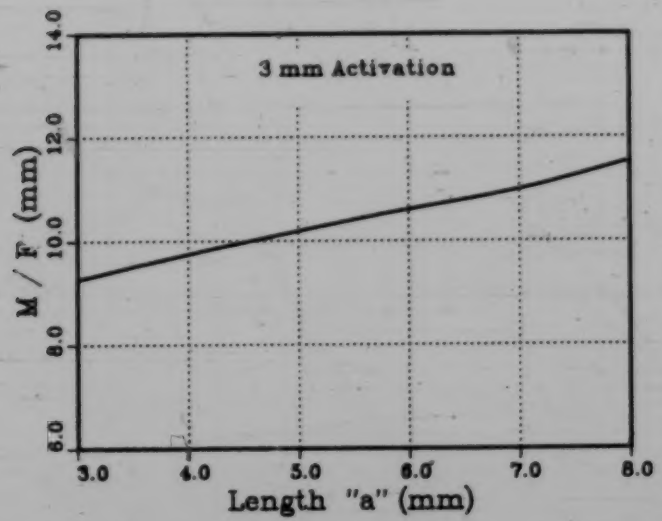


Figure 4.6: $M/F$ value for pre-activated T-springs with different $a$ Length ($0.017" \times 0.025"$ *TMA wire*)

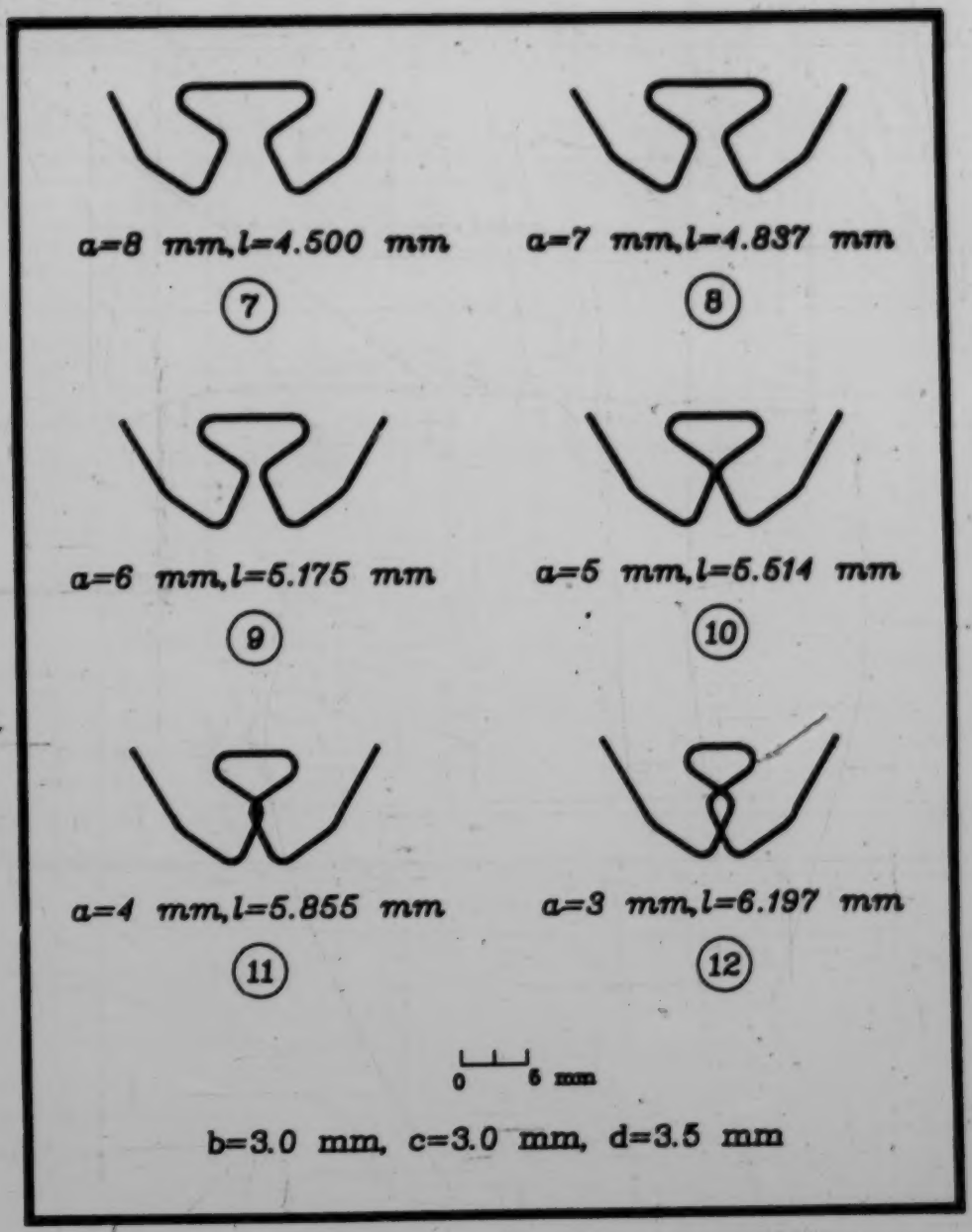


Figure 4.7: Pre-activated T-springs with different lengths $a$ and $l$

Table 4.3: Moments and forces of pre-activated T-springs with different $a$ and $l$ (0.017" × 0.025" TMA wire)

| spring | Length ($mm$) | | Neutral Position | | 24 $mm$ $I.B.D.$* | |
|---|---|---|---|---|---|---|
| # | $a$ | $l$ | $M$ ($N$ $mm$) | $X$ ($mm$) | $M$ ($N$ $mm$) | $T$ ($N$) |
| 12 | 3.0 | 6.20 | 14.435 | 20.762 | 17.729 | 2.447 |
| 11 | 4.0 | 5.86 | 14.342 | 20.762 | 18.040 | 2.257 |
| 10 | 5.0 | 5.51 | 14.250 | 20.762 | 18.308 | 2.101 |
| 9 | 6.0 | 5.18 | 14.158 | 20.762 | 18.543 | 1.972 |
| 8 | 7.0 | 4.84 | 14.066 | 20.762 | 18.749 | 1.826 |
| 7 | 8.0 | 4.50 | 13.976 | 20.762 | 18.938 | 1.770 |

* 3.238 $mm$ *Activation*

the neutral position. This in turn means that for a given spring activation the $I.B.D.$ will be the same for all the springs. This allows a more clinically useful comparison of the above springs. The geometries of these modified springs are shown in Figure 4.7, while the values of moments and forces for the neutral position and 24 $mm$ $I.B.D$ are listed in Table 4.3. Note that 24 $mm$ $I.B.D.$ corresponds to an activation of 3.238 $mm$.

Decreasing $a$ and increasing $l$ seems to have little effect on the moment value as shown in Figure 4.8. This is due to the fact that the possible *increase* in the moment value caused by the *decrease* in $a$ length, as was shown in previous study, is counter-balanced by a *decrease* in the moment required to deform the spring to the neutral position as a result of *increased* arms length ($l$). Therefore, the net moment value is relatively unaffected by the simultaneous *increase* in $a$ and *decrease* $l$. On the other hand, the values of the force *increased* as $a$ *decreased* (and $l$ *increased*). The rate of *increase* in the force value is close to the rate of *increase* caused by only

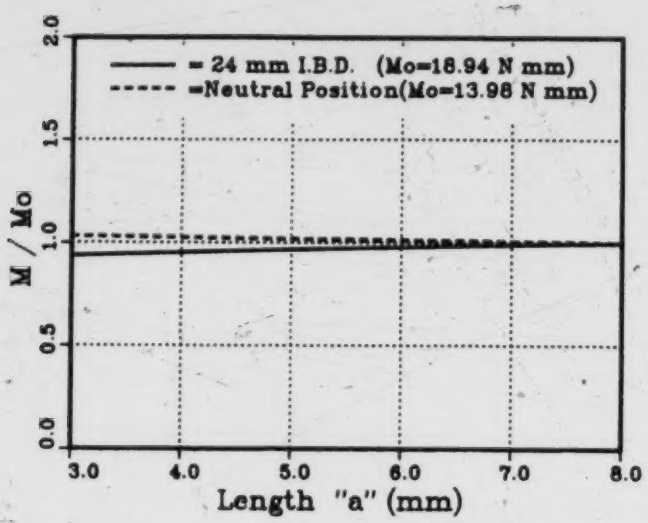


Figure 4.8: $M/M_o$ for pre-activated T-springs with different lengths $a$ and $l$ ($0.017" \times 0.025"$ *TMA wire*)

*decreasing* length $a$, which means that the *increase* in length $l$ does not have an effect on the force value . As a result of the *increase* in the force value, the moment to force ratio *decreases* with the *decrease* in $a$ and *increase* in $l$. The drop in the $M/F$ ratio in this case is higher than the earlier study because the moment value remained approximately constant while the force value *increased*. This drop in moment to force ratio is shown in Figure 4.10. In comparison with the previous study a moment to force ratio around 10 mm, at 3 *mm* activations, now occurs only for $a$ dimensions around 7.0 *mm* not 4-5 *mm* as in the first study.

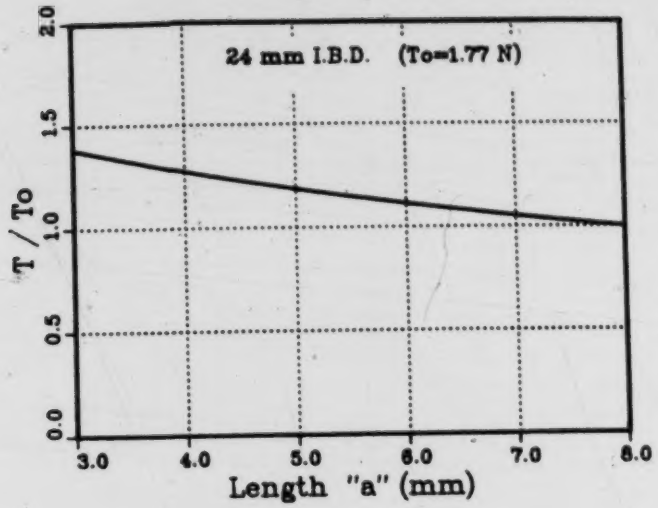


Figure 4.9: $T/T_o$ for pre-activated T-springs with different lengths $a$ and $l$ ($0.017" \times 0.025"$ *TMA wire*)

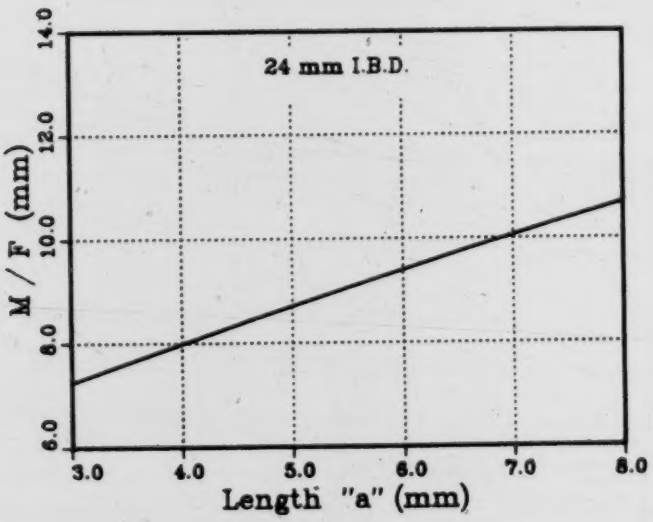


Figure 4.10: $M/F$ for pre-activated T-springs with different lengths $a$ and $l$ ($0.017" \times 0.025"$ *TMA wire*)

### 4.1.2 Combined $a$ and $b$ Lengths Parametric Study

The loop size of the pre-activated T-spring can also be achieved by *decreasing* both lengths $a$ and $b$ simultaneously (see Figure 4.1). This way the overlap in the spring wire that occurred with *decreasing* only length $a$ is avoided. Therefore, another parametric study was performed in which both lengths $a$ and $b$ were reduced, but the ratio $a/b$ was kept constant at 2.667 which is the same ratio in the typical pre-activated T-spring shown in Figure 4.1.

The different spring geometries of this parametric study are shown in Figure 4.11. The difference in loop size between the different springs is clear in this case. Moreover, the *decrease* in horizontal distance between the two ends of the spring caused by reducing length $a$ is offset by the *increase* of this distance caused by decreasing length $b$. Then the different spring designs shown in Figure 4.11 would have approximately the same distance between the two ends. This is verified by comparing the $X$ distance of springs # 13 and # 18 at the neutral position, 20.765 $mm$ and 21.114 $mm$ respectively as given in Table 4.4. Consequently, length $l$ need not be altered in this parametric study as was the case in the previous parametric study. The values of the forces and moments at the neutral position, 3 $mm$ activation, and 24 $mm$ $I.B.D.$ are listed in Table 4.4. The values of forces and moments for 3 $mm$ activation and 24 $mm$ $I.B.D.$ are close because 24 $mm$ $I.B.D.$ corresponds to $2.88 - 3.23$ $mm$ range of activation for the different spring designs given in Figure 4.11.

Plotting the moment values of the different springs as ratios of the moment value of the typical pre-activated T-spring (# 13) results in the curves shown in Figure 4.12. These curves indicate that the moment value *increases* as the loop size gets smaller. The *increase* in the moment value reaches about 12% in the case of spring # 18 ($a = 3.0$ $mm$, $b = 1.125$ $mm$) for 24 $mm$ $I.B.D.$.

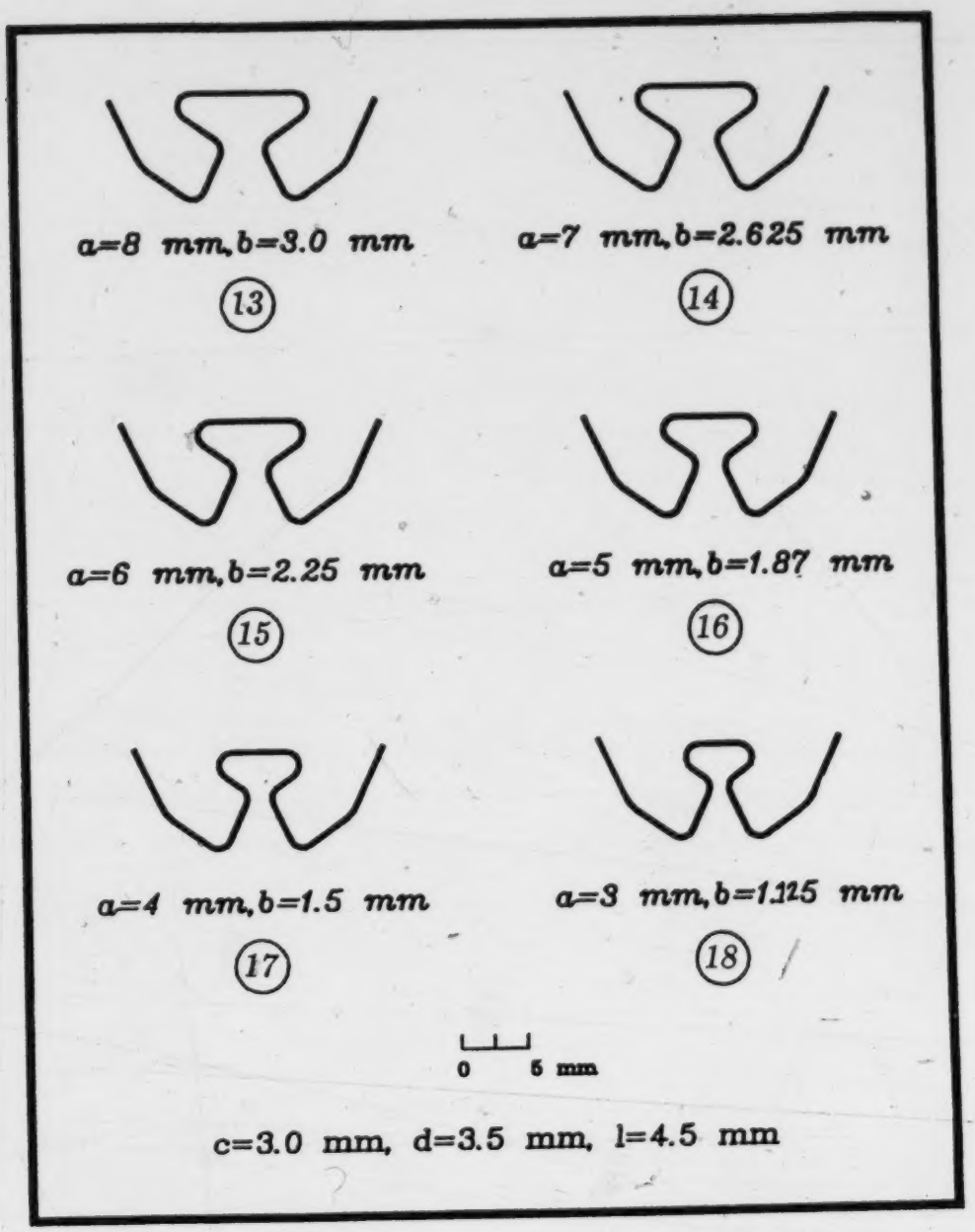


Figure 4.11: Pre-activated T-springs with different lengths $a$ and $b$

Table 4.4: Moments and forces of pre-activated T-springs with different $a$ and $b$ (0.017" x 0.025" TMA wire)

| Spring | Length ($mm$) | | Neutral Position | | 3 $mm$ Activation | | |
|---|---|---|---|---|---|---|---|
| # | $a$ | $b$* | $M$ ($N$ $mm$) | $X$ ($mm$) | $M$ ($N$ $mm$) | $T$ ($N$) | $I.B.D.$ ($mm$) |
| 13 | 8.0 | 3.000 | 13.97 | 20.76 | 18.63 | 1.64 | 23.77 |
| 14 | 7.0 | 2.625 | 14.47 | 20.81 | 19.14 | 1.80 | 23.81 |
| 15 | 6.0 | 2.250 | 15.02 | 20.86 | 19.68 | 2.00 | 23.86 |
| 16 | 5.0 | 1.875 | 15.60 | 20.93 | 20.23 | 2.26 | 23.93 |
| 17 | 4.0 | 1.500 | 16.23 | 21.01 | 20.79 | 2.59 | 24.01 |
| 18 | 3.0 | 1.125 | 16.91 | 21.11 | 21.35 | 3.05 | 24.11 |

| Length ($mm$) | | 24 $mm$ $I.B.D.$ | | |
|---|---|---|---|---|
| $a$ | $b$ | $M$ ($N$ $mm$) | $T$ ($N$) | $Act.$($mm$) |
| 8.0 | 3.000 | 18.93 | 1.77 | 3.24 |
| 7.0 | 2.625 | 19.39 | 1.92 | 3.19 |
| 6.0 | 2.250 | 19.85 | 2.10 | 3.14 |
| 5.0 | 1.875 | 20.32 | 2.32 | 3.07 |
| 4.0 | 1.500 | 20.78 | 2.58 | 2.98 |
| 3.0 | 1.125 | 21.23 | 2.92 | 2.89 |

* $a/b = 2.667$

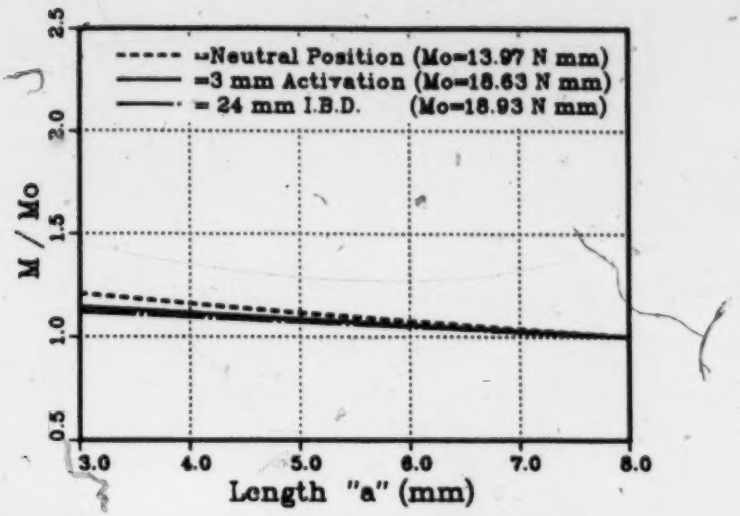


Figure 4.12: $M/M_o$ for pre-activated T-springs with different lengths $a$ and $b$ ($a/b = 2.667$, 0.017" $\times$ 0.025" *TMA wire*)

The ratios of the forces to the force of the typical spring for 3 *mm* activation as well as 24 *mm I.B.D.* are plotted in Figure 4.13. These curves show that the force values *increase* significantly with the *decrease* in the loop size. For example, the force value of spring # 18 is about 65% higher than the typical spring force for 24 *mm I.B.D.* This resulted in the significant drop in the moment to force ratios shown in Figure 4.14. The M/F value for 24 *mm I.B.D.* dropped from 10.7 for the typical spring (# 13) to 7.3 for spring # 18. However, for 5 *mm a* length and 1.87 *mm b* length (spring # 16) the M/F value is 8.77 for 24 *mm I.B.D.*, which is an acceptable ratio to achieve tooth translation without significant tooth tipping, given the fact that the loop width is reduced by 3 *mm*. Also, this spring design can be used with a smaller *I.B.D.*, with the result that the $M/F$ ratio would be higher.

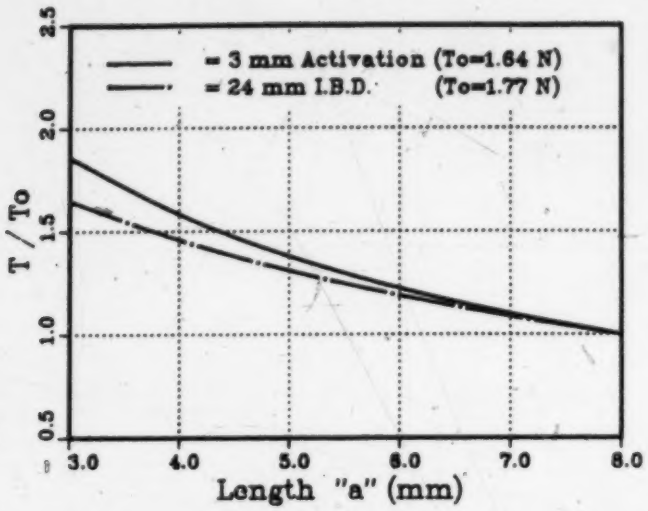


Figure 4.13: $T/T_o$ for pre-activated T-springs with different lengths $a$ and $b$ ($a/b = 2.667,\ 0.017" \times 0.025"\ TMA\ wire$)

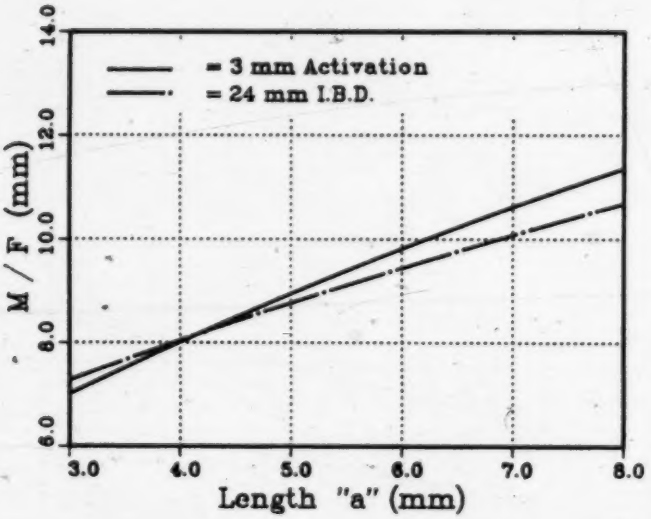


Figure 4.14: $M/F$ for pre-activated T-springs with different lengths $a$ and $b$ ($a/b = 2.667,\ 0.017" \times 0.025"\ TMA\ wire$)

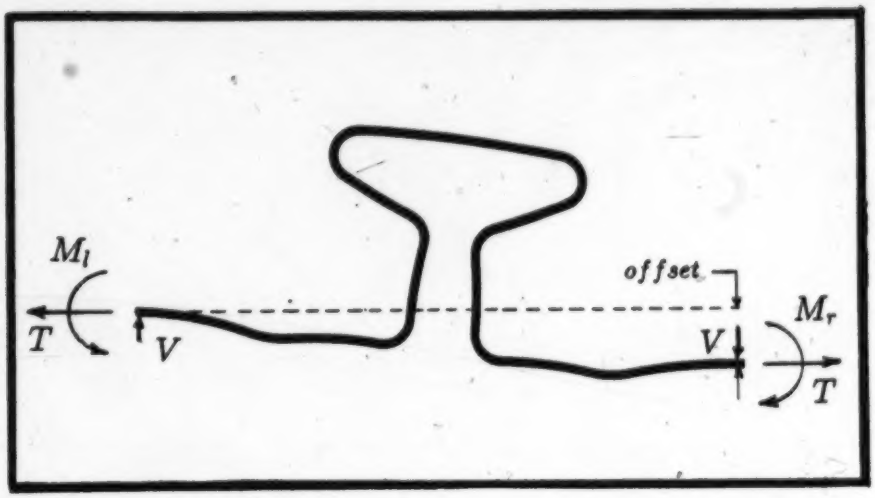


Figure 4.15: Deformed geometry of pre-activated T-spring with bracket offset

### 4.1.3 Bracket Offset Parametric Study

In the previous parametric studies it was assumed that the springs are mounted between two brackets which are at the same horizontal level. However, in some cases there is a vertical offset between the two brackets. Therefore, a parametric study was performed to test the effect of offsetting one the brackets on the values of the forces, shear and tension, and the moments at the two ends of the spring. In this case the full spring has to be considered in the analysis as the deformation of the spring is not symmetric which means that the moment values at the two ends of the spring will be different. This difference is balanced by shear forces acting upward on one the brackets and downward on the other. The direction of these forces and moments are shown in Figure 4.15, which represent the deformed geometry of the typical pre-activated T-spring mounted between two brackets which are 23.76 *mm* apart and with the right bracket 1.5 *mm* lower than the left bracket.

Table 4.5 summaries the results of the parametric study performed on the typical

Table 4.5: Moments and forces of pre-activated T-spring for different bracket offset (0.017" × 0.025" TMA wire)

| bracket | Neutral Position | | 3 *mm* Activation | |
|---|---|---|---|---|
| *offset* (*mm*) | $M_l$ (*N mm*) | $M_r$ (*N mm*) | $M_l$ (*N mm*) | $M_r$ (*N mm*) |
| 0.00 | 13.80 | 13.80 | 18.65 | 18.65 |
| 0.25 | 14.80 | 13.10 | 19.40 | 17.85 |
| 0.50 | 15.70 | 12.30 | 20.16 | 17.11 |
| 0.75 | 16.60 | 11.44 | 20.92 | 16.37 |
| 1.00 | 17.44 | 10.61 | 21.69 | 15.64 |
| 1.25 | 18.33 | 9.79 | 22.46 | 14.91 |
| 1.50 | 19.22 | 8.99 | 23.23 | 14.19 |
| 1.75 | 20.12 | 8.19 | 24.00 | 13.48 |
| 2.00 | 21.02 | 7.40 | 24.79 | 12.77 |

pre-activated spring for different vertical offset value from 0 to 2 mm. In this study the right end of the spring was positioned lower than the left end which means that if the global coordinate system origin is positioned at the left end of the spring then the $Y$ coordinate of right end is equal to the vertical offset value with a negative sign. This is the third boundary condition needed by the segmental shooting technique to analyze the spring with offset.

The left and right moment values at the neutral position for the different offset values are plotted as ratios of the moment value of the spring with zero offset in Figure 4.16. This figure shows that the left moment which is the moment at the end of the spring mounted on the higher bracket *increases* while the moment at the right end *decreases*. The percentage *increase* and the corresponding percentage *decrease* in the two moment values become higher for higher bracket offset values as shown

in the figure. A similar plot is done for the moment values at 3 *mm* activation and is shown in Figure 4.17. Also, in this case the left moment *increases* while the right moment *decreases* with the *increase* in the bracket offset. However, the percentage difference between the two moment values is smaller in the case of 3 *mm* activation than the percentage difference at the neutral position. This suggests that the bracket offset have less effect in the case of higher spring activation, but still the difference between the two values cannot be neglected especially for large vertical offset values. For example, in the case of 2 *mm* offset, the values of left and right moments for 3 mm activation are 24.79 $N$ *mm*, and 12.77 $N$ *mm* respectively, while the tension value is 1.64 $N$ and the shear force is equal to 0.65 $N$. This means that the moment to force ratio at the left bracket is equal to 15.14 *mm* which is high and would cause a clockwise tipping of the left tooth. On the other hand, the $M/F$ ratio at the right end is equal to 7.80, which is low and would, also, result in tipping the right tooth in clockwise direction. Moreover, Figure 4.18 shows that the shear force values *increases* as the vertical offset *increases*, therefore, for large vertical offset the shear values would be high enough to cause the tooth to move vertically. As for the tension, Figure 4.19 indicated that its value in not affected by the vertical offset of the brackets.

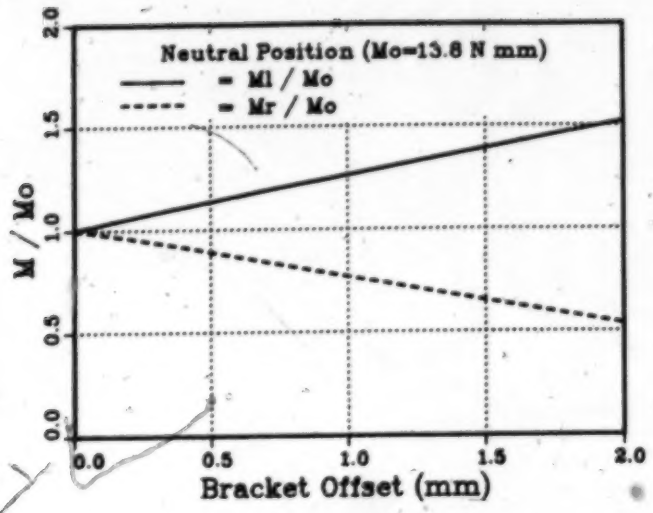


Figure 4.16: $M/M_o$ of pre-activated T-spring for different bracket offset #1
*neutral position* (0.017" × 0.025" *TMA wire*)

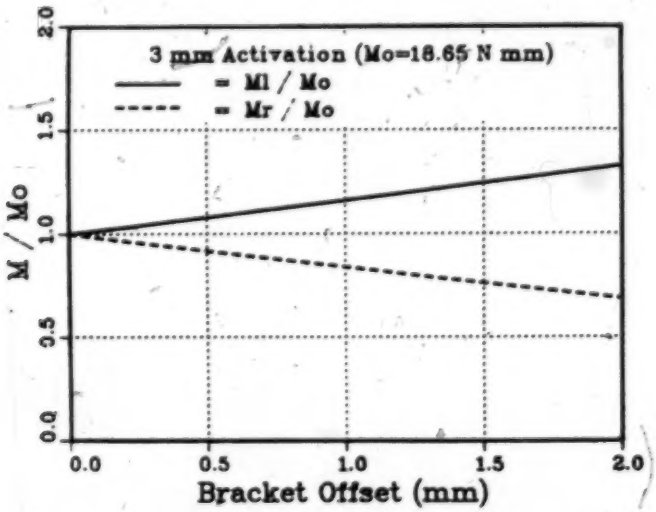


Figure 4.17: $M/M_o$ of pre-activated T-spring for different bracket offset #2
3 *mm activation* (0.017" × 0.025" *TMA wire*)

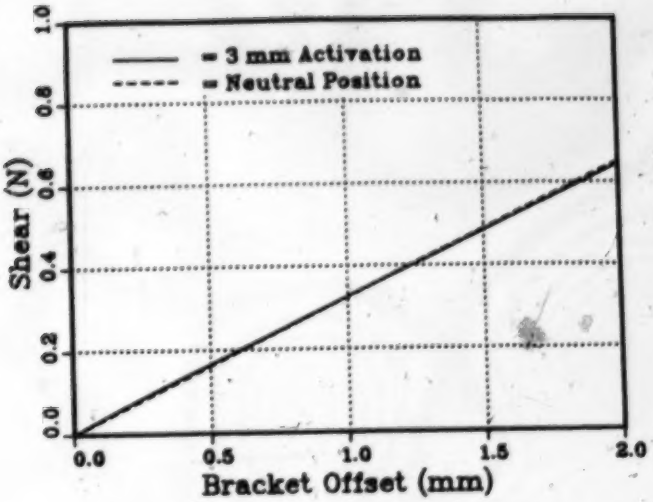


Figure 4.18: Shear of pre-activated T-spring for different bracket offset ($0.017" \times 0.025"$ *TMA wire*)

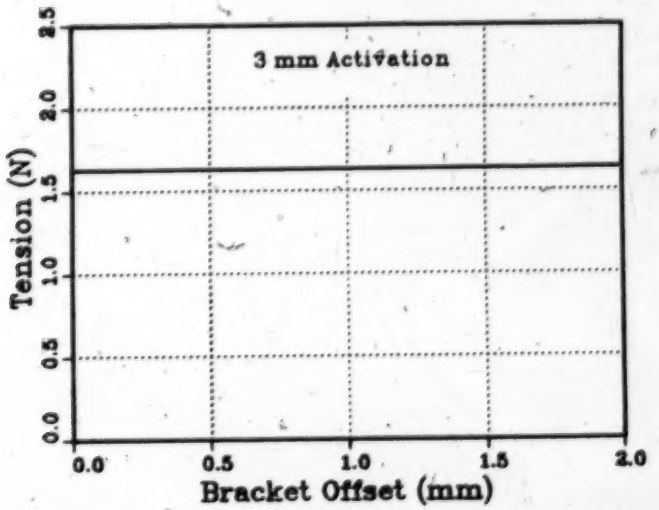


Figure 4.19: Tension of pre-activated T-spring for different bracket offset ($0.017" \times 0.025"$ *TMA wire*)

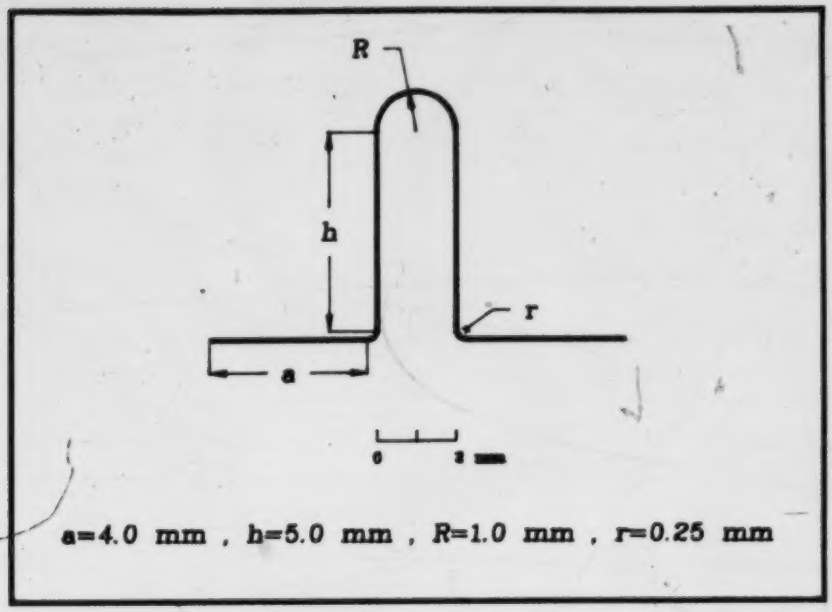


Figure 4.20: Typical vertical loop spring geometry

## 4.2 Vertical Loop Springs Parametric Studies

Vertical loop springs are widely used in orthodontic practice as the primary devices for space closure, and the majority of orthodontists use this simple spring design rather than the complicated pre-activated T-spring discussed earlier. Consequently, it is important to perform a full mechanical analysis for the vertical loop spring design to determine whether it is capable of delivering the range of force and moment values required for proper tooth movement. The typical design for the vertical loop spring is shown in Figure 4.20, and for the symmetric case the half spring can be broken into four different sections, two initially straight with lengths $a$ and $h$, and two initially curved with radii of curvature $r$ and $R$ (each with arc angle = 90°). Throughout this study, length $a$ will be referred to as the arm of the vertical loop spring, $h$ the height of the spring, and $R$ defined as the radius of the loop. The spring is usually fabricated

Table 4.6: Moment and force values of the typical vertical loop spring

| *Act.(mm)* | *M (Nmm)* | *F (N)* | *I.B.D. (mm)* |
|---|---|---|---|
| 0.0 | 0.0 | 0.0 | 10.5 |
| 0.1 | 0.449 | 0.215 | 10.6 |
| 0.2 | 0.895 | 0.431 | 10.7 |
| 0.3 | 1.339 | 0.648 | 10.8 |
| 0.4 | 1.779 | 0.867 | 10.9 |
| 0.5 | 2.217 | 1.088 | 11.0 |
| 0.6 | 2.652 | 1.310 | 11.1 |
| 0.7 | 3.084 | 1.534 | 11.2 |
| 0.8 | 3.514 | 1.760 | 11.3 |
| 0.9 | 3.940 | 1.988 | 11.4 |
| 1.0 | 4.364 | 2.218 | 11.5 |
| 1.1 | * | * | 11.6 |

* *Spring Yielded*

from stainless steel wire, with Young's modulus equal to 174 $GPa$, and the tensile yield strength equal to 1400 $MPa$.

The values of moments and forces for the vertical loop spring, bent from 0.016" diameter stainless steel wire, were determined for different spring activations using the segmental shooting technique program. These values for 0 to 1 $mm$ activation range are listed in Table 4.6. For activation values higher than 1 $mm$ the spring would yield at the mid point of the spring loop according to the stress analysis routine of the program. This means that this spring design has a very limited range of activation compared to the activation range of the pre-activated T-spring. Consequently, this will require more frequent adjustments in order to achieve significant movement of the teeth.

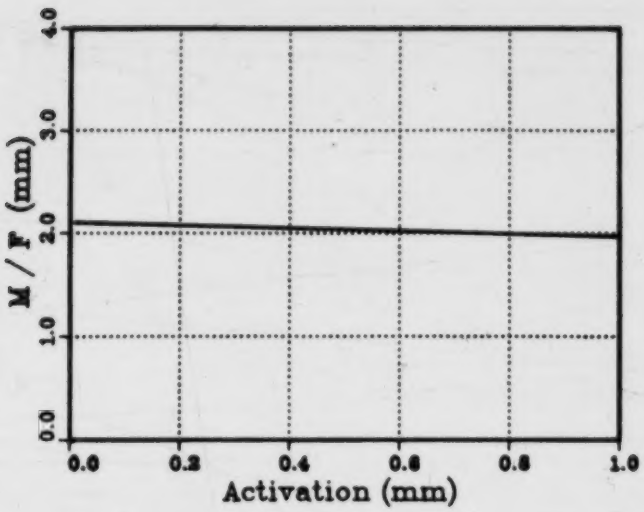


Figure 4.21: Moment to force ratio of the typical vertical loop spring as a function of activation

The moment to force ratio of the typical vertical loop spring is plotted for the different activation values in Figure 4.21. The plot indicates that the ratio is approximately constant at 2 $mm$. This low value, which is below than the desired 10 $mm$, would result in the tipping of the teeth on which the spring is mounted.

From the above analysis and discussion, it can be inferred that the typical vertical loop spring design suffers from two major limitations. First, it has a very limited activation range, and second, its moment to force ratio is very low. Therefore, different parametric studies were performed using the segmental shooting technique program to determine how the typical design of the spring can be altered so that the mechanical performance of this widely used spring can be improved. These different parametric studies will be presented in the following sections.

### 4.2.1 Spring Wire Material and Cross Section Parametric Study

As mentioned above stainless steel wire is generally used for the vertical loop springs. Different wire cross sections are used in practice, with square 0.017" × 0.017" (0.432×0.432 $mm$) cross section being the most common. In order to determine the effect of using different wire cross sections and materials on the values of the moments and forces as well as the activation range, a parametric study was performed in which the typical vertical loop design was analyzed using four different stainless steel cross sections, and four different $TMA$ wire cross sections. The Young's modulus for stainless steel orthodontic wire is 174 $GPa$ while it is equal to 71 $GPa$ for $TMA$. These are the average values obtained from the tension tests discussed in Chapter 3. The tensile yield strength of stainless steel wire was chosen to be 1400 $MPa$ which is an approximate value that corresponds to about 75% of the ultimate tensile strength [26] obtained from the tension tests performed in this study. This is the conventional ratio used in determining the yield strength of the mechanical springs, as both wires, orthodontic and mechanical springs, are manufactured through severe cold drawing processes which result in higher yield strength for the wire close to the ultimate tensile strength. Similarly, the yield strength for $TMA$ wire was chosen to be 1240 $MPa$.

The values of the moments and forces generated by activating the vertical loop spring 1 $mm$ are listed in Table 4.7 for the different materials and cross sections. As shown in the table the moment to force ratio is independent of the material or the cross section of the spring wire, which means the $M/F$ ratio depends only on the spring geometry. The values of the moments and forces of the 0.016" diameter stainless steel were chosen to be the standard, and the ratios of the other moments and forces to the standard values were computed and they are listed in the second

Table 4.7: Moments and forces for different wire sizes and materials typical vertical loop spring (1 *mm* activation)

| Material | $EI$ ($N\ mm^2$) | $M$ ($N\ mm$) | $F$ ($N$) | $M/F$ ($mm$) |
|---|---|---|---|---|
| SS D=0.016" | 233.468 | 4.364 | 2.218 | 1.968 |
| SS 0.016"×0.022" | 545.049 | 10.187 | 5.176 | 1.968 |
| SS 0.016"×0.016" | 396.320 | 7.409 | 3.765 | 1.968 |
| SS 0.010"×0.020" | 121.006 | 2.261 | 1.149 | 1.968 |
| TMA D=0.016" | 96.025 | 1.795 | 0.912 | 1.968 |
| TMA 0.017"×0.025" | 305.502 | 5.711 | 2.902 | 1.968 |
| TMA 0.016"×0.022" | 224.178 | 4.190 | 2.129 | 1.968 |
| TMA 0.017"×0.017" | 207.756 | 3.883 | 1.973 | 1.968 |

| Material | $(EI)/(EI)_o$ | $M/M_o$ | $F/F_o$ | Yield Act.($mm$) |
|---|---|---|---|---|
| SS D = 0.016" | 1.00 | 1.00 | 1.00 | 1.0 |
| SS 0.016"× 0.022" | 2.334 | 2.334 | 2.334 | 1.0 |
| SS 0.016"× 0.016" | 1.698 | 1.698 | 1.698 | 1.0 |
| SS 0.010"× 0.020" | 0.518 | 0.518 | 0.518 | 1.5 |
| TMA D = 0.016" | 0.411 | 0.411 | 0.411 | 2.0 |
| TMA 0.017"× 0.025" | 1.309 | 1.309 | 1.309 | 2.0 |
| TMA 0.016"× 0.022" | 0.960 | 0.960 | 0.960 | 2.0 |
| TMA 0.017"× 0.017" | 0.890 | 0.890 | 0.890 | 2.0 |

*SS = stainless steel , TMA = titanium molybdenum alloy*

part of Table 4.7. Comparing the different ratios leads to the conclusion that the absolute values of the moments and forces generated by the spring deformation are linearly related to the stiffness value of the spring wire ($EI$), which is the product of Young's modulus of the material and the second moment of area or moment of inertia of the wire cross section. Consequently, the parametric studies on the orthodontic springs can be performed only on one standard material and cross section and the values of the forces for a different spring wire would be computed by multiplying the values of the moments and forces of the standard case by the ratio of the actual wire stiffness to the stiffness of the standard wire.

Using a different cross section and more importantly a different material can make it possible to deform the spring to a higher activation before causing it to yield, especially if a material with a relatively low Young's modulus and high yield strength such as $TMA$ is used. The Young's modulus of $TMA$ orthodontic wire is about 40% of the stainless steel wire value, while the yield strength of $TMA$ is about 85% of the yield strength value of the stainless steel. As a result, a typical vertical loop spring bent from $TMA$ wire can be activated up to approximately 2 $mm$ before yielding occurs compared to 1 $mm$ in the case of stainless steel wire. However, $TMA$ wire is more difficult to deform to the correct spring geometry than stainless steel as the wire springs back after being bent. In addition, the cost of $TMA$ wire is higher than that of stainless steel. Finally, it should be noted that even within the same material, cross sections with smaller thickness can allow for higher activations, because the tensile stress due to the bending moment, which is the largest component of the total stress at a given point, is linearly related to the thickness of the wire cross section. ($\sigma_m = Mc/I$, see Appendix E). For example, a vertical loop spring bent from stainless steel wire with 0.01" $\times$ 0.02" (0.254 $\times$ 0.508 $mm$) cross section can be activated up to 1.5 $mm$ compared to 1 $mm$ in the case of the other cross sections

with larger heights, as shown in Table 4.7.

### 4.2.2 Height ($h$) Parametric Study

The first set of geometrical parametric studies performed on the vertical loop spring made changes in the values of length $h$, length $a$ and radius $R$ (see Figure 4.20), which means that the general shape of the spring will be unchanged. The first of these studies involves changing the height, $h$, which was varied from 4 to 9 $mm$. This means that the total height of the springs will vary from 5.25 to 10.25 $mm$ when the radii of the two arcs are added. The geometries of these vertical loop springs with different heights are shown in Figure 4.22 (the scale of the drawing is 3:1), with the values of the moments and forces associated with 1 $mm$ activation of these springs are listed in Table 4.8. As indicated in the table, the vertical loop spring with a height of 4 $mm$ will yield if it is activated 1 mm. The total horizontal length of all the springs in this case is 10.5 $mm$, which result in having the 11.5 $mm$ $I.B.D.$ for the 1 mm activated springs.

The standard in most of the vertical loop spring parametric studies will be the typical spring given in Figure 4.20 (spring #2 in Figure 4.22, which has the dimensions $a = 4.0\ mm$, $r = 0.25\ mm$, $h = 5.0\ mm$, $R = 1.0\ mm$ ). The ratios of the moments and force of the different vertical loop spring with different heights, given in Figure 4.22, at 1 $mm$ activation to the corresponding values of the standard spring are plotted in Figure 4.23. The two curves shown in the figure indicate that the both the moment and force values drop as the height of the spring is *increased*, but the force values drop at a higher rate than the moment values do. As a result, the moment to force ratio will *increase* with the *increase* in the spring height. This is shown in Figure 4.24, in which the moment to force ratio *increases* to 3.8 at a 9 $mm$ height from 1.97 at the

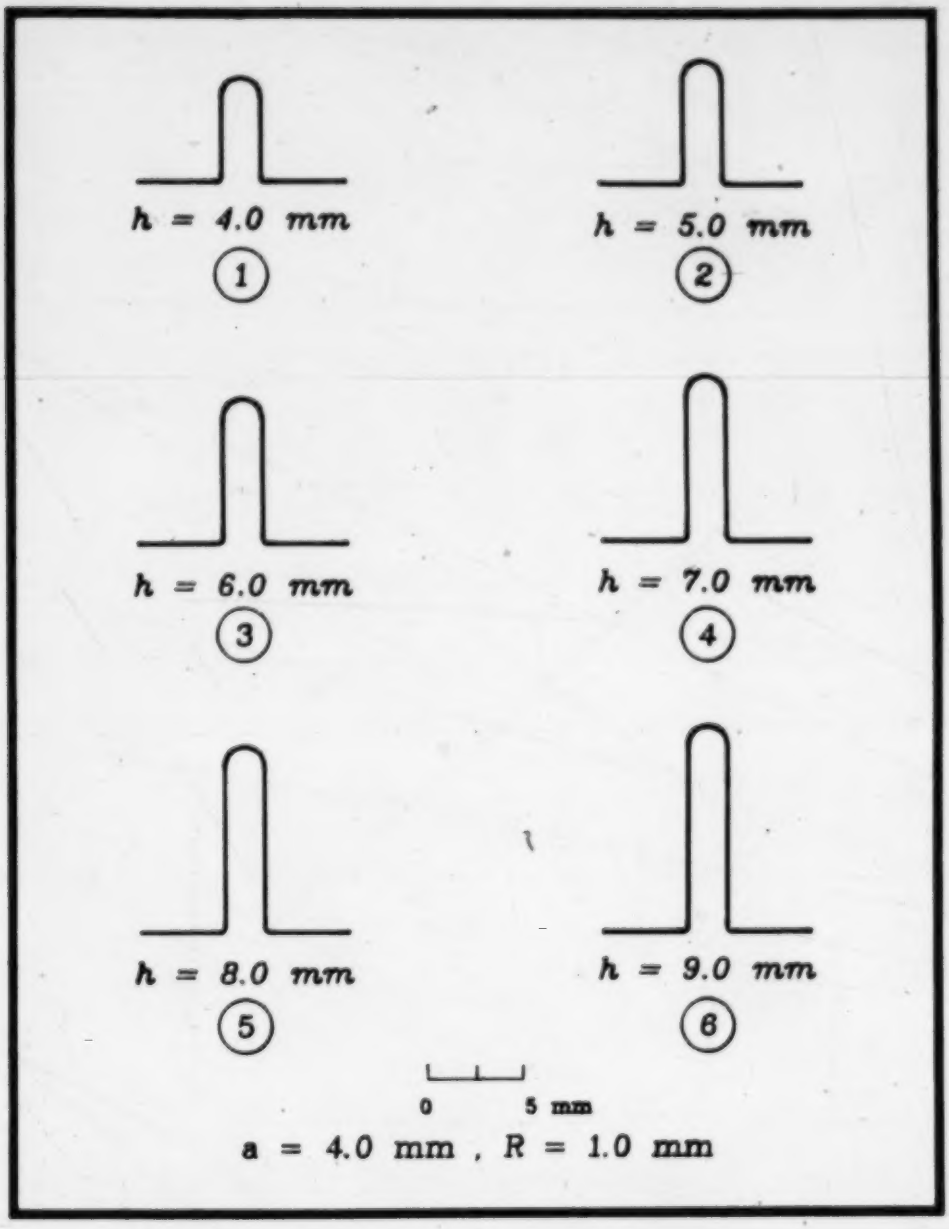


Figure 4.22: Vertical loop springs with different height $h$.

Table 4.8: Moments and forces of vertical loop springs with different $h$

1 $mm$ activation (0.016" round stainless steel wire)

| Spring # | $h$ $(mm)$ | $M$ $(Nmm)$ | $F$ $(N)$ | $I.B.D.$ $(mm)$ |
|---|---|---|---|---|
| 1 | 4 | * | * | 11.5 |
| 2 | 5 | 4.364 | 2.218 | 11.5 |
| 3 | 6 | 3.663 | 1.511 | 11.5 |
| 4 | 7 | 3.126 | 1.083 | 11.5 |
| 5 | 8 | 2.704 | 0.806 | 11.5 |
| 6 | 9 | 2.366 | 0.619 | 11.5 |

* *Spring Yielded*

standard height of 5 $mm$. Moreover, the drop in the absolute values of the moment and force results in lower stress values at the different points of the activated spring. For example, the force value of the spring with 9 mm height at 1 $mm$ activation is about 28% of the force value of the standard spring, while the moment value is about 55% of the standard value. Therefore, the maximum activation of the springs with *increased* height can be higher than the 1 $mm$ limit of the standard case. However, the *increased* height might cause some irritations to the patients as part of vertical loop would be considerably above the gum line.

The effect of increasing the height of the vertical loop spring was also studied experimentally by Burstone and Koenig [27], and they have obtained similar results to the above.

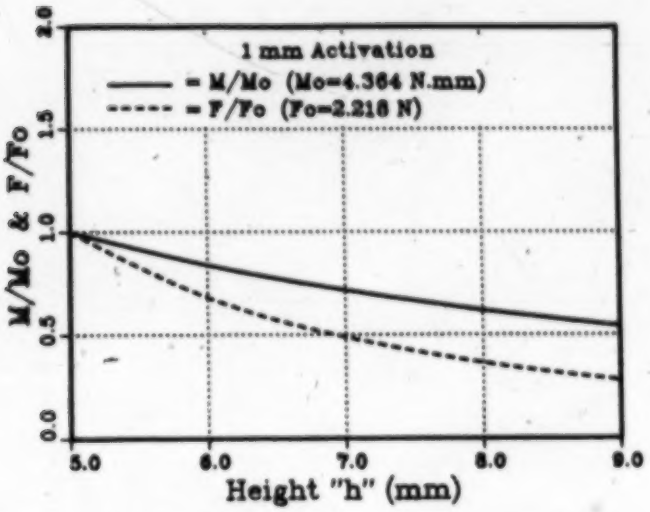


Figure 4.23: $M/M_o$ and $F/F_o$ for vertical springs with different $h$.

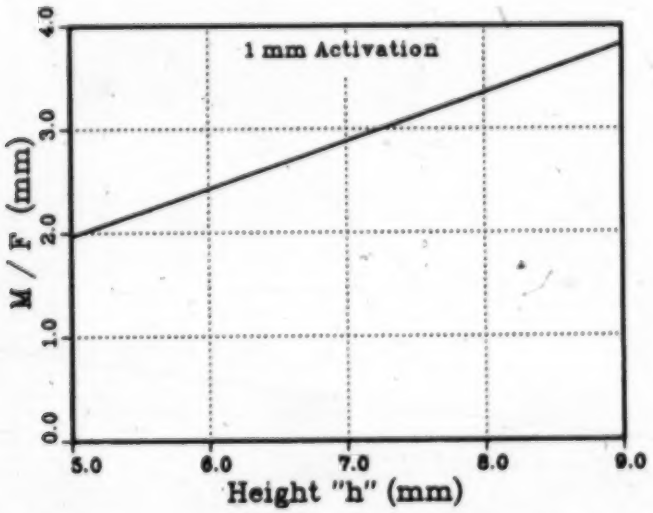


Figure 4.24: $M/F$ values for vertical loop springs with different $h$.

### 4.2.3 Combined loop radius ($R$) and arm length ($a$) parametric study

The objective of the second parametric study performed on the vertical loop spring was to test the effect of increasing the loop radius value ($R$) on the mechanical characteristics of the spring. However, larger loop radius results in an *increase* in the initial horizontal length of the spring. Therefore, the increase in loop radius ($R$) was coupled with a decrease in the arm length ($a$) such that the initial horizontal length of the different springs would be the same. This makes the parametric study more clinically relevant. The initial length of the springs was chosen to be 12 $mm$ for this parametric study.

The geometries of the different vertical loop springs investigated in this parametric study are given in Figure 4.25, with the moments and forces generated by activating these springs 1 $mm$, i.e. positioning them between two brackets 13 $mm$ apart, are listed in Table 4.9. In this parametric study the standard was chosen to be spring # 8 which has a loop radius equals to 1 $mm$ and 4.75 $mm$ arm length. This is different from the arm length of the typical vertical loop ($a = 4\ mm$) previously considered.

Figure 4.26 shows the plots of the ratios of the moments and forces at 1 mm activation of the different springs, given in Figure 4.25, to the corresponding values of the moment and force of the standard spring (#8) in this case . These ratios are plotted in the figure as a function of the loop radius $R$, which was chosen over arm length for convenience. The two curves in the figure show that the moment in this case in not significantly affected by *increasing* the radius and *decreasing* the arm length. This means that the *decrease* in the moment value caused by the *increase* in the radius is counter balanced by the *increase* in the moment value due to the *decreasing* arm length. However, the force value drops as the radius is *increased* and

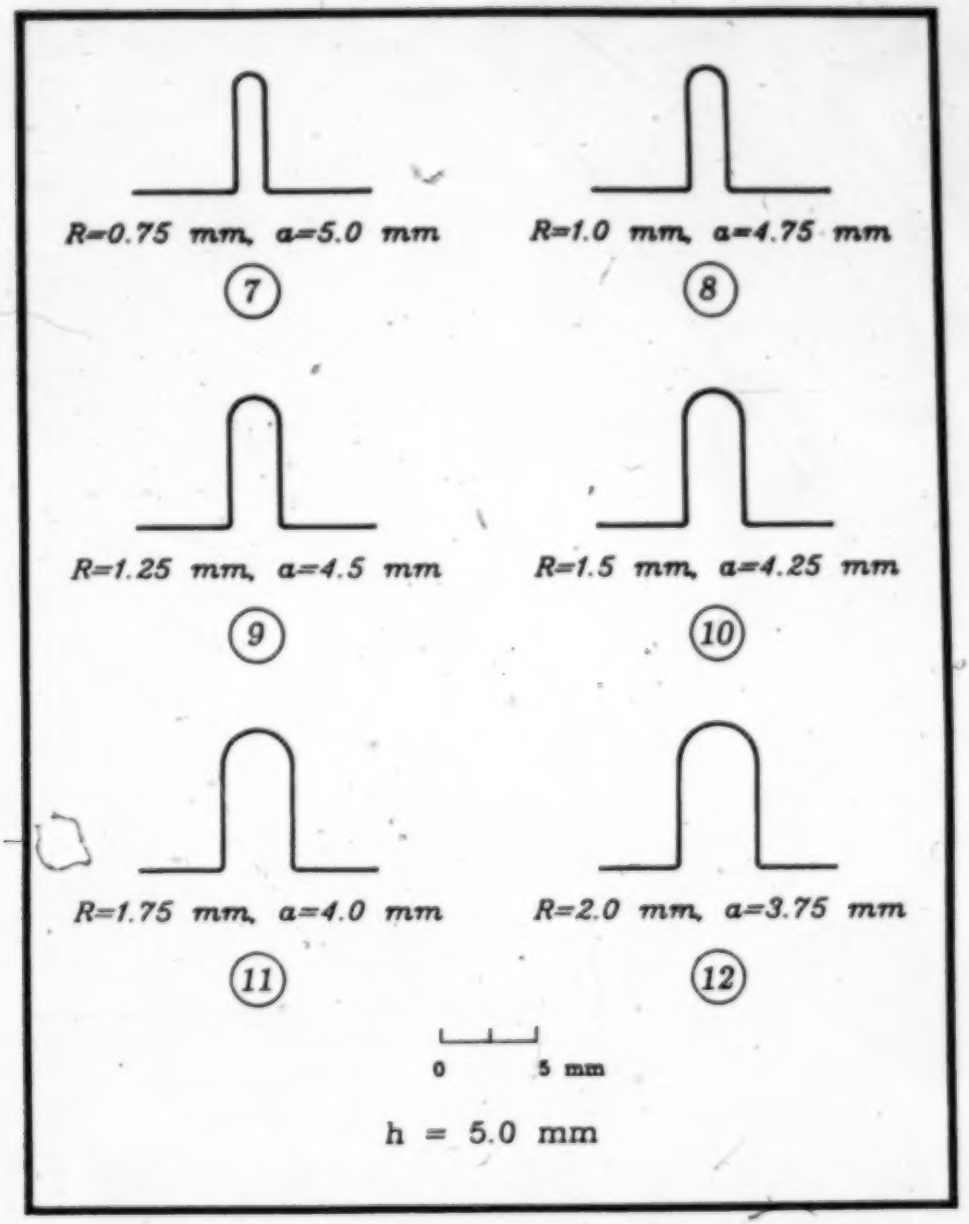


Figure 4.25: Vertical loop springs with different $R$ and $a$ (initial horizontal length = 12 $mm$)

Table 4.9: Moments and forces of vertical springs with different $a$ and $R$

1 $mm$ activated (0.016" round stainless steel wire)

| Spring # | $R$ ($mm$) | $a$ ($mm$) | $M$ ($Nmm$) | $F$ ($N$) | $I.B.D.$ ($mm$) |
|---|---|---|---|---|---|
| 7 | 0.75 | 5.00 | • | • | 13.0 |
| 8 | 1.00 | 4.75 | 3.830 | 2.114 | 13.0 |
| 9 | 1.25 | 4.50 | 3.775 | 1.867 | 13.0 |
| 10 | 1.50 | 4.25 | 3.730 | 1.667 | 13.0 |
| 11 | 1.75 | 4.00 | 3.694 | 1.503 | 13.0 |
| 12 | 2.00 | 3.75 | 3.667 | 1.367 | 13.0 |

• *Spring Yielded*

the arm length is *decreased*, because the drop in the force value due to the *increase* in the radius is higher than the *increase* the force value due to the *decrease* of the arm length. This drop in the force value results in the *increase* in the moment to force ratio as shown in Figure 4.27. However, the *increase* in this ratio is still not large enough such that the spring would cause the translation of the tooth without tipping. For example, the moment to force ratio for the spring with loop radius 2 $mm$ and arm length 3.75 $mm$ (spring # 12) is equal to 2.682 $mm$ which is much lower than the 10 $mm$ targeted value.

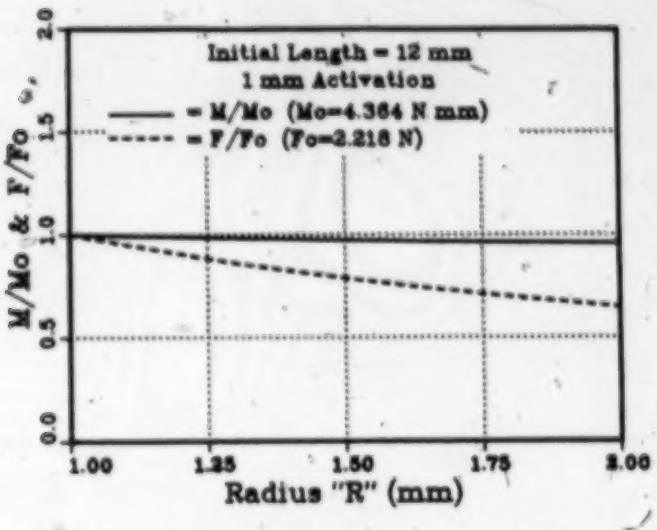


Figure 4.26: $M/M_o$ and $F/F_o$ for vertical springs with different $R$ and $a$

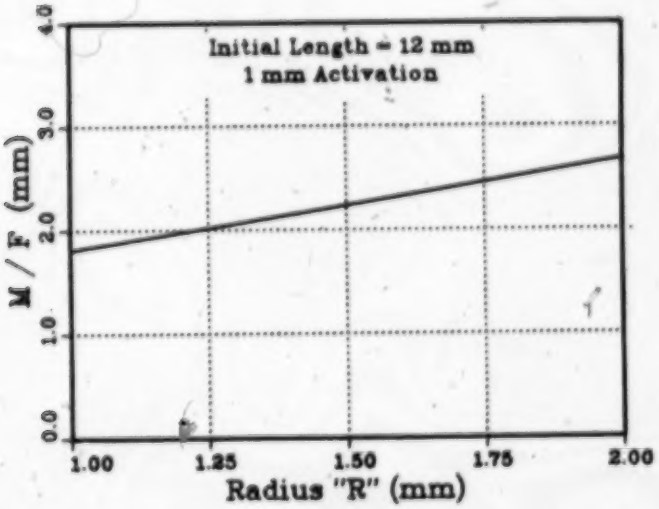


Figure 4.27: $M/F$ values for vertical loop springs with different $R$ and $a$

### 4.2.4 Pre-Activation Angle Parametric Study (0.016" round stainless steel wire)

The results of the previous parametric studies performed on the vertical loop springs indicate that the moment to force ratio of the vertical loop spring cannot be *increased* significantly by merely *increasing* the spring height or loop radius. Therefore, more radical changes to the spring design are necessary so a higher moment can be generated by deforming the spring. This can be done by pre-activating the vertical loop spring arms, which involves initially bending the spring arms such that the spring ends would form an angle with the horizontal plane. This angle is referred to as the pre-activation angle. The geometries of vertical loop springs, with different pre-activation angle in the range 0 to 12.5 degrees for the case of 0.016" round stainless steel wire, are given in Figure 4.28. The values of the moments and forces of these springs at 1 *mm* activation are listed in Table 4.10. It should be noted that similar to the pre-activated T-spring, the activation of this spring design is measured from the neutral position, which is the deformed shape of the spring where the ends have zero slope and the axial force or tension is equal to zero. Moreover, the different pre-activation angles for the different springs of this parametric study resulted in different horizontal distances between the two ends of the spring at the neutral position. This is translated into different values for the inter-bracket distance ($I.B.D.$) at 1 *mm* activation as listed in the table. Furthermore, the table indicates that a stainless steel vertical loop spring will yield if the pre-activation angle exceeds 10°.

In order to show the effect of the pre-activation on the mechanical characteristics of the vertical loop springs, the ratios of the moments and forces, generated by activating these springs shown in Figure 4.28 1 *mm*, to the corresponding moment and force values of the typical vertical loop spring, i.e. with zero pre-activation angle, are

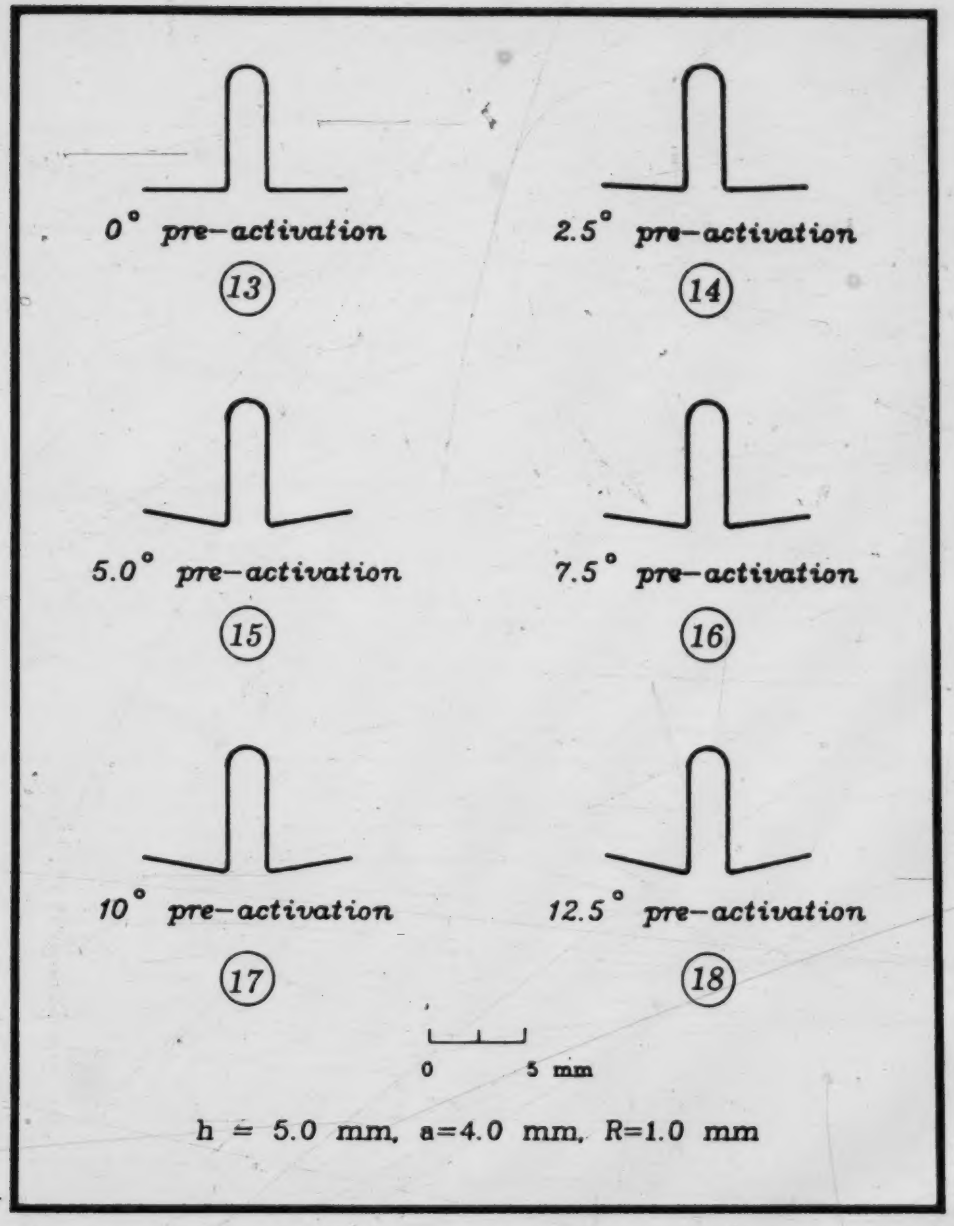


Figure 4.28: Vertical loop springs with different pre-activation angles (0.016" round stainless steel wire)

Table 4.10: Moments and forces of stainless steel pre-activated vertical springs
1 *mm* activation (0.016" round stainless steel wire)

| Spring # | Angle (*deg.*) | *M* (*Nmm*) | *F* (*N*) | *I.B.D.* (*mm*) |
|---|---|---|---|---|
| 13 | 0.0° | 4.364 | 2.2176 | 11.500 |
| 14 | 2.5° | 5.257 | 2.22006 | 11.338 |
| 15 | 5.0° | 6.148 | 2.22368 | 11.176 |
| 16 | 7.5° | 7.038 | 2.22845 | 11.013 |
| 17 | 10.0° | 7.927 | 2.23438 | 10.849 |
| 18 | 12.5° | * | * | |

* *Spring Yielded*

plotted in Figure 4.29. The curves in this figure show that the force value is not affected by the pre-activation of the spring, while as expected the moment value *increases* as the initial pre-activation is increased. This results in higher values for the moment to force ratios of the vertical loop springs with higher pre-activation angles as shown in Figure 4.30. For example, the value of moment to force ratio of the 10° pre-activated spring at 1 *mm* activation is 3.5 *mm* which is reasonably higher than the value of typical vertical loop (2 *mm*), but still not close to the 10 *mm* desired value.

The moment to force ratio of the typical vertical loop spring is approximately constant through the activation range of the spring with a value around 2 *mm*. This would not be the case for any pre-activated spring, because a significant initial moment is needed to deform the spring to the neutral position before applying any axial forces or tensions to activate the spring.

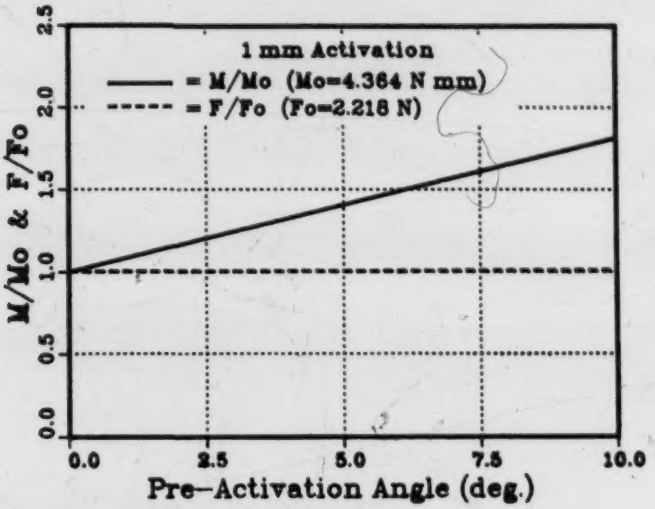


Figure 4.29: $M/M_o$ and $F/F_o$ for stainless steel pre-activated vertical springs (0.016" round stainless steel wire)

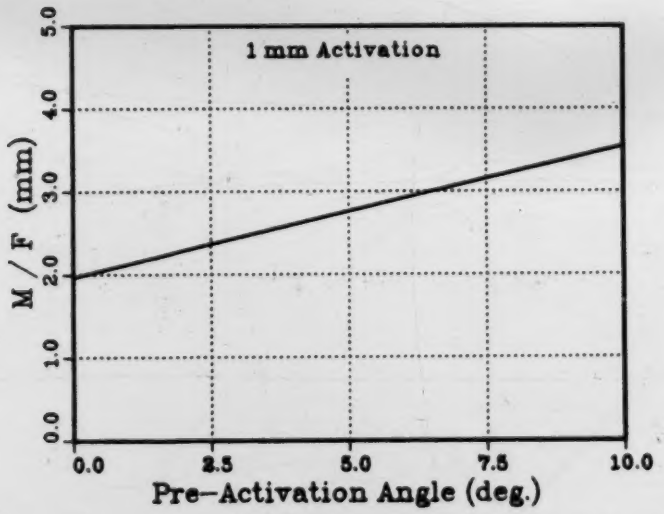


Figure 4.30: $M/F$ value for stainless steel pre-activated vertical springs (0.016" round stainless steel wire)

Table 4.11: Moments and forces of 10° pre-activated vertical spring

| *Act.(mm)* | *M (Nmm)* | *F (N)* | *I.B.D. (mm)* |
|---|---|---|---|
| 0.0 | 3.702 | 0.00 | 9.84 |
| 0.05 | 3.921 | 0.109 | 9.89 |
| 0.1 | 4.139 | 0.218 | 9.94 |
| 0.2 | 4.572 | 0.437 | 10.04 |
| 0.3 | 5.002 | 0.657 | 10.14 |
| 0.4 | 5.429 | 0.877 | 10.24 |
| 0.5 | 5.853 | 1.101 | 10.34 |
| 0.6 | 6.274 | 1.325 | 10.44 |
| 0.7 | 6.692 | 1.550 | 10.54 |
| 0.8 | 7.107 | 1.777 | 10.64 |
| 0.9 | 7.518 | 2.005 | 10.74 |
| 1.0 | 7.927 | 2.234 | 10.84 |
| 1.1 | 8.332 | 2.466 | 10.94 |
| 1.2 | * | * | 11.04 |

* *Spring Yielded*

In order to understand how the pre-activated vertical loop springs behave through their activation range, the stainless steel vertical loop spring with 10° pre-activation angle (spring # 17 in Figure 4.28) was analyzed at different activation values from 0 to 1.1 $mm$ . Note that the spring is expected to yield for activations greater than 1.1 $mm$ as was indicated by the stress calculation routine of the program. The values of the moments, forces and the $I.B.D.$ of this spring at the different activations are listed in Table 4.11. The moment to force ratio is plotted as a function of activation in Figure 4.31. The curve in this figure indicates that the $M/F$ ratio of the 10° pre-activated spring is higher than 10 $mm$ for activations lower than 0.2 $mm$ with the

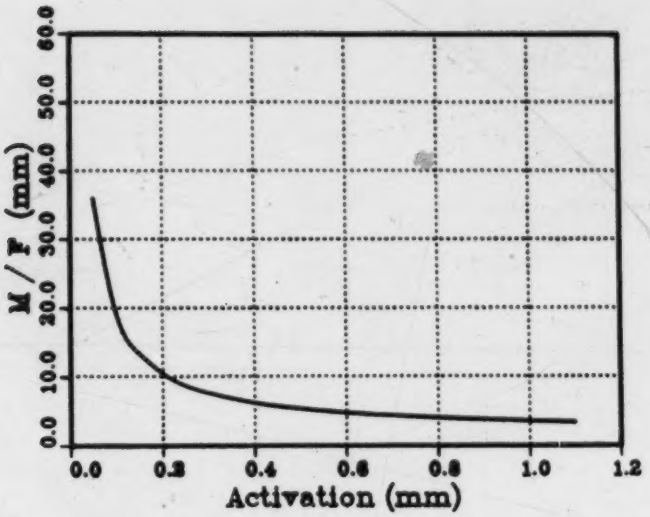


Figure 4.31: $M/F$ values of 10° pre-activated vertical loop spring (0.016" round stainless steel wire)

moment values in the range of 3.70 $N\ mm$ to 4.57 $N\ mm$, while the force values are less than 0.44 $N$. This means that the possible tipping of the tooth at the higher activations caused by low moment to force ratio could be corrected by the sufficiently high moment values at the low activations. As the small changes in the spring activation considered in the above argument are difficult to measure, other modifications in the vertical loop design and material were considered in order to achieve more predictable results for the space closure mechanisms.

It should be noted here that orthodontists appear to achieve better results by using the typical vertical loop spring than would be expected by the analyses above. According to these analyses the teeth would tip as a result of the low moment to force ratio, but the amount of tipping observed in some actual cases is not as large as might be expected. The discrepancy in the results can be attributed to the fact that

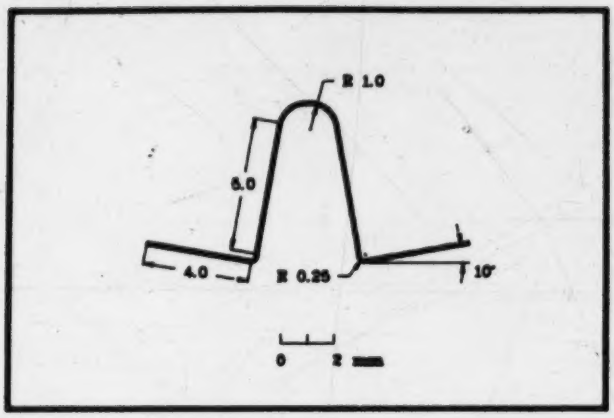


Figure 4.32: Yielded typical vertical loop spring initial geometry

the activation range of the typical vertical loop spring (no pre-activation) is limited to 1 *mm* which means that there is a good probability that orthodontists often yield the spring while mounting it to the patients teeth. This yielding usually occurs at the mid point of the spring loop where the maximum bending moment exists. The result of the spring yielding at this point is the change in the initial geometry of the spring to a similar geometry to the one shown in Figure 4.32.

The spring given in Figure 4.32, is a 10° pre-activated vertical loop spring but the pre-activation is introduced by bending the loop rather than bending the arms as was the case in the pre-activated spring discussed earlier. The values of the moments and forces generated by activating this spring from 0 to 1.0 *mm*, measured from the neutral position, are listed in Table 4.12. Comparing these values with the values of moments and forces of the normal 10° pre-activated vertical loop spring (spring # 17 Figure 4.28) presented earlier, one realizes that both springs have approximately

Table 4.12: Moments and forces of 10° pre-activated spring by loop yielding

vertical loop spring (0.016" round stainless steel wire)

| *Act.(mm)* | *M (Nmm)* | *F (N)* | *M/F (mm)* | *I.B.D. (mm)* |
|---|---|---|---|---|
| 0.0 | 3.777 | 0.00 | ∞ | 11.59 |
| 0.05 | 4.006 | 0.120 | 33.383 | 11.64 |
| 0.1 | 4.234 | 0.241 | 17.568 | 11.69 |
| 0.2 | 4.688 | 0.480 | 9.686 | 11.79 |
| 0.3 | 5.140 | 0.730 | 7.041 | 11.89 |
| 0.4 | 5.588 | 0.979 | 5.708 | 11.99 |
| 0.5 | 6.033 | 1.229 | 4.909 | 12.09 |
| 0.6 | 6.475 | 1.484 | 4.363 | 12.19 |
| 0.7 | 6.914 | 1.741 | 3.971 | 12.29 |
| 0.8 | 7.350 | 2.000 | 3.675 | 12.39 |
| 0.9 | 7.783 | 2.264 | 3.438 | 12.49 |
| 1.0 | 8.212 | 2.530 | 3.246 | 12.59 |
| 1.1 | * | * | * | 12.69 |

* *Spring Yielded*

the same mechanical characteristics. This could explain the better results achieved sometimes by orthodontists when using the typical vertical loop spring without pre-activation.

### 4.2.5 Pre-Activation Angle Parametric Study (0.016" × 0.022" *TMA* wire)

As discussed above, pre-activation of the vertical loop spring arms improved the moment to force ratio of the spring, as the moment values are higher. However, in the case of vertical loop springs bent from stainless steel wire, the maximum pre-activation angle is about 10°, as yielding occurs in the case of larger angles. For such small pre-activation angles the *increase* in the moment value is not high enough to *increase* the moment to force ratio significantly especially at higher activations. Therefore, another parametric study was performed on the pre-activated vertical loop springs, but using *TMA* as the wire material instead of stainless steel. As the Young's modulus of the *TMA* is about 40% of the Young's modulus value of the stainless steel while the yield strength of *TMA* is close to the yield strength of stainless steel, then the pre-activation angle can be *increased* if *TMA* is used. For example, it was found that a vertical loop spring, bent form 0.016"×0.022" *TMA* wire, can have a pre-activation angle up to 35° before the spring yields when activated more than 1 *mm*.

The geometries of pre-activated vertical loop springs bent form 0.016"×0.022" *TMA* wire, with arm lengths of 4 *mm*, height of 5 *mm*, and a loop radius of 1 *mm* and that have different pre-activation angles from 10 to 35 degrees, are given in Figure 4.33. The values of the moments and forces of these springs at 1 *mm* activation are given in Table 4.13. As shown in the table a higher pre-activation angle results in smaller inter-bracket distance.

The ratios of the moments and forces listed in Table 4.13 to the corresponding moment and force values of the typical *TMA* vertical loop spring without pre-activation are plotted in Figure 4.34. Similar to the stainless steel parametric study the force value is unaffected by the pre-activation of the spring arms, while the

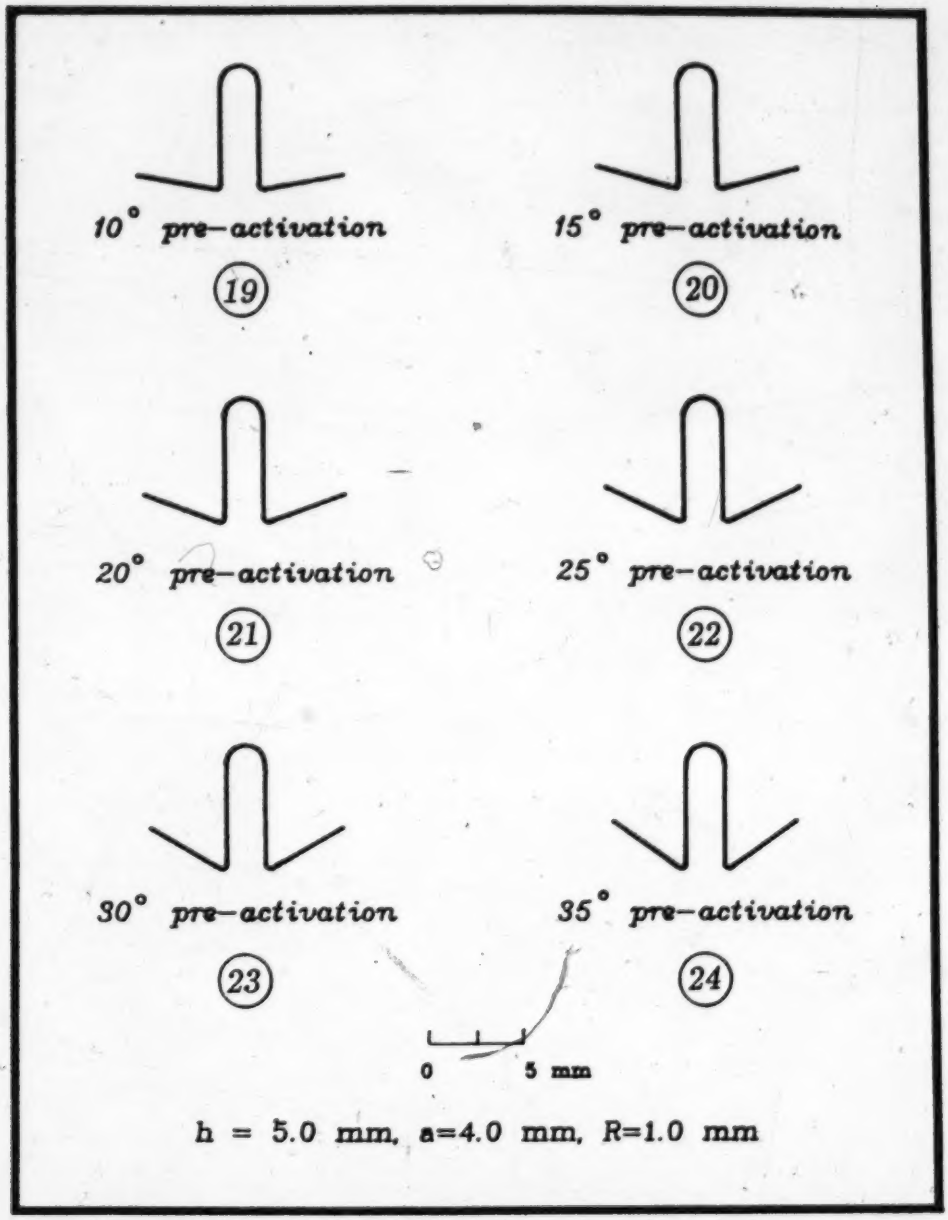


Figure 4.33: *TMA* Vertical loop springs with different pre-activation angles (0.016" × 0.022" *TMA* wire)

Table 4.13: Moments and forces of $TMA$ pre-activated vertical springs

1 $mm$ activation (0.016" × 0.022" $TMA$ wire)

| Spring # | Angle ($deg.$) | $M$ ($Nmm$) | $F$ ($N$) | $I.B.D.$ ($mm$) |
|---|---|---|---|---|
| - | 0.0° | 4.190 | 2.12908 | 11.500 |
| - | 5.0° | 5.902 | 2.13492 | 11.176 |
| 19 | 10.0° | 7.610 | 2.14519 | 10.849 |
| 20 | 15.0° | 9.313 | 2.15992 | 10.521 |
| 21 | 20.0° | 11.010 | 2.17916 | 10.191 |
| 22 | 25.0° | 12.701 | 2.20298 | 9.860 |
| 23 | 30.0° | 14.385 | 2.23151 | 9.529 |
| 24 | 35.0° | 16.063 | 2.26488 | 9.198 |
| - | 40.0° | * | * | * |

* *Spring Yielded*

moment value *increases* considerably with the *increase* in the pre-activation angle. This *increase* in the moment values resulted in the significant increase in the moment to force ratio value shown by the curve in Figure 4.35. The $M/F$ ratio at 1 $mm$ activation reaches 7 $mm$ for the 35° pre-activated vertical loop spring, which is up significantly form the 2 mm value of the typical spring.

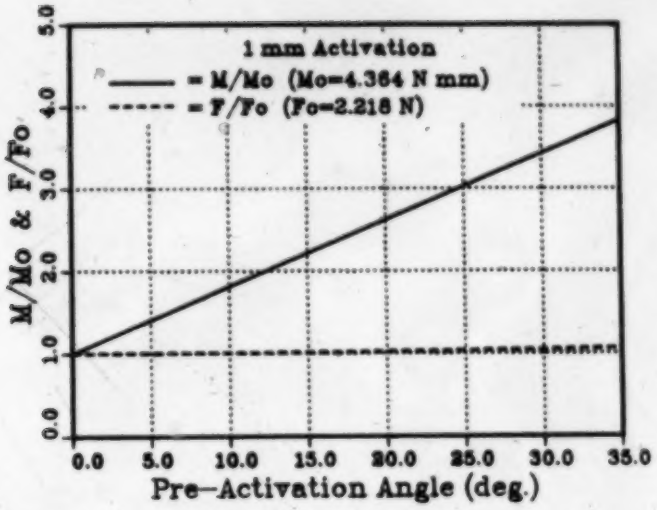


Figure 4.34: $M/M_o$ and $F/F_o$ for $TMA$ pre-activated vertical springs (0.016"×0.022" $TMA$ wire)

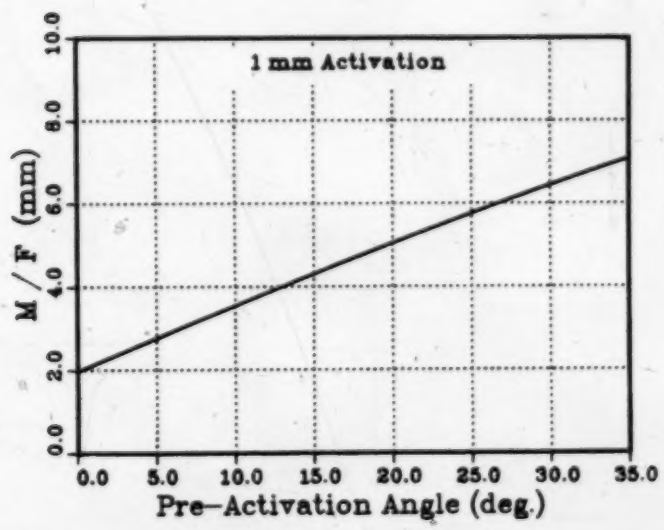


Figure 4.35: $M/F$ value for $TMA$ pre-activated vertical springs (0.016"×0.022" $TMA$ wire)

Table 4.14: Moments and forces of $TMA$ 35° pre-activated vertical spring

| *Act.(mm)* | *M (Nmm)* | *F (N)* | *I.B.D. (mm)* |
|---|---|---|---|
| 0.0 | 12.318 | 0.0 | 8.198 |
| 0.1 | 12.709 | 0.226 | 8.298 |
| 0.2 | 13.096 | 0.452 | 8.398 |
| 0.3 | 13.480 | 0.678 | 8.498 |
| 0.4 | 13.859 | 0.903 | 8.598 |
| 0.5 | 14.236 | 1.130 | 8.698 |
| 0.6 | 14.608 | 1.356 | 8.798 |
| 0.7 | 14.977 | 1.583 | 8.898 |
| 0.8 | 15.343 | 1.810 | 8.998 |
| 0.9 | 15.705 | 2.037 | 9.098 |
| 1.0 | 16.063 | 2.265 | 9.198 |
| 1.1 | 16.418 | 2.493 | 9.298 |
| 1.2 | 16.770 | 2.723 | 9.398 |
| 1.3 | * | * | 9.498 |

* *Spring Yielded*

In order to see how the 35° pre-activated vertical loop spring behaves over its activation range, a detailed analysis was performed on this spring to determine the values of the moments and forces generated by the different activation of this spring from 0 to 1.2 $mm$. The values of these moments and forces are listed in Table 4.14, which includes also the $I.B.D.$ corresponding to each activation. For activations higher than 1.2 $mm$ the spring would yield. The value of the moment at the neutral position (zero activation) is 12.318 $N\ mm$ which is a large initial value and this explains the higher moment to force ratio obtained at the higher activation for this spring design. The plot of this ratio for the different activations of the spring is

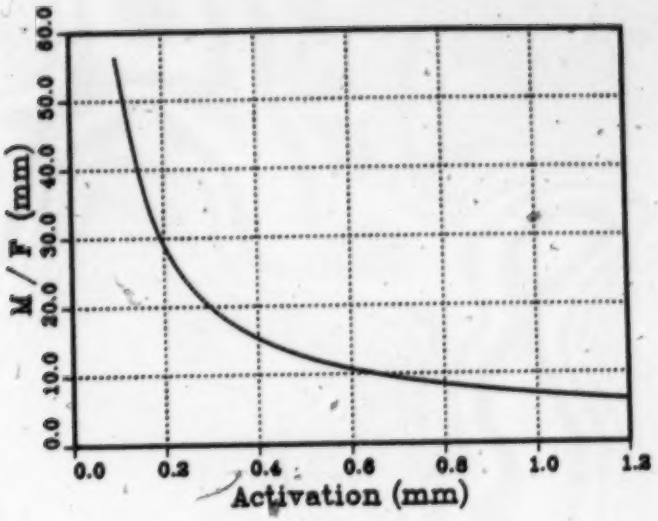


Figure 4.36: $M/F$ values of 35° $TMA$ pre-activated vertical spring (0.016"×0.022" $TMA$ wire)

shown of Figure 4.36. The curve in the figure indicates that for activations lower than 0.7 *mm* the moment to force ratio is higher than 10 *mm* with the force value being 1.583 $N$ at 0.7 *mm* activation. This is an improvement over the 10° stainless steel pre-activated vertical loop spring for which the value of $M/F$ would be higher than 10 *mm* only for activations below 0.2 *mm*.

In conclusion, the $TMA$ pre-activated vertical loop springs have much better mechanical characteristics, for closing space in the dental arch, than the typical vertical loops and the stainless steel pre-activated ones. The disadvantage, however, is the difficulty in forming $TMA$ wire to the desired shape.

### 4.2.6 Loop and Arm Helices Parametric Study

Various design modifications can be employed to the typical vertical loop spring design, in an attempt to overcome its major limitations of small activation range and low moment to force ratio. In this parametric study, the effect of adding helices to the spring loop and arm is studied to see whether such a modification would achieve the desired mechanical characteristics of an orthodontic spring.

The geometries of the different spring designs which will be discussed in this parametric study are shown Figure 4.37, in which the dimensions of the different sections of the springs are given on the drawings which are drawn with 4:1 scale. The material for these springs was chosen to be 0.016" × 0.022" $TMA$ wire. Spring # 25 is referred to as vertical spring with a loop helix, spring # 26 is identified by the added arm and loop helices, while springs # 27 and #28 are pre-activated vertical springs with arm and loop helices. The initial horizontal length of springs # 25 and #26 was chosen to be 12 $mm$, and in the case of the pre-activated springs #27 and #28 the arm length was varied so that the horizontal distance at the neutral position would be also 12 $mm$. The same initial horizontal length or neutral position for all the springs makes it more practical to compare the performance of the different spring designs, as they would have equal activation values for a given inter-bracket distance. The full activation range of each of these springs was analyzed usually in 0.25 $mm$ activation increments until the stress calculation routine of the program indicates that the spring stresses approach yield.

The analysis results for spring # 25 are listed in Table 4.15. This is a normal vertical loop spring with extra helix within the spring loop. As indicated in the table, this spring can be activated up to 3.5 $mm$ without yielding, which is a big improvement over the $TMA$ typical vertical loop spring which has an elastic activation

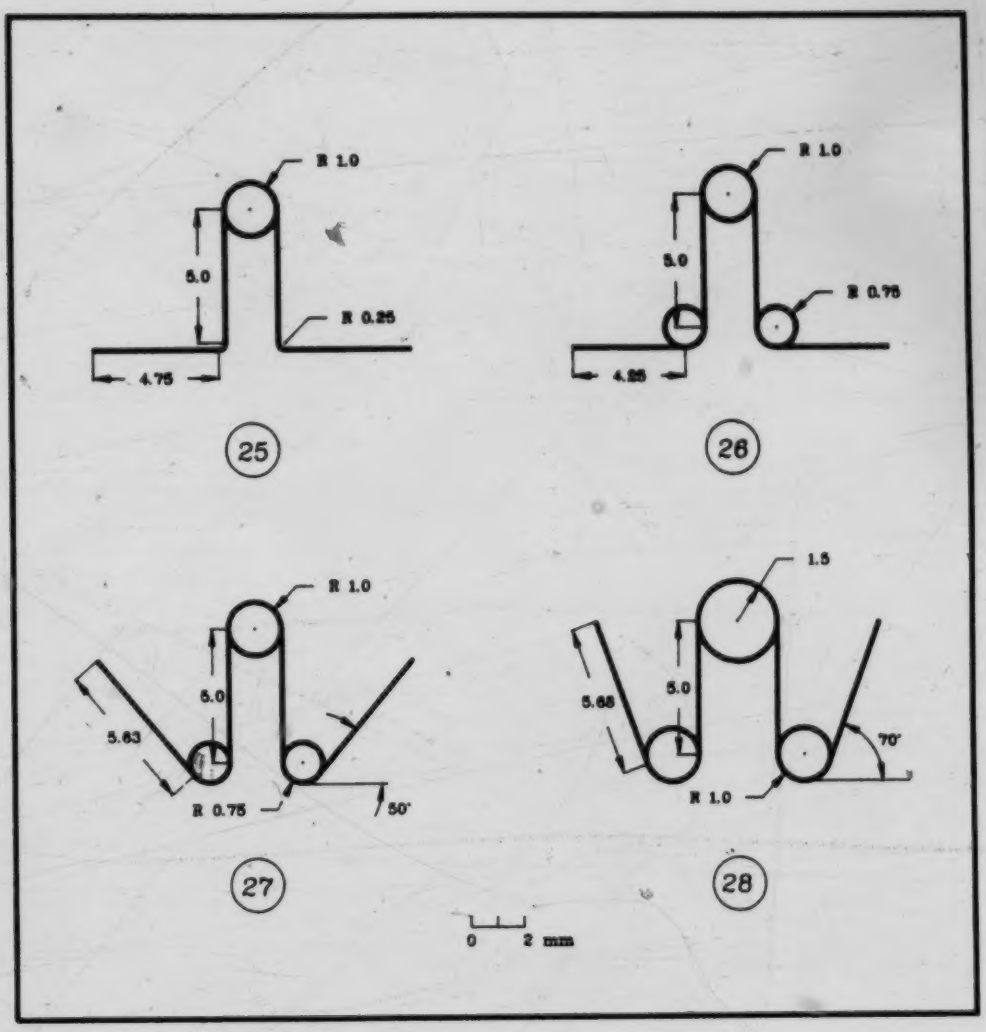


Figure 4.37: Vertical springs with loop and arm helices geometries
(0.016"×0.022" $\mathring{T}MA$ wire)

Table 4.15: Moments and forces for vertical spring with loop helix #25

| *Act.(mm)* | *M (Nmm)* | *F (N)* | *I.B.D. (mm)* |
|---|---|---|---|
| 0.0 | 0.0 | 0.0 | 12.0 |
| 0.1 | 0.347 | 0.131 | 12.1 |
| 0.2 | 0.692 | 0.263 | 12.2 |
| 0.4 | 1.379 | 0.531 | 12.4 |
| 0.6 | 2.060 | 0.805 | 12.6 |
| 0.8 | 2.736 | 1.084 | 12.8 |
| 1.0 | 3.406 | 1.371 | 13.0 |
| 1.25 | 4.236 | 1.739 | 13.25 |
| 1.5 | 5.056 | 2.119 | 13.5 |
| 1.75 | 5.867 | 2.510 | 13.75 |
| 2.0 | 6.669 | 2.923 | 14.0 |
| 2.25 | 7.460 | 3.350 | 14.25 |
| 2.5 | 8.240 | 3.796 | 14.5 |
| 2.75 | 9.008 | 4.260 | 14.75 |
| 3.0 | 9.764 | 4.753 | 15.0 |
| 3.25 | 10.506 | 5.270 | 15.25 |
| 3.5 | 11.233 | 5.816 | 15.5 |
| 3.75 | * | * | 15.75 |

* *Spring Yielded*

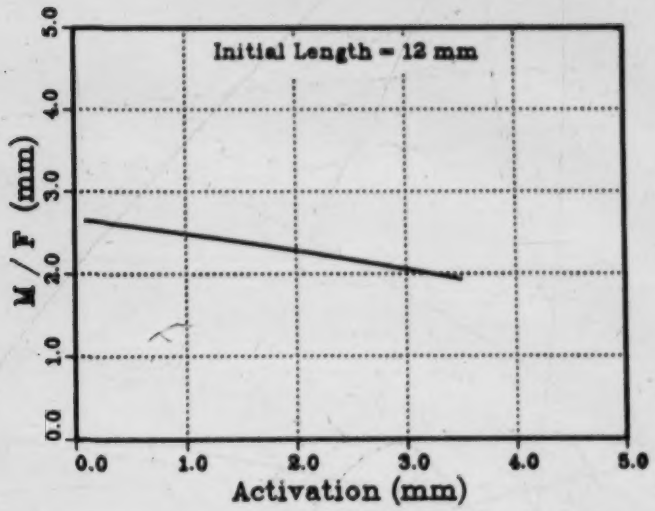


Figure 4.38: $M/F$ values for the vertical loop spring with loop helix (spring # 25, 0.016" × 0.022" $TMA$ wire)

range of only 2 $mm$. The increase in the activation range is due to the decrease in the moments and forces values. This decrease is caused by the added length and higher flexibility of the spring due to the existence of the loop helix.

The moment to force ratio of spring # 25 is plotted in Figure 4.38 for the different activation values. The ratio values for this spring design are slightly higher than the $M/F$ values of the typical vertical loop, but still much lower than the targeted values.

The second design modification to be considered in this parametric study is to add helices to the arms of the vertical loop spring with the loop helix. This design is shown as spring # 26 in Figure 4.37. The values of the moments and forces for the different activation values of this spring are listed in Table 4.16. Comparing these values to the moments and forces of the previous spring, one realizes that added arm helices cause a further reduction in the values of the forces and moments, which

Table 4.16: Moments and forces for vertical spring with loop and arm helices #26

| *Act.(mm)* | *M (Nmm)* | *F (N)* | *I.B.D. (mm)* |
|---|---|---|---|
| 0.0 | 0.0 | 0.0 | 12.0 |
| 0.25 | 0.564 | 0.233 | 12.25 |
| 0.5 | 1.124 | 0.471 | 12.5 |
| 0.75 | 1.679 | 0.714 | 12.75 |
| 1.0 | 2.231 | 0.963 | 13.0 |
| 1.25 | 2.780 | 1.218 | 13.25 |
| 1.5 | 3.325 | 1.481 | 13.5 |
| 1.75 | 3.866 | 1.751 | 13.75 |
| 2.0 | 4.404 | 2.030 | 14.0 |
| 2.25 | 4.939 | 2.319 | 14.25 |
| 2.5 | 5.470 | 2.619 | 14.5 |
| 2.75 | 5.998 | 2.931 | 14.75 |
| 3.0 | 6.521 | 3.256 | 15.0 |
| 3.25 | 7.042 | 3.597 | 15.25 |
| 3.5 | 7.559 | 3.953 | 15.5 |
| 3.75 | 8.071 | 4.329 | 15.75 |
| 4.0 | 8.578 | 4.724 | 16.0 |
| 4.25 | * | * | 16.25 |

* *Spring Yielded*

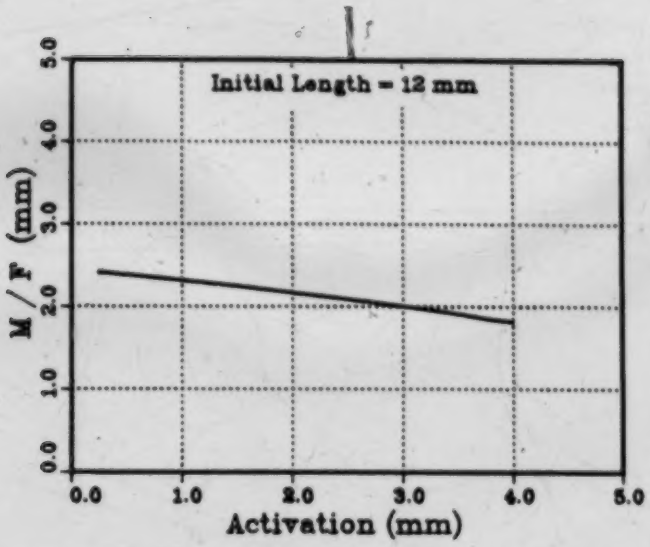


Figure 4.39: $M/F$ values for the vertical spring with loop and arm helices (spring # 26, 0.016" × 0.022" $TMA$ wire)

allowed this spring to have a slightly larger activation range (4.0 $mm$ compared to 3.5 $mm$ previous case).

The moment to force ratios of spring # 26 are plotted in Figure 4.39. As shown in the figure the M/F of this spring values are around the 2 $mm$ value. This leads to the conclusion that adding helices to the arms and the loop of the vertical spring will not increase the moment to force ratio. This is due to the fact that the rate of decrease in the absolute values of both the moments and forces, caused by the addition of the helices, is approximately the same.

Table 4.17: Moments and forces for 50° pre-activated spring with helices #27

| *Act.(mm)* | *M (N mm)* | *F (N)* | *I.B.D. (mm)* |
|---|---|---|---|
| 0.0 | 8.936 | 0.0 | 12.0 |
| 0.25 | 9.318 | 0.213 | 12.25 |
| 0.5 | 9.692 | 0.429 | 12.5 |
| 0.75 | 10.057 | 0.645 | 12.75 |
| 1.0 | 10.413 | 0.863 | 13.0 |
| 1.5 | 11.099 | 1.304 | 13.5 |
| 2.0 | 11.752 | 1.756 | 14.0 |
| 2.5 | 12.371 | 2.221 | 14.5 |
| 3.0 | 12.957 | 2.703 | 15.0 |
| 3.5 | 13.509 | 3.207 | 15.5 |
| 4.0 | 14.027 | 3.738 | 16.0 |
| 4.25 | 14.272 | 4.015 | 16.25 |
| 4.5 | * | * | 16.5 |

* *Spring Yielded*

The parametric study performed on the pre-activated vertical loop springs showed that pre-activation is a good technique to increase the moment to force ratio of the orthodontic springs, but there is limit to the size of the pre-activation angle. Furthermore, the maximum activation range of the pre-activated vertical loops was shown to be only in the 1 *mm* range before yielding occurs. However, one advantage of having an arm helix and a loop helix is that they allow for the arm to be bent to a larger pre-activation angles. This fact was employed in another design modification to the vertical loop spring in which the arms of spring #26 were pre-activated, to give spring # 27. The arm length was increased in this case so that the spring would have a 12 *mm* neutral position. The pre-activation angle of this spring is 50° as shown

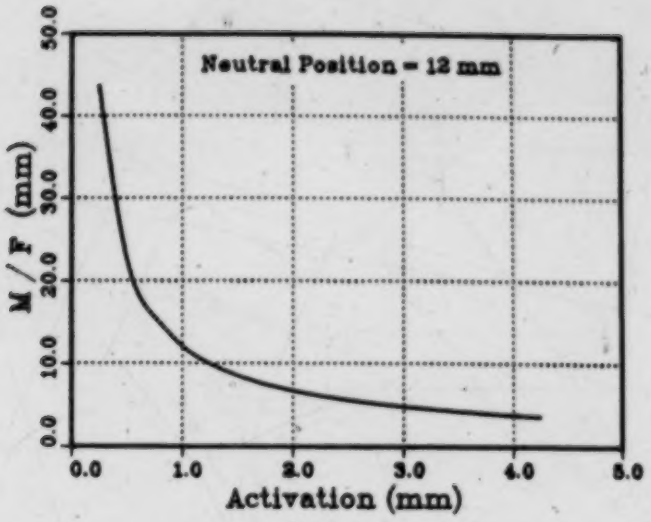


Figure 4.40: $M/F$ values for 50° pre-activated vertical spring with helices (spring # 27, 0.016" × 0.022" $TMA$ wire)

in the figure. This pre-activation angle was chosen such that the spring would have at least 4 $mm$ activation before yielding. The same criterion was followed in the selection of the pre-activation angle of spring # 28 shown in Figure 4.37.

The values of the moments and forces for the different activation values of spring # 27 are listed in Table 4.17, while the moment to force ratio of this spring is plotted in Figure 4.40. The curve in Figure 4.40 shows that the spring has a moment to force ratio higher than 10 mm for activations lower than 1.2 $mm$, with a force value equals to 0.86 $N$ at 1 $mm$ activation. This force value, even though it is low, is sufficient to achieve the tooth motion in most cases. However, the goal is to achieve the 10 $mm$ moment to force ratio for higher activations, which can be accomplished by increasing the radii of the helices.

The last spring analyzed in this parametric study is spring # 28 shown in Figure

4.37. In the design of this spring, the conclusions of the previous parametric studies were incorporated. As can be seen in the drawing of the spring, the radius of the arm helix was increased to 1 *mm*, and the loop helix radius was increased to 1.5 *mm*. The increased size of the helices allowed for a higher pre-activation angle of 70°. Moreover, this design modification allowed for a higher activation range of this spring to 5.25 *mm*. Table 4.18 summarizes the results of the analysis performed on this spring.

Comparing the force values of spring # 27 given in Table 4.17 with the force values of spring # 28, one realizes that the force values in the last case dropped significantly from the previous one. For example, at 2 *mm* activation the force value for spring # 27 is 1.756 *N*, while for spring # 28 it is equal to 1.106 *N*, which is about 40% lower than the previous value. This drop in the force value is the cause of the higher activation range for spring #28. As shown in Figure 4.41 these lower force values and the slightly higher moment values for this spring resulted in significantly higher values for the moment to force ratio of this vertical loop spring design. The curve in this figure indicates that the desired 10 *mm* moment to force ratio is achieved at 2.5 *mm* activation which is much better than all the previous vertical loop designs discussed earlier in this chapter. The mechanical characteristics of this spring approach the good characteristics of the pre-activated T-spring with, from clinicians point of a view, a less complicated design to duplicate than the T-spring. In addition, the width and height of this spring are less that of the typical pre-activated T-spring. From the above discussion it can concluded that vertical loop springs which have large loop radius, loop top and sides helices, and pre-activated arms, have the best mechanical features of all the design modification of the typical vertical loop spring. Their good features makes them strong candidates to replace the pre-activated T-springs, when and where tissue irritation is a concern, to achieve the desired goal of tooth translation without tipping.

Table 4.18: Moments and forces for 70° pre-activated spring with helices #28

| *Act.(mm)* | *M (N mm)* | *F (N)* | *I.B.D. (mm)* |
|---|---|---|---|
| 0.0 | 10.210 | 0.0 | 12.0 |
| 0.25 | 10.508 | 0.137 | 12.25 |
| 0.5 | 10.802 | 0.274 | 12.5 |
| 0.75 | 11.090 | 0.412 | 12.75 |
| 1.0 | 11.373 | 0.550 | 13.0 |
| 1.5 | 11.924 | 0.826 | 13.5 |
| 2.0 | 12.456 | 1.106 | 14.0 |
| 2.5 | 12.968 | 1.339 | 14.5 |
| 3.0 | 13.462 | 1.680 | 15.0 |
| 3.5 | 13.937 | 1.978 | 15.5 |
| 4.0 | 14.394 | 2.285 | 16.0 |
| 4.5 | 14.832 | 2.604 | 16.5 |
| 5.0 | 15.251 | 2.937 | 17.0 |
| 5.25 | * | * | 17.25 |

* *Spring Yielded*

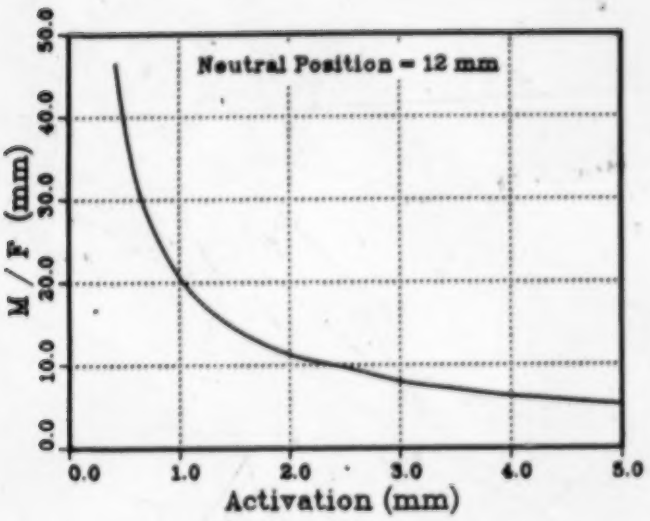


Figure 4.41: $M/F$ values for 70° pre-activated vertical spring with helices (spring # 28, 0.016" × 0.022" $TMA$ wire)

# Chapter 5

# Conclusions

The objective of this research was to develop a numerical technique that could be efficiently used in the analysis of orthodontic appliances. Of the several numerical techniques which have been used for these analyses, a segmental shooting technique (developed originally for the analysis of large deformation of initially straight flexible bars) has shown to have several advantages. The segmental technique equations were first modified so that not only the deformation of initially straight bars could be analyzed, but also bars with initial curvature. This has been done as orthodontic springs were be represented as a combination of initially straight and initially curved wire sections. These modified equations were incorporated in the development of a general computer code that is capable of analyzing a wide variety of orthodontic spring geometries including pre-activated springs either symmetric or non-symmetric and with various force and geometric boundary conditions. The analysis computation time of the segmental shooting technique is significantly less than the time required by the other techniques of analysis. This is due to the fact that the solutions for the forces and for a certain deformed shape are done in one step rather than several steps as it is the case for finite element and finite difference techniques. Furthermore, as

the solution is done as a series of initial value problems, there is no need for large computer memories unlike the finite element technique.

The analysis performed using the segmental shooting technique was verified analytically, numerically, and experimentally. The technique was tested, first, for the case of the deflection of an initially curved cantilever rod loaded by a horizontal force at the free end, and the results were compared to those obtained by the analytical solution given by Frisch-Fay [23]. Second, analysis of some standard T-springs were compared to the results obtained experimentally and by finite element and finite difference numerical techniques. Finally, a numerical and experimental comparison was performed for the analysis of a pre-activated T-spring. In all of these comparative studies, the output of the segmental shooting technique compared favourably to the other techniques. This is in addition to the fact that segmental approach gave similar results to the other numerical techniques with significantly less computational time.

Having verified the results of the segmental shooting technique, several parametric studies could be performed using the developed computer code. This was due to the fact that the time required to analyze some of the most complex orthodontic spring designs is less than 10 minutes on an IBM 386/387 microcomputer. The parametric studies evaluated the effect of changing some of the geometric parameters of the existing orthodontic springs designs as well as the effect of having different spring wire material and cross section dimensions. Moreover, new spring designs were analyzed to test their applicability in the orthodontic practice.

Two groups of parametric studies were performed, one on pre-activated T-springs and the second on vertical loop springs. The results of the pre-activated T-spring parametric studies revealed that the current typical design has a very good mechanical characteristics and is capable of achieving translational tooth movement. However, it was also shown that if the loop size was reduced by about 50% these good mechanical

characteristics would not be significantly altered, and this an advantage in terms of patient comfort. Another study on the pre-activated spring showed that bracket misalignment would result in different moment to force ratios at the two ends of the spring; this leads to different types of teeth movement at the posterior and anterior segments of the dental arch.

The parametric studies of the vertical loop spring indicated that by increasing the loop height and radius the low moment to force ratio that characterized this spring could be increased slightly. However, it was shown that pre-activation of the spring arms is the design modification to be employed in order to achieve significant increases in the moment to force ratio of this spring.

In conclusion, the computer model that has been developed to represent the mechanical behaviour of the orthodontic appliances is accurate, efficient and an excellent replacement of the previous analysis techniques.

# References


[1] **Mohl, N.D.**, "Introduction to Occlusion", In: Mohl, N., Zarb, G., Carlsson and G., Rugh, J. (eds), A Textbook of Occlusion, Ch. 1, Quintessence Co., 1988.

[2] **Caputo, A. and Standlee J.** , "Prerestorative Orthodontics". In: Caputo, A. and Standlee J., Biomechanics in Clinical Dentistry, Ch. 4, Quintessence Co., 1987.

[3] **Faulkner, M.G., Fuchshuber, P., Haberstock, D. and Mioduchowski, A.**, "A Parametric Study of the Force/Moment Systems Produced by T-Loop Retraction Springs". *Journal of Biomechanics*, (accepted for publication).

[4] **DePorter, D. and Zarb, G.**, "The Periodontium". In: Mohl, N., Zarb, G., Carlsson, G., Rugh, J. (eds), A Textbook of Occlusion, Ch. 1, Quintessence Co., 1988.

[5] **Quinn, R.S. and Yoshikawa, D.**, " A Reassessment of Force Magnitude in Orthodontics", *American Journal of Orthodontics*, Vol. 88, No. 3, pp. 252-260, 1985.

[6] **Smith, R.J. and Burstone, C.J.**, "Mechanics of Tooth Movement", *American Journal of Orthodontics*, Vol. 85, No.4, pp. 294-307, 1984.

[7] **Tanne, K., Koenig, H.K. and Burstone, C.J.**, "Moment to Force Ratios and the Center of Rotation", *American Journal of Orthodontics and Dentofacial Orthopedics*, Vol. 94, No. 5, pp. 426-431, 1988.

[8] **Burstone, C.J.**, "Application of Bioengineering to Clinical Orthodontics", In: Graber, T.M. and Swain, B.F. (eds), Current Orthodontic Concepts and Techniques, Vol. 1, Ch. 5, W.B. Sanders Co., 1975.

[9] **Burstone, C.J.**, "The Segmented Arch Approach to Space Closure", *American Journal of Orthodontics*, Vol. 82, No. 5, pp. 361-378, 1982.

[10] **Paulich, S.**, "Measuring of Orthodontic Forces", *American Journal of Orthodontics and Oral Surgery*, Vol. 25, pp. 817-849, 1939.

[11] **Solonche, D.J., Burstone, C.J. and Ratches, J.**, " A Computer Controlled Device For Determining the Mechanical Behaviour of Orthodontic Appliances", Abstract, 30th Annual Conference on Engineering in Medicine and Biology, Los Angeles, Nov. 1977.

[12] **Paquien, J.**, "The Measurement of Forces and Moments Delivered by Dental Appliances", M.Sc. Thesis, The University of Manitoba, 1978.

[13] **Faulkner, M.G., Hay, A., Fuchshuber, P. and Haberstock, D.**, "Development of a System for the Measurement of Forces and Moments Created by Orthodontic Appliances", *Proceedings of the VI International Congress on Experimental Mechanics*, Vol. 1, pp. 384-389, 1988.

[14] **Waters, N.E., Stephens, C.D. and Houston W.J.**, " The Mechanics of Plain and Looped Arches: Part 2", *British Journal of Orthodontics*, Vol.3, pp. 161-167, 1975.

[15] **Koenig, H.A. and Burstone, C.J.**, " Analysis of Generalized Curved Beams for Orthodontic Applications", *Journal of Biomechanics*, Vol. 7, pp. 429-435, 1974.

[16] **DeFranco, J.C., Koenig, H.A and Burstone, C.J.**, "Three Dimensional Large Displacement Analysis of Orthodontic Appliances", *Journal of Biomechanics*, Vol. 9, pp. 793-801, 1976.

[17] **Yang, T.Y. and Baldwin, J.J.**, "Analysis of Space Closing Springs in Orthodontics", *Journal of Biomechanics*, Vol. 7, pp. 21-28, 1974.

[18] **Grief, R., Coltman, M., Gailus, M. and Shapiro, E.**, "Force Generation From Orthodontic Appliances", *Journal of Biomechanical Engineering*, Vol. 104, pp. 280-289, 1982.

[19] **Miyakawa, O. and Shiokawa, N.**, "A New Method for Finite Element Simulation of Orthodontic Appliance - Teeth - Periodontium - Alveolus System", *Journal of Biomechanics*, Vol. 18, No. 4, pp. 277-284, 1985.

[20] **Fuchshuber, P.**, "An Experimental and Numerical Analysis of Orthodontic T Springs", M.Sc. Thesis, University of Alberta, 1987.

[21] **Faulkner, M.G. and Stredulinsky, D.C.**, "Nonlinear Bending of Inextensible Thin Rods Under Distributed and Concentrated Loads", *Transactions of the C.S.M.E*, Vol. 4, No. 2, 1977.

[22] **Stredulinsky, D.**, "Large Deformations of Thin Inextensible Elastic Rods", M.Sc. Thesis, University of Alberta, 1975.

[23] **Frisch-Fay, R.**, Flexible Bars, Chapter 4, Butterworths, 1962.

[24] **Koenig, H.A., Vanderby, R., Solonche, D.J. and Burstone, C.J.**, "Force Systems From Orthodontic Appliances: An Analytical Experimental Comparison", *Journal of Biomechanical Engineering*, Vol. 102, pp. 294-300, 1980.

[25] **Goldberg, A., Vanderby, J. and Burstone, C.J.**, "Reduction in the Modulus of Elasticity in Orthodontic Wires", *Journal of Dental Research*, Vol. 56 No. 10, pp. 1227-1231, 1977.

[26] **Kusy, R.P. and Greenberg, A.R.**, "Effects of Composition and Cross Section on the Elastic Properties of Orthodontic Wires", *The Angle Orthodontist*, Vol. 51, No. 4, pp. 325-341, 1981.

[27] **Burstone C.J. and Koenig, H.A.**, "Optimizing Anterior and Canine Retraction", *American Journal of Orthodontics*, Vol. 70, No. 1, pp. 1-16, 1976.

# Appendix A

# Segmental Shooting Technique Program Listing

The source code of the segmental shooting technique program is listed below. The programming language used is **Turbo Pascal**. The program is composed of **GLOBE, INPUT**, and **PLOT** units as well as the main **SEGTEC** program. The declaration of the input data records and the global variables of the program is done in the **GLOBE** unit (pages 139-141). The **INPUT** units contains the parameters and geometry input routines (procedures) that allow the program to be user friendly (pages 142-149), while the **PLOT** unit is composed of the plotting routines which enable the plotting of the deformed geometries of the springs on the screen (pages 150-153). The **SEGTEC** main program contains the boundary input routines (pages 157-163), the segmental technique routines (pages 163-170), the shooting and Newton-Raphson routines for 1, 2 and 3 unknowns (pages 170-174) and the stress calculation routine (pages 175-176).

```
{*************************************************************************}
{*                                                                       *}
{* ---------------------- University of Alberta ----------------------- *}
{* ----------------- Mechanical Engineering Department ----------------- *}
{*                                                                       *}
{* ============   Orthodontic Springs Analysis Program  ============== *}
{*                                                                       *}
{*                                                                       *}
{*       This program numerically analyses orthodontic springs using     *}
{*   the Segmental Shooting Technique to determine the forces,moments    *}
{*   and the deformed geometries of the activated springs.               *}
{*                                                                       *}
{*                                                                       *}
{*                    K O S A Y    E L - R A Y E S                       *}
{*                                                                       *}
{*                          M.Sc.  June, 1989                            *}
{*                                                                       *}
{*                                                                       *}
{*  Copyright © 1989                                                     *}
{*  All rights reserved. No part of the software may be reproduced or    *}
{*  distributed in any form or by any means, without the prior written   *}
{*  permission of the author.                                            *}
{*                                                                       *}
{*************************************************************************}

{*********************   definition of variables   **********************
 *                                                                       *
 *   M1    = Moment at the starting node of segment                      *
 *   V1    = Shear at the starting node of segment                       *
 *   M1    = Tension at the starting node of segment                     *
 *   MU1   = non-dimentional Moment  at the starting node of the segment *
 *   NU1   = non-dimentional Shear   at the starting node of the segment *
 *   TAU1  = non-dimentional Tension at the starting node of the segment *
 *   M2    = Moment at the ending node of segment                        *
 *   V2    = Shear at the ending node of segment                         *
 *   M2    = Tension at the ending node of segment                       *
 *   MU2   = non-dimentional moment at the ending node of the segment    *
 *   NU2   = non-dimentional shear at the ending node of the segment     *
 *   TAU2  = non-dimentional Tension at the ending node of the segment   *
 *   H     = difference in height between the two nodes of the segment   *
 *   BETA  = the angle from the local x-axis to tangent at the start node*
 *   FAY   = the angle from the local x-axis to tangent at the end node  *
 *   GAMA  = the angle from the global X-axis to tangent at of each node *
 *   XS    = the global X-coordinate of each node                        *
 *   YS    = the global Y-coordinate of each node                        *
 *   DELTA= segment length                                               *
 *   RAD   = radius of curvature of the segment                          *
 *   EI    = Spring wire stiffness                                       *
 *                                                                       *
 *************************************************************************}

UNIT GLOBE;

INTERFACE
{*************       ORTHODONTAL SPRINGS GENERAL PROGRAM       ***********}

        TYPE    REAL=DOUBLE;
```

```
TYPE    INPUTDATA=RECORD
        CASEN,N,NUM,NP:                                  INTEGER;
        E,INR,TOL,YIELD:                                 REAL;
        DIAM,WIDTH,HEIGTH,AREA:                          REAL;
        DELTAS,RADS:ARRAY[1..30] OF                      REAL;
        NS:ARRAY[1..30] OF                               INTEGER;
        END;

TYPE    INPUTFORCES=RECORD
        XG1,YG1,GAMA1:                                   REAL;
        MOMENT,TENSION,SHEAR:                            REAL;
        INVAL,QS:ARRAY[1..6] OF                          REAL;
        XPOS,YPOS,ACT:                                   REAL;
        UN,MFLAG,TFLAG,SFLAG,LF:                         INTEGER;
        UNK:ARRAY[1..6] OF                               INTEGER;
        MVL,TVL,SVL:STRING[10];
        END;

TYPE    ARR5=ARRAY[0..20] OF                             REAL;
        ARR6=ARRAY[1..3,1..3] OF                         REAL;
        ARR7=ARRAY[1..3] OF                              REAL;
        ARR9=ARRAY[1..30] OF                             REAL;
        ARR10=ARRAY[1..6] OF                             REAL;
        ARR13=ARRAY[0..80,1..3] OF                       REAL;
        ARR14=ARRAY[1..3] OF                             REAL;
        ARR4=ARRAY[1..30] OF                             INTEGER;
        ARR8=ARRAY[1..10000] OF                          INTEGER;
        ARR11=ARRAY[1..6] OF                             INTEGER;
        STR=STRING[10];

VAR     X1,Y1,GAMMA1,X2,Y2,GAMMA2:                       REAL;
        MU1,MU2,TAU1,TAU2,NU1,NU2,H,R:                   REAL;
        M1,M2,T1,T2,V1,V2,B1,G1,D1:                      REAL;
        BETA,GAMA,FAY:                                   REAL;
        XG,YG,X,Y:                                       REAL;
        PLOT:FILE OF                                     REAL;
        DELTA,RAD:                                       REAL;
        LENG,LENG3,CHECK,CHECK2,CHECK3:                  REAL;
        F1F110,F1F101,F1F011,F1F111:                     REAL;
        F2F110,F2F101,F2F011,F2F111:                     REAL;
        F3F110,F3F101,F3F011,F3F111:                     REAL;
        F1F10,F1F01,F1F11:                               REAL;
        F2F10,F2F01,F2F11:                               REAL;
        FF1,FF0:                                         REAL;
        WF1,WF2,WF3:                                     REAL;
        SF,STRESS,STRESST,STRESSM,CENTER:                REAL;
        SEGT,SEGMAX,SEGMIN,SHEARSTRESS,CX:               REAL;
        RADIUS,TMAX,TENMAX,SHEARMAX:                     REAL;
        MOM,FORC,MFR,sheer:                              REAL;
        DD,angle,act:                                    REAL;
        LENGTH,EI,LOAD,MUE,M:                            REAL;
        R1,R2,ANG,WF:                                    REAL;
        MINLAPS,SECLAPS,JYMAX,JSMAX,THOULAPS:INTEGER;
        JMIN,JLD,percent,COUNTER,JYLD:                   INTEGER;
        I,J,K,L,MM,W,KK,CODE,NPLOT,LF:                   INTEGER;
        FLAG1,FLAG2,FLAG3,FLAG4,FLAG5,CHOICE:INTEGER;
        NU,NN,N,CASEN:                                   INTEGER;
```

```
                XYDATA:FILE OF                          INTEGER;
                OPTION:                                 INTEGER;
                Z:ARR13;
                ZZ:ARR14;
                INP:INPUTDATA;
                BD:INPUTFORCES;
                ALPHA:ARR5;
                JAC:ARR6;
                FUN,DIF:ARR7;
                CH,SYMMETRIC,DUM:CHAR;
                IV,ST1,ST2,ST3:STRING[12];
                OLDPIX,YPIX,NEWPIX,POS:BYTE;
                NEWPIX1,NEWPIX2,NEWPIX3:BYTE;
                XPL,YPL:ARR8;
                NAME,IPD,VL,PT,FNAME:STRING[12];
                RADS,DELTAS:ARR9;
                P,Q:ARR10;
                FST:STRING[12];
                NS:ARR4;
                INDATA:FILE OF INPUTDATA;
                BCOND:FILE OF INPUTFORCES;
                GIM,PRT,OUT,GEOM:TEXT;
                month,day,year,dayofweek:WORD;
                HOUR1,MINUTE1,SECOND1,SEC1001:WORD;
                HOUR2,MINUTE2,SECOND2,SEC1002:WORD;
                INFO,IV2:STRING[80];
                GOON:BOOLEAN;

IMPLEMENTATION
END.
```

```
UNIT INPUT;
{$N+}
INTERFACE
USES CRT,
     GRAPH,
     PRINTER,
     DOS,
     GLOBE;

PROCEDURE NEWDATA;
PROCEDURE LOADDATA;
PROCEDURE EDITDATA;
PROCEDURE PRINTDATA;
PROCEDURE READREAL(VAR RVAR:REAL);
PROCEDURE READINT(VAR IVAR:INTEGER);
PROCEDURE DIRECTORY(ST1,ST2:STR);

IMPLEMENTATION

{******************** VARIABLE READING PROCEDURES   ********************}
     {--------------READ REAL---------------}
PROCEDURE READREAL(VAR RVAR:REAL);
  LABEL S10;
  VAR IV:STRING[20];
  CODE:INTEGER;
  BEGIN
 {$R-}
S10: READLN(IV);
     VAL(IV,RVAR,CODE);
   _ IF CODE <> 0 THEN
             BEGIN
      WRITELN('          !!!!!   Improper input. Please Try again.  !!!!!! ');
             GOTO S10;
             END;
 {$R+}
 END;
    {---------------READ INTEGER---------------}

PROCEDURE READINT(VAR IVAR:INTEGER);
  LABEL S10;
  VAR IV:STRING[20];
  CODE:INTEGER;
  BEGIN
 {$R-}
S10: READLN(IV);
     VAL(IV,IVAR,CODE);
     IF CODE <> 0 THEN
             BEGIN
      WRITELN('          !!!!!   Improper input. Please Try again.  !!!!!! ');
             GOTO S10;
             END;
 {$R+}
 END;

{********************   LISTING OF DATA FILES PROCEDURE  ******************}

PROCEDURE DIRECTORY(ST1,ST2:STR);
```

```
        VAR     DIRINFO:SEARCHREC;
        BEGIN
                GOTOXY(1,15);
                ST3:=ST1+'*'+ST2;
                FINDFIRST(ST3,ARCHIVE,DIRINFO);
                WHILE DOSERROR=0 DO
                        BEGIN
                                WRITE('    ',DIRINFO.NAME);
                                FINDNEXT(DIRINFO);
                        END;
                WRITELN;
    END;

{*************************    INPUTING NEW DATA    *************************}

PROCEDURE NEWDATA;
BEGIN
  CLRSCR;
  GOTOXY(1,4);
  TEXTCOLOR(WHITE);
  WRITELN('                              N E W    D A T A    I N P U T ');
  WRITELN('                              ~~~~~~~~~~~~~~~~~~~~~~~~~~~~~ ');
  WRITELN;
  TEXTCOLOR(LIGHTCYAN);
  WRITE('                        Input the number of different sections : ');
  READINT(INP.NUM);
  WRITE('                        Input total number of segments for the spring : ');
  READINT(INP.N);
  WRITE('                        Input solver tolerance value  eg.(1E-8)  : ');
  READREAL(INP.TOL);
  WRITE('                        Input Young's Modulus (MPa)      : ');
  READREAL(INP.E);
  WRITE('                        Input Yield strength (MPa)       : ');
  READREAL(INP.YIELD);
  WRITELN;
  WRITE('              Is the cross section Rectangular "R" or Circular "C" ? ');
  REPEAT
    CH := READKEY;
    CH := UPCASE(CH);
  UNTIL CH IN ['C','R'];
  WRITELN(ch);
  IF CH='R' THEN
      BEGIN
        WRITE('                        Input the cross section Width (inches): ');
        READREAL(INP.WIDTH);
        INP.WIDTH:=INP.WIDTH*25.4;
        WRITE('                        Input the cross section Height (inches): ');
        READREAL(INP.HEIGTH);
        INP.HEIGTH:=INP.HEIGTH*25.4;
        INP.AREA:=INP.WIDTH*INP.HEIGTH;
        INP.INR:=INP.HEIGTH*SQR(INP.HEIGTH)*INP.WIDTH/12.0;
        INP.DIAM:=0.0;
      END;
    IF CH='C' THEN
       BEGIN
        WRITE('                        Input the cross section Diameter (inches): ');
        READREAL(INP.DIAM);
```

```
      INP.DIAM:=INP.DIAM*25.4;
      INP.AREA:= PI*SQR(INP.DIAM)/4;
      INP.INR:= PI*SQR(INP.DIAM)*SQR(INP.DIAM)/64;
      INP.WIDTH:=0.0;
      INP.HEIGTH:=0.0;
     END;
EI:=INP.E*INP.INR;
FOR KK:=1 TO INP.NUM DO
     BEGIN
     CLRSCR;
     TEXTCOLOR(WHITE);
     GOTOXY(1,4);
     WRITELN('                                    G E O M E T R Y');
     WRITELN('                                    ~~~~~~~~~~~~~~~');
     TEXTCOLOR(LIGHTCYAN);
     WRITELN;
     WRITELN('                                Geometry for Section ',KK);
     WRITELN;
     WRITE('                        Is the section Curved "C"  or Straight "S" ?');
     REPEAT
        CH := READKEY;
        CH := UPCASE(CH);
        UNTIL CH IN ['C','S'];
        WRITELN(ch);
        IF CH='C' THEN
        BEGIN
        WRITE('                                 Angle (degrees)              = ');
        READREAL(ANGLE);
        WRITE('                                 Radius of curvature (mm)     = ');
        WRITELN('                              Counterclockwise is positive.');
        READREAL(INP.RADS[KK]);
        WRITE('                                 Number of segments           = ');
        READINT(INP.NS[KK]);
        LENG:=ANGLE*PI/180*ABS(INP.RADS[KK]);
        INP.DELTAS[KK]:=LENG/INP.NS[KK];
        END;
        IF CH='S' THEN
        BEGIN
        WRITE('                                 Length (mm)                  = ');
        READREAL(LENG);
        WRITE('                                 Number of segments           = ');
        READINT(INP.NS[KK]);
        INP.RADS[KK]:=1.0E30;
        INP.DELTAS[KK]:=LENG/INP.NS[KK];
        END;
      WRITELN('                        ******************************************');
      END;
      WRITELN;
      CLRSCR;
      GOTOXY(1,4);
      TEXTCOLOR(WHITE);
      WRITELN('                          S A V I N G   I N P U T E D   D A T A ');
      WRITELN('                          ~~~~~~~~~~~~~~~~~~~~~~~~~~~~~~~~~~~');
      WRITELN;
      TEXTCOLOR(LIGHTCYAN);
      WRITE('                                 Geometry file name : ');READLN(IPD);
      IPD:=IPD+'.DAT';
      ASSIGN(INDATA,IPD);REWRITE(INDATA);
```

```
        WRITE(INDATA,INP);
        CLOSE(INDATA);
END;

{************************ LOADING THE DATA ***********************************}

PROCEDURE LOADDATA;
BEGIN
{$I-}
  CODE:=99;
  CLRSCR;
  REPEAT
    TEXTCOLOR(WHITE);
    GOTOXY(1,4);
    WRITELN('                                D A T A   L O A D I N G');
    WRITELN('                                ~~~~~~~~~~~~~~~~~~~~~~~');
    WRITELN;
    TEXTCOLOR(LIGHTCYAN);
    WRITE('                  Input data file name or type "L" to list files : ');
    READLN(IPD);
    IF (IPD='L') OR (IPD='l')  THEN
      BEGIN
        WRITELN;
        WRITE('                                  Input the path "e.g. D:\TURBO" : ');
        READLN(IPD);
        ST1:=IPD;
        ST2:='.DAT';
        CLRSCR;
        DIRECTORY(ST1,ST2);
      END
      ELSE
        BEGIN
        IPD:=IPD+'.DAT';
        ASSIGN(INDATA,IPD);RESET(INDATA);
        CODE:=IORESULT;
        IF CODE <> 0 THEN
        GOTOXY(1,23);
        WRITELN('                          File was not found.    Please try again. ');
        END;
   UNTIL CODE=0;
{$I+}
        READ(INDATA,INP);
        EI:=INP.E*INP.INR;
  END;

{************************   EDITING THE DATA   ***************************}

PROCEDURE EDITDATA;
LABEL S1000,S2000;
BEGIN
CLRSCR;
TEXTCOLOR(WHITE);
GOTOXY(1,4);
WRITELN('                                D A T A   E D I T I N G');
WRITELN('                                ~~~~~~~~~~~~~~~~~~~~~~~');
WRITELN;
TEXTCOLOR(LIGHTCYAN);
WRITELN('                          1. Total number of  segments');
```

```
WRITELN('                              2. Solver tolerance value   ');
WRITELN('                              3. Young's modulus          ');
WRITELN('                              4. Material Yield strength  ');
WRITELN('                              5. Wire cross section       ');
WRITELN('                              6. Geometry                 ');
WRITELN('                              7. Exit data editing');
WRITELN;
WRITE('                          Number of the parameter to be edited ====> ');
GOON:=FALSE;
REPEAT;
  CH := READKEY;WRITELN(CH);
  IF CH IN ['1','2','3','4','5','6','7'] THEN GOON := TRUE;
  IF NOT GOON THEN
  WRITELN(' Use only a number between 1 and 7.    Please try again.');
UNTIL  GOON;
CASE CH OF
  '7':BEGIN
        WRITELN;
        WRITE(' Would you like to save the changes in data  Y/N : ');
        REPEAT
          CH := READKEY;
          CH := UPCASE(CH);
        UNTIL CH IN ['Y','N'];
        WRITELN(ch);
        IF CH='Y' THEN
           BEGIN
           WRITE('                              Name of new data file : ');
           READLN(IPD);
           IPD:=IPD+'.DAT';
           ASSIGN(INDATA,IPD);REWRITE(INDATA);
           WRITE(INDATA,INP);
           CLOSE(INDATA);
           END;
           EXIT;
     END;
  '1':BEGIN
        WRITE('  Number of segments = ',INP.N,'     New value = ');
        READINT(INP.N);
      END;
  '2':BEGIN
        WRITE('  Tolerance value    = ',INP.TOL,'   New value = ');
        READREAL(INP.TOL);
      END;
  '3':BEGIN
        WRITE('  Young's modulus  = ',INP.E:9:0,'   New value = ');
        READREAL(INP.E);
      END;
  '4':BEGIN
        WRITE('  Yield strength   = ',INP.YIELD:3:4,' New value = ');
        READREAL(INP.YIELD);
      END;
  '5':BEGIN
        WRITE(' Is the cross section Rectangular "R" or Circular "C"  ?');
        REPEAT
          CH := READKEY;
          CH := UPCASE(CH);
        UNTIL CH IN ['C','R'];
        WRITELN(ch);
```

```
      IF CH='R' THEN
      BEGIN
      WRITELN;
      WRITE('                Input the cross section Width (inches) : ');
      READREAL(INP.WIDTH);
      INP.WIDTH:=INP.WIDTH*25.4;
      WRITELN;
      WRITE('                Input the cross section Height (inches): ');
      READREAL(INP.HEIGTH);
      INP.HEIGTH:=INP.HEIGTH*25.4;
      INP.AREA:=INP.WIDTH*INP.HEIGTH;
      INP.INR:=INP.HEIGTH*SQR(INP.HEIGTH)*INP.WIDTH/12.0;
      INP.DIAM:=0.0;
      END;
      IF CH='C' THEN
      BEGIN
      WRITELN;
      WRITE('                    Input the cross section Diameter (inches): ');
      READREAL(INP.DIAM);
      INP.DIAM:=INP.DIAM*25.4;
      INP.AREA:= PI*SQR(INP.DIAM)/4;
      INP.INR:= PI*SQR(INP.DIAM)*SQR(INP.DIAM)/64;
      INP.WIDTH:=0.0;
      INP.HEIGTH:=0.0;
      END;
      EI:=INP.E*INP.INR;
    END;
'6':BEGIN
      S2000: CLRSCR;
      GOTOXY(1,4);
      TEXTCOLOR(WHITE);
      WRITELN('          S E C T I O N   D E S C R I P T I O N ');
      WRITELN('    ************************************************');
      WRITELN('    * Pt.#     # of Seg:    Leng.       Angle        Radius *');
      WRITELN('    ************************************************');
      FOR W:=1 TO INP.NUM DO
          BEGIN
          LENG:=INP.DELTAS[W]*INP.NS[W];
          ANGLE:=LENG/ABS(INP.RADS[W])*180/PI;
          WRITE('                *',W:3);
          WRITE(INP.NS[W]:9,LENG:13:3,ANGLE:12:2,'        ');
          IF INP.RADS[W]>1.0E15 THEN WRITELN('  ---      *');
          IF INP.RADS[W]<1.0E15 THEN WRITELN(INP.RADS[W]:7:4,'    *');
          END;
      WRITELN('    ************************************************');
      WRITELN;
      TEXTCOLOR(LIGHTCYAN);
      WRITELN('                          Input 0 to exit geometry editing.');
      WRITELN;
      WRITE('                         Input part number to be changed  ===> ');
      READINT(W);
      IF W=0 THEN GOTO S1000;
      WRITE('                 Is the section Curved "C"  or Straight "S" : ');
      REPEAT
        CH := READKEY;
        CH := UPCASE(CH);
      UNTIL CH IN ['C','S'];
      WRITELN(ch);
```

```
            IF CH='C' THEN
               BEGIN
               WRITE('                                Angle (degrees)          = ');
               READREAL(ANGLE);
               WRITE('                                Radius of curvature (mm) = ');
               READREAL(INP.RADS[W]);
               WRITE('                                Number of segments       = ');
               READINT(INP.NS[W]);
               LENG:=ANGLE*PI/180*ABS(INP.RADS[W]);
               INP.DELTAS[W]:=LENG/INP.NS[W];
               END;
            IF CH='S' THEN
               BEGIN
               WRITE('                                Length (mm)              = ');
               READREAL(LENG);
               WRITE('                                Number of segments       = ');
               READINT(INP.NS[W]);
               INP.RADS[W]:=1.0E30;
               INP.DELTAS[W]:=LENG/INP.NS[W];
               END;
            GOTO S2000;
    S1000:
            END;
            END;        { END OF THE CASE }
            EI:=INP.E*INP.INR;
            EDITDATA;
            END;

    {*******************   PRINT DATA PROCEDURE   ************************}

    PROCEDURE PRINTDATA;
     BEGIN
      CLRSCR;
      GOTOXY(1,8);
      WRITELN('                    Specify the LISTING device : ');
      WRITELN;
      WRITELN('    1. Screen       2. Printer      3. Save as a TEXT file ');
      WRITELN;
      WRITE('                                 =====>  ');
      GOON:=FALSE;
      REPEAT;
       CH := READKEY;WRITELN(CH);
       IF CH IN ['1','2','3'] THEN GOON := TRUE;
       IF NOT GOON THEN
       WRITELN('    Use only a number between 1 and 3.   Please try again.');
      UNTIL  GOON;
      CASE CH OF
            '1':ASSIGN(PRT,'');
            '2':ASSIGN(PRT,'PRN');
            '3':BEGIN
                WRITE('                              Input geometry file name : ');
                READLN(IPD);
                ASSIGN(PRT,IPD);
                END;
      END;
      REWRITE(PRT);
      CLRSCR;
      WRITELN(PRT);WRITELN(PRT);
```

```
  WRITELN(PRT);WRITELN(PRT);
  WRITELN(PRT,'************ I N P U T   P A R A M E T E R S ********** ');
  WRITELN(PRT);
  WRITELN(PRT);
  WRITELN(PRT,'           Number of different parts = ',INP.NUM);
  WRITELN(PRT,'           Total number of segments  = ',INP.N);
  WRITELN(PRT,'           Tolerance value           = ',INP.TOL);
  WRITELN(PRT,'           Young's modulus (MPa)     = ',INP.E:6:0);
  WRITELN(PRT,'           Yield strength (MPa)      = ',INP.YIELD:5:2);
  IF INP.DIAM=0.0 THEN
    BEGIN
        WRITELN(PRT,'    Cross section width       = ',INP.WIDTH:3:6,' mm');
        WRITELN(PRT,'    Cross section height      = ',INP.HEIGTH:3:6,' mm');
    END;
  IF INP.WIDTH=0.0 THEN
        WRITELN(PRT,'    Cross section diameter    = ',INP.DIAM:3:6,' mm');
        WRITELN(PRT,'    Cross section area        = ',INP.AREA:3:6,' mm^2');
        WRITELN(PRT,'    Moment of inertia         = ',INP.INR:3:6,' mm^4');
        WRITELN(PRT);WRITELN(PRT);
        TEXTCOLOR(YELLOW);
        GOTOXY(29,24);
        WRITELN('Press any key to continue  ');
        CH:=READKEY;
        TEXTCOLOR(WHITE);
        CLRSCR;
        WRITELN(PRT);WRITELN(PRT);
        WRITELN(PRT,'          S E C T I O N   D E S C R I P T I O N ');
        WRITELN(PRT,'*************************************************');
        WRITELN(PRT,'* Pt.#    # of Seg     Leng.       Angle       Radius  *');
        WRITELN(PRT,'*************************************************');
        FOR W:=1 TO INP.NUM DO
        BEGIN
                LENG:=INP.DELTAS[W]*INP.NS[W];
                        ANGLE:=LENG/ABS(INP.RADS[W])*180/PI;
                WRITE(PRT,'                *',W:3);
                WRITE(PRT,INP.NS[W]:9,LENG:13:3,ANGLE:12:2,'        ');
                IF INP.RADS[W]>1.0E15 THEN WRITELN(PRT,'    -       *');
                IF INP.RADS[W]<1.0E15 THEN WRITELN(PRT,INP.RADS[W]:7:4,'    *');
         END;
        WRITELN(PRT,'*************************************************');
        WRITELN;
        TEXTCOLOR(YELLOW);
        GOTOXY(29,24);
        WRITELN('Press any key to continue  ');
        CH:=READKEY;
        TEXTCOLOR(WHITE);
        CLOSE(PRT);
  END;
END.
```

```
UNIT PLOT;
{$N+}
INTERFACE
   USES
       CRT,
       GRAPH,
       PRINTER,
       DOS,
       GLOBE;

PROCEDURE PLOTGEOM;
PROCEDURE LOADPLOT;
PROCEDURE SAVEPLOT;

IMPLEMENTATION
       {*****************LOADING OLD PLOT FILE***************}
PROCEDURE LOADPLOT;
       VAR     I,N: INTEGER;
  BEGIN
    CLRSCR;
    TEXTCOLOR(WHITE);
    GOTOXY(1,4);
    WRITELN('                          P L O T   L O A D I N G');
    WRITELN('                          ~~~~~~~~~~~~~~~~~~~~~~~');
    TEXTCOLOR(LIGHTCYAN);
    GOTOXY(1,9);
    WRITE('                           Input plot file name : ');
    READLN(NAME);
    GOTOXY(1,12);
    WRITE('                        Input the number of data points : ');
    READ(N);
    FNAME:=NAME+'.PLT';
        ASSIGN(XYDATA,FNAME);
        RESET(XYDATA);
        FOR I:= 1 TO N DO
                READ(XYDATA,XPL[I]);
        FOR I:= 1 TO N DO
                READ(XYDATA,YPL[I]);
        NPLOT:=N;
        PLOTGEOM;
END;

{*********************   PLOTTING PROCEDURE    *************************}

PROCEDURE PLOTGEOM;
        VAR XMAX,YMAX,XNORM,YNORM:     INTEGER;
            XMAXP,XMAXN,YMAXP,YMAXN:   INTEGER;
            I,J,K,L,N,FLAG6,XSHIFT,YSHIFT: INTEGER;
            GraphDriver,GraphMode,ErrorCode: INTEGER;
            XVAL,YVAL,XS,YS: REAL;
BEGIN
        N:=NPLOT;
        DetectGraph(GraphDriver,GraphMode);
        CASE GraphDriver Of
        CGA:BEGIN
                GraphMode:=CGAHI;
                XNORM:=640;
                YNORM:=200;
```

```
                XSHIFT:=400;
                YSHIFT:=150;
            END;
        EGA:BEGIN
                GraphMode:=EGAHI;
                XNORM:=640;
                YNORM:=380;
                XSHIFT:=292;
                YSHIFT:=220;
            END;
        VGA:BEGIN
                GraphMode:=VGAHI;
                XNORM:=640;
                YNORM:=480;
                XSHIFT:=300;
                YSHIFT:=200;
            END;
HERCMONO:BEGIN
                GraphMode:=HERCMONOHI;
                XNORM:=720;
                YNORM:=348;
                XSHIFT:=400;
                YSHIFT:=150;
            END;
  END;          {CASE}
      XMAXP:=0;
      XMAXN:=0;
      YMAXP:=0;
      YMAXN:=0;
      FOR I:=1 TO N DO
              BEGIN
              IF XPL[I] < 0 THEN
                      BEGIN
                      IF XPL[I] < XMAXN THEN XMAXN:=XPL[I];
                      END;
                      IF XPL[I] >= 0 THEN
                      BEGIN
                      IF XPL[I] > XMAXP THEN XMAXP:=XPL[I];
                      END;
                      IF YPL[I] < 0 THEN
                      BEGIN
                      IF YPL[I] < YMAXN THEN YMAXN:=YPL[I];
                      END;
                      IF YPL[I] >= 0 THEN
                      BEGIN
                      IF YPL[I] > YMAXP THEN YMAXP:=YPL[I];
                      END;
              END;
      XMAX:=XMAXP-XMAXN;
      YMAX:=YMAXP-YMAXN;
      XNORM:=XNORM-XSHIFT;
      YNORM:=YNORM-YSHIFT;
      XS:=XSHIFT/2;
      YS:=YSHIFT/2;
      XVAL:=XNORM/XMAX;
      YVAL:=YNORM/YMAX;
      FOR I:=1 TO N DO
              BEGIN
```

```
                XPL[I]:=XPL[I]-XMAXN;
                XPL[I]:=ROUND(XS+XPL[I]*XVAL);
                YPL[I]:=YPL[I]-YMAXN;
                YPL[I]:=ROUND(YS+YNORM-YPL[I]*YVAL);
                END;
        InitGraph(Graphdriver,Graphmode,'');
        ErrorCode:=GraphResult;
        IF ErrorCode<>grOK THEN
                BEGIN
                WRITELN('Graphics Error: ',GraphErrorMsg(ErrorCode));
                WRITELN('You probably do not have a graphics card!)');
                GOTOXY(29,24);
                WRITELN('Press any key to continue.');
                CH:=READKEY;
                EXIT;
                END;
        SetBkColor(BLUE);
        SetColor(WHITE);
        Rectangle(0,0,639,349);
        Rectangle(1,1,638,348);
        Rectangle(2,2,637,347);
        Rectangle(5,5,635,345);
        MoveTo(90,30);
        SetTextStyle(1, HORIZDIR, 5);
        SetColor(LIGHTCYAN);
        OUTTEXT('Deflected Spring Shape');
        Line(336,322,363,322);
        Line(336,322,336,318);
        Line(363,318,363,322);
        Line(349,322,349,320);
        SetColor(WHITE);
        FOR I:=2 TO N DO
        LINE(XPL[I-1],YPL[I-1],XPL[I],YPL[I]);
        CH:=READKEY;
        CLOSEGRAPH;

         {***RETURNING THE DATA TO ITS ORIGINAL FORM   *****}

        XVAL:=XMAX/XNORM;
        YVAL:=YMAX/YNORM;
        FOR I:=1 TO N DO
                BEGIN
                XPL[I]:=ROUND(XMAXN+(XPL[I]-XS)*XVAL);
                YPL[I]:=-1*ROUND(YMAXN+(YPL[I]-YS-YNORM)*YVAL);
                END;
END;

{************************   SAVING THE DATA   ***************************}

PROCEDURE SAVEPLOT;
  BEGIN
        CLRSCR;
        GOTOXY(1,4);
        WRITE('                                  Plot file name : ');READLN(NAME);
        FNAME:=NAME+'.PLT';
        ASSIGN(XYDATA,FNAME);REWRITE(XYDATA);
        FOR J:=1 TO INP.N DO
                WRITE(XYDATA,XPL[J]);
```

```
        FOR J:=1 TO INP.N DO
                WRITE(XYDATA,YPL[J]);
        CLOSE(XYDATA);
  END;

END.
```

```
PROGRAM SEGMENTAL_TECHNIQUE(INPUT,OUTPUT);
{$N+}

{**************      ORTHODONTAL SPRINGS GENERAL PROGRAM      ************}

        USES    DOS,
                CRT,
                PRINTER,
                GLOBE,
                INPUT,
                PLOT,
                GRAPH;

{************************  DEFINING THE POWER FUNCTION  ********************}

FUNCTION PW(X,R:REAL):                                              REAL;
        BEGIN
                IF X=0.0 THEN PW:=0.0;
                IF X>0.0 THEN PW:=EXP(R*LN(X));
                IF X<0.0 THEN PW:=-1.0*EXP(R*LN(ABS(X)));
        END;


PROCEDURE FIRSTNODE;                                                FORWARD;
PROCEDURE CLASSIFY_SEGMENT;                                         FORWARD;
PROCEDURE COMPUTE_FORCES;                                           FORWARD;
PROCEDURE ONE_D_SECANT;                                             FORWARD;
PROCEDURE FALSE_POSITION_2;                                         FORWARD;
PROCEDURE FALSE_POSITION_3;                                         FORWARD;
PROCEDURE DATAMENU;                                                 FORWARD;
PROCEDURE PLOTMENU;                                                 FORWARD;
PROCEDURE BOUNDARY;                                                 FORWARD;
PROCEDURE CALFORCES;                                                FORWARD;
PROCEDURE BOUNDMENU;                                                FORWARD;
PROCEDURE LOADBOUND;                                                FORWARD;
PROCEDURE PRINTBOUND;                                               FORWARD;
PROCEDURE OUTSCREEN;                                                FORWARD;
PROCEDURE SOLVE(N:INTEGER;AA:ARR6;BB:ARR7;VAR XX:ARR7);             FORWARD;
PROCEDURE CHECKYIELD;                                               FORWARD;
PROCEDURE BEGINNING;                                                FORWARD;

{************************  BEGINNING  ************************************}

PROCEDURE BEGINNING;
    VAR XMAX,YMAX:                          INTEGER;
        XMAXP,XMAXN,YMAXP,YMAXN:            INTEGER;
        I,J,K,L,N,FLAG6,XSHIFT,YSHIFT:      INTEGER;
        GraphDriver,GraphMode,ErrorCode:    INTEGER;
        XVAL,YVAL,XS,YS:                    REAL;

    BEGIN
      N:=NPLOT;
      DetectGraph(GraphDriver,GraphMode);
      CASE GraphDriver Of
            CGA:BEGIN
                GRAPHMODE:=CGAHI;
```

```
            XMAX:=635;
            YMAX:=195;
            END;
        EGA:BEGIN
            GraphMode:=EGAHI;
            XMAX:=635;
            YMAX:=345;
            END;
        VGA:BEGIN
            GraphMode:=VGAHI;
            XMAX:=635;
            YMAX:=475;
            END;
  HERCMONO:BEGIN
            GraphMode:=HERCMONOHI;
            XMAX:=715;
            YMAX:=343;
            END;
END;          {CASE}
 InitGraph(Graphdriver,Graphmode,'');
 ErrorCode:=GraphResult;
 IF ErrorCode<>grOK THEN
 begin
   Gotoxy(17,10);
   writeln('Graphics not installed... press any key to continue');
 end;
 SetBkColor(BLUE);
 SetColor(WHITE);
 Rectangle(5,5,XMAX,YMAX);
 INC(XMAX,3);
 INC(YMAX,3);
 Rectangle(2,2,XMAX,YMAX);
 INC(XMAX,1);
 INC(YMAX,1);
 Rectangle(1,1,XMAX,YMAX);
 INC(XMAX,1);
 INC(YMAX,1);
 Rectangle(0,0,XMAX,YMAX);
 MoveTo(215,25);
 SetTextStyle(1, HORIZDIR, 5);
 SetColor(yellow);
 OUTTEXT('Segmental');
 moveto(135,70);
 outtext('Shooting Technique');
 SetTextStyle(1, HORIZDIR, 4);
 moveto(75,165);
 SetColor(lightred);
 OUTTEXT('Orthodontic Spring Performance');
 moveto(240,205);
 outtext('Evaluation');
 moveto(170,280);
 SetTextStyle(1, HORIZDIR, 1);
 SetColor(cyan);
 OUTTEXT('Created by : Kosay El-Rayes  M.Sc.');
 moveto(265,305);
 OUTTEXT('June 1989');
 Setcolor(white);
 rectangle(160,275,495,330);
```

```
      rectangle(158,273,487,332);
      CH:=READKEY;
      CLOSEGRAPH;
END;

{*****************   INPUT PARAMETERS & PRIMARY CALCULATIONS   ***************}

PROCEDURE MENU;
BEGIN
  TEXTBACKGROUND(BLUE);
  TEXTCOLOR(WHITE);
  CLRSCR;
  GOTOXY(1,4);
  WRITELN('                                  M A I N   M E N U ');
  WRITELN('                                  ~~~~~~~~~~~~~~~~~ ');
  TEXTCOLOR(LIGHTCYAN);
  WRITELN;
  WRITELN('                                 1. Input Data Menu ');
  WRITELN('                                 2. Forces & Boundary Menu');
  WRITELN('                                 3. Calculate Forces   ');
  WRITELN('                                 4. Plotting Menu   ');
  WRITELN('                                 5. Output Summary');
  WRITELN('                                 6. Quit             ');
  WRITELN;
  WRITE('                                    =====>');
  GOON := FALSE;
  REPEAT
     CH := READKEY;WRITELN(CH);
     IF CH IN ['1','2','3','4','5','6'] THEN GOON := TRUE;
     IF NOT GOON THEN
     WRITELN(' Use only a number between 1 and 5.    Please try again.');
  UNTIL  GOON;
        CASE CH OF
                '1' : DATAMENU;
                '2' : BOUNDMENU;
                '3' : CALFORCES;
                '4' : PLOTMENU;
                '5' : OUTSCREEN;
                '6' : BEGIN
        WRITELN;
        WRITE('                          Are you sure you want to quit  Y/N ? ');
        REPEAT
        CH:=READKEY; WRITELN(CH);
        CH:=UPCASE(CH);
        UNTIL CH IN ['Y','N'];
        IF CH='Y' THEN HALT;
        MENU;
                        END;
        END;
        END;

{*************************    INPUT DATA MENU    ***************************}

PROCEDURE DATAMENU;
BEGIN
  TEXTCOLOR(WHITE);
  CLRSCR;
  GOTOXY(1,4);
```

```
WRITELN('                          I N P U T   D A T A   M E N U ');
WRITELN('                          ~~~~~~~~~~~~~~~~~~~~~~~~~~~~~ ');
TEXTCOLOR(LIGHTCYAN);
WRITELN;
WRITELN('                                  1. Input new data     ');
WRITELN('                                  2. Load existing data ');
WRITELN('                                  3. Edit data          ');
WRITELN('                                  4. Print data         ');
WRITELN('                                  5. Return to Main Menu');
WRITELN;
WRITE('                                       *****> ');
GOON:=FALSE;
REPEAT;
  CH := READKEY;WRITELN(CH);
  IF CH IN ['1','2','3','4','5'] THEN GOON := TRUE;
  IF NOT GOON THEN
  WRITELN('   Use only a number between 1 and 5.    Please try again. ');
  UNTIL  GOON;
  CASE CH OF
      '1':BEGIN
          NEWDATA;
          DATAMENU;
          END;
      '2':BEGIN
          LOADDATA;
          DATAMENU;
          END;
      '3':BEGIN
          EDITDATA;
          DATAMENU;
          END;
      '4':BEGIN
          PRINTDATA;
          DATAMENU;
          END;
      '5':MENU;
  END;
END;

(********************   BOUNDARY CONDITIONS MAIN MENU  ********************)

PROCEDURE BOUNDMENU;
  BEGIN
    TEXTCOLOR(WHITE);
    CLRSCR;
    GOTOXY(1,4);
    WRITELN('                  B O U N D A R Y   C O N D I T I O N S   M E N U');
    WRITELN('                  ~~~~~~~~~~~~~~~~~~~~~~~~~~~~~~~~~~~~~~~~~~~~~');
    WRITELN;
    TEXTCOLOR(LIGHTCYAN);
    WRITELN('                                1. Input new boundary ');
    WRITELN('                                2. Load boundary');
    WRITELN('                                3. Print boundary');
    WRITELN('                                4. Return to main menu');
    WRITELN;
    WRITE('                                     *****> ');
    GOON:=FALSE;
```

```
    REPEAT;
       CH := READKEY;WRITELN(CH);
       IF CH IN ['1','2','3','4'] THEN GOON := TRUE;
       IF NOT GOON THEN
       WRITELN('              Use only a number between 1 and 4.    Please try again. ');
    UNTIL  GOON;
    CASE CH OF
       '1':BOUNDARY;
       '2':LOADBOUND;
       '3':PRINTBOUND;
       '4':MENU;
    END;
  END;

{********************   BOUNDARY CONDITIONS PROCEDURE   ******************}

PROCEDURE BOUNDARY;
   LABEL 51000,52000,53000,54000;
  BEGIN
   CLRSCR;
   WRITELN;
   TEXTCOLOR(WHITE);
   WRITELN('***********   N E W   B O U N D A R Y  I N P U T  **********');
   WRITELN;
   I:=1;
   BD.UN:=0;
   BD.MFLAG:=0;
   BD.TFLAG:=0;
   BD.SFLAG:=0;
   BD.ACT:=0.0;
   WRITELN;
   WRITELN('                          F I R S T   N O D E   D A T A');
   WRITELN('                          ~~~~~~~~~~~~~~~~~~~~~~~~~~~ ');
   WRITELN;
   TEXTCOLOR(LIGHTCYAN);
   WRITELN('Input the following data for the final position of the FIRST node:');
   WRITELN;
   WRITE('                          Input GLOBAL X - coordinate : ');
   READREAL(BD.XG1);
   WRITELN;
   WRITE('                          Input GLOBAL Y - coordinate : ');
   READREAL(BD.YG1);
   WRITELN;
   WRITE('                          Input ANGLE with X - axis   : ');
   READREAL(BD.GAMA1);
   WRITELN;
   CLRSCR;
   TEXTCOLOR(LIGHTGRAY);
   GOTOXY(1,3);
   WRITELN('-for the Moment, Shear&Axial forces input "U" if the value is unknown.');
   WRITELN;
   WRITELN('-for right hand system, Moment is positive for clockwise rotation. ');
   WRITELN;
   WRITELN(' -         force is positive if in tension. ');
   WRITELN;
   WRITELN(' -         force is positive if upward.     ');
   WRITELN;
   TEXTCOLOR(lightred);
```

```
    GOTOXY(49,3);
    WRITELN('U');
    GOTOXY(28,5);
    WRITELN('Moment');
    GOTOXY(5,7);
    WRITELN('Axial');
    GOTOXY(5,9);
    WRITELN('Shear');
    TEXTCOLOR(LIGHTCYAN);
S1000:
    WRITELN;
    WRITE('                          Input the MOMENT      (N mm) : ');
    READLN(BD.MVL);
    CODE:=0;
    IF BD.MVL='u' THEN BD.MVL:='U';
    IF BD.MVL='U' THEN
        BEGIN
          INC(BD.UN);
          WRITELN;
          WRITE('                        Input initial guess for the MOMENT :');
          READLN(BD.INVAL[BD.UN]);
          BD.MFLAG:=1;
        END
        ELSE VAL(BD.MVL,BD.MOMENT,CODE);
        IF (CODE<>0) THEN
           BEGIN
            WRITELN('                Improper input.    Please try again.');
            GOTO S1000;
           END;
        WRITELN;
S2000:
    WRITE('                          Input the AXIAL force     (N) : ');
    READLN(BD.TVL);
    CODE:=0;
    IF BD.TVL='u' THEN BD.TVL:='U';
    IF BD.TVL='U' THEN
         BEGIN
           INC(BD.UN);
           WRITELN;
           WRITE('                          Input initial guess for the AXIAL force ');
           READLN(BD.INVAL[BD.UN]);
           BD.TFLAG:=1;
         END
         ELSE VAL(BD.TVL,BD.TENSION,CODE);
         IF (CODE<>0) THEN
            BEGIN
              WRITELN('                Improper input.    Please try again.');
                 GOTO S2000;
                 END;
         WRITELN;
S3000:
WRITE('                        Input the SHEAR force     (N) : ');READLN(BD.SVL);
CODE:=0;
IF BD.SVL='u' THEN BD.SVL:='U';
IF BD.SVL='U' THEN
    BEGIN
      INC(BD.UN);
      WRITELN;
```

```
      WRITE('                          Input initial guess for the SHEAR force ');
      READLN(BD.INVAL[BD.UN]);
      BD.SFLAG:=1;
    END
ELSE VAL(BD.SVL,BD.SHEAR,CODE);
IF (CODE<>0) THEN
   BEGIN
     WRITELN('          Improper input.    Please try again.');
     GOTO 53000;
   END;
FOR L:= 1 TO BD.UN DO
        BEGIN
              Z[0,L]:=BD.INVAL[L];
              Z[1,L]:=BD.INVAL[L]+0.05*BD.INVAL[L];
        END;
54000:

FOR L:= 1 TO BD.UN DO
BEGIN
  CLRSCR;
  TEXTCOLOR(WHITE);
  GOTOXY(1,4);
  WRITELN('                    B O U N D A R Y   C O N D I T I O N S');
  WRITELN('                    ~~~~~~~~~~~~~~~~~~~~~~~~~~~~~~~~~~~ ');
  TEXTCOLOR(LIGHTCYAN);
  WRITELN;
  WRITELN('                                  1.  X - coordinate  ');
  WRITELN('                                  2.  Y - coordinate  ');
  WRITELN('                                  3.  Angle with X - axis ');
  WRITELN('                                  4.  Moment  ');
  WRITELN('                                  5.  Shear   ');
  WRITELN('                                  6.  Tension ');
  WRITELN;
  IF L=1 THEN FST:='1st';
  IF L=2 THEN FST:='2nd';
  IF L=3 THEN FST:='3rd';
  WRITELN('Choose the number of the ',FST,' known value at the LAST NODE ===> ');
  GOON:=FALSE;
REPEAT
   CH := READKEY;WRITELN(CH);
   IF CH IN ['1','2','3','4','5','6'] THEN GOON := TRUE;
   IF NOT GOON THEN
   WRITELN('          Use only a number between 1 and 6.    Please try again. ');
UNTIL  GOON;
VAL(CH,BD.UNK[L],CODE);
CASE BD.UNK[L] OF
    1:BEGIN
        WRITE('          Input the NEUTRAL X - position : ');
        READREAL(BD.XPOS);
        BD.QS[L]:=BD.XPOS;
        BD.LF:=L;
      END;
    2:BEGIN
        WRITE('          Input NEUTRAL Y - position : ');
        READREAL(BD.YPOS);
        BD.QS[L]:=BD.YPOS;
      END;
    3:WRITE('          Input Angle with X - axis     : ');
```

```
    4:WRITE('            Input the known Moment (N mm) : ');
    5:WRITE('            Input the known Tension   (N) : ');
    6:WRITE('            Input the known Shear     (N) : ');
  END;
       IF BD.UNK[L] > 2 THEN
             BEGIN
                READREAL(BD.QS[L]);
             END;
  END;
  CLRSCR;
  TEXTCOLOR(WHITE);
  GOTOXY(1,4);
  WRITELN('                          S A V I N G   B O U N D A R Y   D A T A ');
  WRITELN('                          ~~~~~~~~~~~~~~~~~~~~~~~~~~~~~~~~~~~~~~');
  GOTOXY(1,10);
  TEXTCOLOR(LIGHTCYAN);
  WRITE('                                    Boundary file name : ');READLN(IPD);
  IPD:=IPD+'.BD';
  ASSIGN(BCOND,IPD);REWRITE(BCOND);
  WRITE(BCOND,BD);
  CLOSE(BCOND);
  BOUNDMENU;
END;

{************************   BOUNDARY LOADING   ***************************}

PROCEDURE LOADBOUND;
  BEGIN
    CODE:=99;
{$I-}
   CLRSCR;
   REPEAT
    TEXTCOLOR(WHITE);
    GOTOXY(1,4);
    WRITELN('                          B O U N D A R Y   L O A D I N G ');
    WRITELN('                          ~~~~~~~~~~~~~~~~~~~~~~~~~~~~~~');
    WRITELN;WRITELN;
    TEXTCOLOR(LIHTCYAN);
    WRITE('          Input boundary file name or type "L" to list files : ');
    READLN(IPD);
    IF (IPD='L') OR (IPD='l')  THEN
        BEGIN
          WRITE('           Input the data DISC DRIVE "e.g. A:" : ');
          READLN(IPD);                    ST1:=IPD;
          ST2:='.BD';
          CLRSCR;
          DIRECTORY(ST1,ST2);
        END
        ELSE
          BEGIN
            IPD:=IPD+'.BD';
            ASSIGN(BCOND,IPD);RESET(BCOND);
            CODE:=IORESULT;
            IF CODE <> 0 THEN
            GOTOXY(1,23);
            WRITELN('          File was not found.    Please try again. ');
          END;
   UNTIL CODE=0;
```

```
{$I+}
        READ(BCOND,BD);
        FOR L:= 1 TO BD.UN DO
                BEGIN
                        Z[0,L]:=BD.INVAL[L];
                        Z[1,L]:=BD.INVAL[L]+0.05*BD.INVAL[L];
                END;
        BOUNDMENU;
END;

{*****************   PRINTING THE BOUNDARY CONDITIONS  *****************}

PROCEDURE PRINTBOUND;
  BEGIN
    CLRSCR;
    GOTOXY(1,8);
    WRITELN('                              Specify the LISTING device : ');
    WRITELN;
    WRITELN('            1. Screen       2. Printer      3. Save as a TEXT file ');
    WRITELN;
    WRITE('                                    =====>  ');
    GOON := FALSE;
    REPEAT
    CH := READKEY;WRITELN(CH);
    IF CH IN ['1','2','3'] THEN GOON := TRUE;
    IF NOT GOON THEN
    WRITELN('           Use only a number between 1 and 3.    Please try again. ');
    UNTIL  GOON;
    CASE CH OF
        '1':ASSIGN(PRT,'');
        '2':ASSIGN(PRT,'PRN');
        '3':BEGIN
            WRITE('    Input the name of BOUNDARY text file : ');READLN(IPD);
            ASSIGN(PRT,IPD);
            END;
     END;
     CLRSCR;
     REWRITE(PRT);
     GOTOXY(1,4);
    WRITELN(PRT,'          *********  FIRST NODE  INPUT DATA  **********');
    WRITELN(PRT);
    WRITELN(PRT,'                    X - coordinate       = ',BD.XG1:3:3);
    WRITELN(PRT,'                    Y - coordinate       = ',BD.YG1:3:3);
    WRITELN(PRT,'                    Angle with X - axis  = ',BD.GAMA1:3:3);
    WRITELN(PRT,'                    Moment         (N mm) = ',BD.MVL:3);
    WRITELN(PRT,'                    Axial force      (N) = ',BD.TVL:3);
    WRITELN(PRT,'                    Shear force      (N) = ',BD.SVL:3);
    WRITELN(PRT);
    WRITELN(PRT,'                Initial guesses for the UNKNOWN quantities ');
    WRITELN(PRT);
    FOR KK:=1 TO BD.UN DO
        BEGIN
          WRITELN('     'BD.INVAL[KK]);
        END;
  WRITELN(PRT);
  WRITELN(PRT,'          *********  LAST NODE KNOWN VALUES  **********');
  BD.QS[BD.LF]:=BD.XPOS;
  FOR KK:=1 TO BD.UN DO
```

```
      BEGIN
        CASE BD.UNK[KK] OF
        1:WRITELN(PRT,'        X - coordinate        = ',BD.QS[KK]:3:3);
        2:WRITELN(PRT,'        Y - coordinate        = ',BD.QS[KK]:3:3);
        3:WRITELN(PRT,'        Angle with  X - axis  = ',BD.QS[KK]:3:3);
        4:WRITELN(PRT,'        Moment          (g mm) = ',BD.QS[KK]:3:3);
        5:WRITELN(PRT,'        Shear             (g) = ',BD.QS[KK]:3:3);
        6:WRITELN(PRT,'         Tension          (g) = ',BD.QS[KK]:3:3);
      END;
   END;
        WRITELN(PRT,'      ********************************************');
        CH:=READKEY;
        CLOSE(PRT);
        BOUNDMENU;
        END;

{************************** FORCE CALCULATION **********************}

PROCEDURE CALFORCES;
   BEGIN
{$R-}
   CLRSCR;
   TEXTCOLOR(LIGHTCYAN);
   GOTOXY(1,8);
   WRITELN('                    Specify the LISTING device : ');
   WRITELN;
   WRITELN('      1. Screen       2. Printer      3. Save as a TEXT file');
   WRITELN;
   WRITE('                                  ======>  ');
   GOON := FALSE;
   REPEAT
     CH := READKEY;WRITELN(CH);
     IF CH IN ['1','2','3'] THEN GOON := TRUE;
     IF NOT GOON THEN
     WRITELN('          Use only a number between 1 and 3.    Please try again.');
   UNTIL GOON;
   CASE CH OF
        '1':ASSIGN(OUT,'');
        '2':ASSIGN(OUT,'PRN');
        '3':BEGIN
            WRITE('                  Input the name of output text file : ');
            READLN(IPD);
            ASSIGN(OUT,IPD);
            END;
   END;
   REWRITE(OUT);
   CLRSCR;
   WRITELN(OUT);
   FLAG1:=0;
   FLAG2:=0;
   FLAG3:=0;
   FLAG4:=0;
   FLAG5:=0;
   POS:=1;
   TENMAX:=0.0;
   SHEARMAX:=0.0;
   GOTOXY(1,4);
   WRITE('          Would you like to save the geometry on a text file  Y/N ?:');
```

```
GOON := FALSE;
REPEAT
     CH := READKEY;WRITELN(CH);
     CH:=UPCASE(CH);
     IF CH IN ['Y','N'] THEN GOON := TRUE;
     IF NOT GOON THEN
     WRITELN('                          Use only Y or N.    Please try again. ');
UNTIL GOON;
IF CH='Y' THEN
     BEGIN
       FLAG4:=1;
       WRITE('            Input the name of geometry output text file : ');
       READLN(IPD);
       ASSIGN(GEOM,IPD);
       REWRITE(GEOM);
     END;
WRITELN;
WRITELN('                              Would you like to specify:');
WRITELN;
WRITELN('             Activation "A" or Inter Bracket Distance (I.B.D.) "I" : ');
WRITELN;
WRITE('                                    =====>');
GOON := FALSE;
REPEAT
  CH := READKEY;WRITELN(CH);
  CH:=UPCASE(CH);
  IF CH IN ['A','I'] THEN GOON := TRUE;
  IF NOT GOON THEN
  WRITELN('                  Use only an I or an A.    Please try again.');
UNTIL GOON;
  IF CH='A' THEN
     BEGIN
       WRITELN;
       WRITE('                               Activation    : ');
       READREAL(BD.ACT);
       WRITELN;
       BD.QS[BD.LF]:=BD.XPOS+BD.ACT;
     END;
  IF CH='I' THEN
  BEGIN
     WRITELN;
     WRITE('                             I.B.D.       : ');
     READREAL(BD.QS[BD.LF]);
  END;
  JYLD:=20000;
  WRITELN('                This program automatically checks for yielding.');
  JLD:=20000;
  FLAG5:=1;                {YIELD CHECK AUTOMATIC}
  WRITELN;
  WRITE('        Would you like to print the intermediate node values  Y/N ?');
  GOON := FALSE;
  REPEAT
  CH := READKEY;WRITELN(CH);
  CH:=UPCASE(CH);
  IF CH IN ['Y','N'] THEN GOON := TRUE;
  IF NOT GOON THEN
  WRITELN('                   Use only a Y or an N.    Please try again.');
  UNTIL GOON;
```

```
   IF CH='Y' THEN
      BEGIN
              WRITELN;
              WRITE('                    Input the printing step :');
              READINT(INP.NP);
      END
      ELSE
      INP.NP:=INP.N;
      CLRSCR;
      WRITELN;
      MM:=0;
      I:=1;
      GETTIME(HOUR1,MINUTE1,SECOND1,SEC1001);
      WRITELN(OUT);

{          *****   S O L U T I O N          ***)


 IF BD.UN=3 THEN FALSE_POSITION_3;
 IF BD.UN=2 THEN FALSE_POSITION_2;
 IF BD.UN=1 THEN ONE_D_SECANT;
 IF BD.UN=0 THEN
      BEGIN
              FLAG1:=1;
              FIRSTNODE;
      END;
 TEXTCOLOR(GREEN);
 GOTOXY(46,19);
 WRITELN('Starting time  ',HOUR1,':',MINUTE1,':',SECOND1,':',SEC1001);
 GETTIME(HOUR2,MINUTE2,SECOND2,SEC1002);
 GOTOXY(46,20);
 WRITELN('Ending time    ',HOUR2,':',MINUTE2,':',SECOND2,':',SEC1002);
 MINLAPS:=MINUTE2-MINUTE1;
 IF MINLAPS<0 THEN MINLAPS:=MINLAPS+60;
 SECLAPS:=SECOND2-SECOND1;
 IF SECLAPS<0 THEN
      BEGIN
          SECLAPS:=SECLAPS+60;
          MINLAPS:=MINLAPS-1;
      END;
THOULAPS:=SEC1002-SEC1001;
IF THOULAPS<0 THEN
      BEGIN
          THOULAPS:=THOULAPS+100;
          SECLAPS:=SECLAPS-1;
      END;
 GOTOXY(46,22);
 TEXTCOLOR(LIGHTGREEN);
 WRITELN('Elapsed time    0:',MINLAPS,':',SECLAPS,':',THOULAPS);
 TEXTCOLOR(YELLOW);
 GOTOXY(1,23);
 WRITELN;
 WRITELN('                              Press any key to continue.');
 CH:=READKEY;
 CLRSCR;
 TEXTCOLOR(LIGHTCYAN);
 GOTOXY(1,10);
 WRITELN('                  Input parametric study information ');
```

```
    WRITELN;
    WRITELN('                or type "S" to print same information:');
    WRITELN;
    WRITE('      ');
    READLN(IV2);
    IF (IV2='S') OR (IV2='s') THEN INFO:=INFO
    ELSE INFO:=IV2;
    GETDATE(YEAR,MONTH,DAY,DAYOFWEEK);
    CLRSCR;
    WRITELN(OUT);
    WRITELN(OUT,'~~~
```

```
   WRITELN('    ',DAY,'/',MONTH,'/',YEAR,'    ',INFO);
   WRITELN('~~~~~~~~~~~~~~~~~~~~~~~~~~~~~~~~~~~~~~~~~~~~~~~~~~~~~~~~~~~~~~~~');
   WRITELN('  Activation          = ',BD.ACT:2:2,' mm                    ');
   WRITELN('  Total segments      = ',INP.N,'                          ');
   WRITELN('  Young's Modulus     = ',INP.E:6:0,' MPa                   ');
   WRITELN('  Moment of Inertia   = ',INP.INR:1:7,' mm^4                ');
   WRITELN('  Solver Tolerance    = ',INP.TOL);
   WRITELN('                      Iterations Required = ',I);
   WRITELN('~~~~~~~~~~~~~~~~~~~~~~~~~~~~~~~~~~~~~~~~~~~~~~~~~~~~~~~~~~~~~~~~');
   WRITELN('First Node Values          Last Node Values          ');
   WRITELN('~~~~~~~~~~~~~~~~~          ~~~~~~~~~~~~~~~~          ');
   WRITELN('Moment = ',MOM:4:3,' N mm       Moment = ',M2:4:3,' N mm      ');
   WRITELN('Force  = ',FORC:4:3,' N            Force  = ',T2:4:3,' N      ');
   WRITELN('Shear  = ',SHEER:4:3,' N           Shear  = ',V2:4:3,' N      ');
   IF FORC<> 0 THEN
   WRITELN('M/F Ratio = ',MOM/FORC:4:3,'        M/F Ratio = ',M2/T2:4:3,' ');
   WRITELN('X = ',X1:3:3,' mm                  X = ',X2:3:3,' mm ');
   WRITELN('Y = ',Y1:3:3,' mm                  Y = ',Y2:3:3,' mm ');
   WRITELN('Gamma = ',GAMMA1:2:4,' rad         Gamma = ',GAMMA2:2:4,' rad ');
   WRITELN('~~~~~~~~~~~~~~~~~~~~~~~~~~~~~~~~~~~~~~~~~~~~~~~~~~~~~~~~~~~~~~~~');
   WRITELN('          Maximum Tensile stress = ',TENMAX:4:2,' MPa');
   WRITELN('         Maximum Shear stress    = ',SHEARMAX:4:2,' MPa');
   WRITELN('~~~~~~~~~~~~~~~~~~~~~~~~~~~~~~~~~~~~~~~~~~~~~~~~~~~~~~~~~~~~~~~~');
   CH:=READKEY;
   MENU;
END;

(*********************   FIRST NODE DATA   ***************************)

 {   For the incremental solution it is required to know six values
     at the starting node which are :

                          1. global X-coordinate.
                          2. global Y-coordinate.
                          3. angle from tangent to X-axis.
                          4. global moment value.
                          5. global tension value.
                                              6. global shear value.

     If some of these values are unknown then the values ZZ[1],ZZ[2] ...ect
     will be assigned to them and the known  values at the other end of
     the  spring  will be assigned to  QS1, QS2 ...  etc. in  the solver
     respectivily.
 }
PROCEDURE FIRSTNODE;
  BEGIN
    XG:=BD.XG1;                    { FIRST NODE GLOBAL X-COORDINATE}
    YG:=BD.YG1;                    { FIRST NODE GLOBAL Y-COORDINATE}
    GAMA:=BD.GAMA1;                { FIRST NODE TANGENT SLOPE }
    L:=1;
    IF BD.MFLAG=1 THEN
       BEGIN
                M1:=ZZ[L];     { FIRST NODE MOMENT VALUE  }
                L:=L+1;
       END
       ELSE M1:=BD.MOMENT;
    IF BD.TFLAG=1 THEN
       BEGIN
```

```
                T1:=ZZ[L];
                L:=L+1;
            END
            ELSE T1:=BD.TENSION;
        IF BD.SFLAG=1 THEN
            V1:=ZZ[L]
            ELSE V1:=BD.SHEAR;
        K:=0;
        IF  FLAG1=1 THEN
            BEGIN
              TEXTCOLOR(YELLOW);
              GOTOXY(29,24);
              WRITE('Press any key to continue.');
              CH:=READKEY;
              CLRSCR;
              GOTOXY(25,23);
              TEXTCOLOR(LIGHTMAGENTA);
              WRITELN('Press PAUSE key to pause program.');
              GOTOXY(32,24);
              WRITELN('RETURN to continue');
              TEXTCOLOR(LIGHTCYAN);
              YPIX:=3;
              NEWPIX:=4;
              OLDPIX:=NEWPIX;
              GOTOXY(2,YPIX);
              WRITELN('              Segment = ',K);
              TEXTCOLOR(CYAN);
              WRITELN('    M1 = ',M1:3:3,' Nmm  T1     = ',T1:3:3,' N    ');
              WRITELN('    V1 = ',V1:3:3,' N    X      = ',XG:3:4,' mm   ');
              WRITELN('    Y  = ',Y1:3:3,' mm   Gamma  = ',GAMA:2:4,' rad    ');
              IF FLAG4=1 THEN WRITELN(GEOM,XG:3:6,YG:3:6);
            END;
         IF FLAG1=1 THEN
              BEGIN
                  MOM:=M1;
                  FORC:=T1;
                  SHEER:=V1;
                  X1:=XG;
                  Y1:=YG;
                  GAMMA1:=GAMA;
              END;
          IF FLAG1=1 THEN
               BEGIN
                 L:=1;
                 XPL[L]:=ROUND(100*XG);
                 YPL[L]:=ROUND(100*YG);
                 L:=L+1;
               END;
CLASSIFY_SEGMENT;
END;

(**********************   CLASSIFYING THE SEGMENTS   ********************)

PROCEDURE CLASSIFY_SEGMENT;
  BEGIN
    J:=0;
    FOR KK:=1 TO INP.NUM DO
        BEGIN
```

```
                FOR W:=1 TO INP.NS[KK] DO
                        BEGIN
                                INC(J);
                                RAD:=INP.RADS[KK];
                                DELTA:=INP.DELTAS[KK];
                                COMPUTE_FORCES;
                        END;
        END;
    FOR NU:=1 TO BD.UN DO
    Q[NU]:=P[BD.UNK[NU]];
END;

{********************    COMPUTING THE FORCES FOR    ******************
 **************    CONSTANT CURVATURE OR LINEAR SEGMENTS    ************}

PROCEDURE COMPUTE_FORCES;
   BEGIN
        MU1:=M1*DELTA/EI;
        TAU1:=T1*SQR(DELTA)/EI;
        NU1:=V1*SQR(DELTA)/EI;
        X:=XG/DELTA;
        Y:=YG/DELTA;
        INC(FLAG3);
        IF (FLAG1=0) AND (FLAG3=200) THEN
                BEGIN
                        TEXTCOLOR(15);
                        GOTOXY(64,5);
                        WRITE('      ');
                        GOTOXY(61,4);
                        WRITE('Segment:');
                        GOTOXY(60,5);
                        TEXTCOLOR(12);
                        WRITE('    ',J);
                        FLAG3:=0;
                        GOTOXY(1,POS);
                        TEXTCOLOR(YELLOW);
                END;
        MUE:=MU1+DELTA/RAD;
        BETA:=-(3*MUE+NU1)/6;
        K:=3;
        ALPHA[K-3]:=BETA;
        ALPHA[K-2]:=MU1+DELTA/RAD;
        ALPHA[K-1]:=NU1/2;
        FAY:=ALPHA[K-3]+ALPHA[K-2]+ALPHA[K-1];
        MU2:=ALPHA[K-2]+2*ALPHA[K-1];
        NU2:=2*ALPHA[K-1];
        H:=ALPHA[K-3]+ALPHA[K-2]/2+ALPHA[K-1]/3;
        REPEAT
                ALPHA[K]:=TAU1*ALPHA[K-2]/(K*(K-1));
                FAY:=FAY+ALPHA[K];
                MU2:=MU2+K*ALPHA[K];
                H:=H+ALPHA[K]/(K+1);
                NU2:=NU2+K*(K-1)*ALPHA[K];
                K:=K+1;
        UNTIL ABS(ALPHA[K-1]+ALPHA[K-2])<=INP.TOL;
        MU2:=MU2-DELTA/RAD;
        TAU2:=TAU1+NU1*BETA-NU2*FAY;
        X:=X+(COS(GAMA-BETA)-H*SIN(GAMA-BETA));
```

```
        Y:=Y+(SIN(GAMA-BETA)+H*COS(GAMA-BETA));
        GAMA:=GAMA-BETA+FAY;
        M2:=MU2*EI/DELTA;
        T2:=TAU2*EI/SQR(DELTA);
        V2:=NU2*EI/SQR(DELTA);
        XG:=X*DELTA;
        YG:=Y*DELTA;
        IF (FLAG1=1) AND (FLAG4=1)THEN
              WRITELN(GEOM,XG:3:6,YG:3:6);
        IF (FLAG1=1) AND (FLAG5=1) THEN CHECKYIELD;
        IF FLAG1=1 THEN FLAG2:=FLAG2+1;
        IF (FLAG1=1) AND (FLAG2=INP.NP) THEN
          BEGIN
           FLAG2:=0;
           {      **   PRINTER   ** }
           TEXTCOLOR(LIGHTCYAN);
           INC(YPIX,5);
           IF YPIX>=19 THEN YPIX:=3;
           GOTOXY(2,YPIX);
           WRITELN('            Segment = ',J);
           TEXTCOLOR(CYAN);
           WRITELN('   M2 = ',M2:3:3,' Nmm  T2    = ',T2:3:3,' N');
           WRITELN('   V2 = ',V2:3:3,' N    X     = ',XG:3:4,' mm');
           WRITELN('   Y  = ',YG:3:3,' mm   Gamma = ',GAMMA2:2:4,' rad');
          END;
       IF FLAG1=1 THEN
              BEGIN
                     XPL[L]:=ROUND(100*XG);
                     YPL[L]:=ROUND(100*YG);
                     L:=L+1;
              END;
        M1:=M2;
        T1:=T2;
        V1:=V2;
        X2:=XG;
        Y2:=YG;
        GAMMA2:=GAMA;
        P[1]:=XG;       P[2]:=YG;       P[3]:=GAMA;
        P[4]:=M2;       P[5]:=V2;       P[6]:=T2;
  END;

{******************   ONE DIMENSIONAL SECANT METHOD ROUTINE   ***********}

PROCEDURE ONE_D_SECANT;
  BEGIN
    ZZ[1]:=Z[I-1,1];
    FIRSTNODE;
    FFO:=(Q[1]-BD.QS[1]);
    ZZ[1]:=Z[I,1];
    FIRSTNODE;
    REPEAT
        FF1:=(Q[1]-BD.QS[1]);
        INC(POS);
        WRITELN('   FF1=',FF1);
        Z[I+1,1]:=Z[I,1]-((Z[I,1]-Z[I-1,1])/(FF1-FFO))*FF1;
        I:=I+1;
        FFO:=FF1;
        ZZ[1]:=Z[I,1];
```

```
        IF (ABS(FFO)<=INP.TOL) THEN FLAG1:=1;
        FIRSTNODE;
        IF (ABS(FFO)<=INP.TOL) OR (I=100) THEN MM:=1;
        WRITELN(I);
    UNTIL MM=1;
END;

{*****************   TWO DIMENSIONAL FALSE_POSITION ROUTINE   **************}

PROCEDURE FALSE_POSITION_2;
   BEGIN
     I:=1;
     MM:=0;
     WF1:=1.0;
     WF2:=1.0;
   REPEAT;
        ZZ[1]:=Z[I,1];
        ZZ[2]:=Z[I-1,2];
        TEXTCOLOR(YELLOW);
        GOTOXY(1,POS);
        WRITE('    First pass.');
        FIRSTNODE;
        F1F10:=Q[1]-BD.QS[1];
        F2F10:=Q[2]-BD.QS[2];
        ZZ[1]:=Z[I-1,1];
        ZZ[2]:=Z[I,2];
        WRITE('    Second pass.');
        FIRSTNODE;
        F1FO1:=Q[1]-BD.QS[1];
        F2FO1:=Q[2]-BD.QS[2];
        ZZ[1]:=Z[I,1];
        ZZ[2]:=Z[I,2];
        WRITE('    Final pass.  ');
        FIRSTNODE;
        F1F11:=Q[1]-BD.QS[1];
        F2F11:=Q[2]-BD.QS[2];
        IF (ABS(F1F11)<=INP.TOL) AND (ABS(F2F11)<=INP.TOL) THEN FLAG1:=1;
        TEXTCOLOR(WHITE);
        WRITELN('              Iteration ',I,' completed.');
        TEXTCOLOR(CYAN);
        WRITELN('    ',F1F11,'    ',F2F11);
        IF FLAG1=1 THEN FIRSTNODE;
        WRITELN;
        INC(POS,2);

        {     *   FALSE POSITION [NEWTON-RAPHSON] SOLUTION   *}

        JAC[1,1]:=(F1F11-F1FO1)/(Z[I,1]-Z[I-1,1]);
        JAC[1,2]:=(F1F11-F1F10)/(Z[I,2]-Z[I-1,2]);
        JAC[2,1]:=(F2F11-F2FO1)/(Z[I,1]-Z[I-1,1]);
        JAC[2,2]:=(F2F11-F2F10)/(Z[I,2]-Z[I-1,2]);
        DD:=JAC[1,1]*JAC[2,2]-JAC[2,1]*JAC[1,2];
        Z[I+1,1]:=Z[I,1]-(JAC[2,2]*F1F11-JAC[1,2]*F2F11)/DD*WF1;
        Z[I+1,2]:=Z[I,2]-(JAC[1,1]*F2F11-JAC[2,1]*F1F11)/DD*WF2;
        IF (ABS(F1F11)<=1.0E-2) AND (ABS(F2F11)<=1.0E-2) THEN
               BEGIN
                     WF1:=1.0;
                     WF2:=1.0;
```

```
                END;
        IF (ABS(F1F11)<=INP.TOL) AND (ABS(F2F11)<=INP.TOL) THEN MM:=1;
        I:=I+1;
    UNTIL MM=1;
    WRITELN(OUT);
  END;

{********************   THREE DIMENTIONAL FALSE POSITION   ****************}

PROCEDURE FALSE_POSITION_3;
    LABEL S1000;
  BEGIN
    CLRSCR;
    I:=1;
    MM:=0;
    FLAG1:=0;
    WF1:=1.0;
    WF2:=1.0;
    WF3:=1.0;
    REPEAT
        ZZ[1]:=Z[I,1];
        ZZ[2]:=Z[I,2];
        ZZ[3]:=Z[I-1,3];
                TEXTCOLOR(YELLOW);
                WRITE('    First pass.');
                FIRSTNODE;
        F1F110:=Q[1]-BD.QS[1];
        F2F110:=Q[2]-BD.QS[2];
        F3F110:=Q[3]-BD.QS[3];
        ZZ[1]:=Z[I,1];
        ZZ[2]:=Z[I-1,2];
        ZZ[3]:=Z[I,3];
                WRITE('    Second pass.');
                FIRSTNODE;
        F1F101:=Q[1]-BD.QS[1];
        F2F101:=Q[2]-BD.QS[2];
        F3F101:=Q[3]-BD.QS[3];
        ZZ[1]:=Z[I-1,1];
        ZZ[2]:=Z[I,2];
        ZZ[3]:=Z[I,3];
        WRITE('    Third pass.  ');
        FIRSTNODE;
        F1FO11:=Q[1]-BD.QS[1];
        F2FO11:=Q[2]-BD.QS[2];
        F3FO11:=Q[3]-BD.QS[3];
        ZZ[1]:=Z[I,1];
        ZZ[2]:=Z[I,2];
        ZZ[3]:=Z[I,3];
        WRITE('    Final pass.');
        FIRSTNODE;
        TEXTCOLOR(15);
        WRITE('            Iteration ',I,' completed.');
        F1F111:=Q[1]-BD.QS[1];
        F2F111:=Q[2]-BD.QS[2];
        F3F111:=Q[3]-BD.QS[3];
        INC(POS,3);
        TEXTCOLOR(CYAN);
        WRITELN;
```

```
        WRITELN('  ',F1F111,'     ',F2F111);
        WRITELN('                 ',F3F111);
        IF (ABS(F1F111)<=INP.TOL) AND (ABS(F2F111)<=INP.TOL) AND
                (ABS(F3F111)<=INP.TOL) THEN
                        BEGIN
                                MM:=1;
                                FLAG1:=1;
                                FIRSTNODE;
                        END;
        IF MM=1 THEN GOTO S1000;
        IF  (ABS(F1F111)<=1.0E-2) AND (ABS(F2F111)<=1.0E-2) AND
                (ABS(F3F111)<=1.0E-2) THEN
                        BEGIN
                                WF1:=1.0;
                                WF2:=1.0;
                                WF3:=1.0;
                        END;
        JAC[1,1]:=(F1F111-F1F011)/(Z[I,1]-Z[I-1,1]);
        JAC[1,2]:=(F1F111-F1F101)/(Z[I,2]-Z[I-1,2]);
        JAC[1,3]:=(F1F111-F1F110)/(Z[I,3]-Z[I-1,3]);
        JAC[2,1]:=(F2F111-F2F011)/(Z[I,1]-Z[I-1,1]);
        JAC[2,2]:=(F2F111-F2F101)/(Z[I,2]-Z[I-1,2]);
        JAC[2,3]:=(F2F111-F2F110)/(Z[I,3]-Z[I-1,3]);
        JAC[3,1]:=(F3F111-F3F011)/(Z[I,1]-Z[I-1,1]);
        JAC[3,2]:=(F3F111-F3F101)/(Z[I,2]-Z[I-1,2]);
        JAC[3,3]:=(F3F111-F3F110)/(Z[I,3]-Z[I-1,3]);
        FUN[1]:=-1*F1F111;
        FUN[2]:=-1*F2F111;
        FUN[3]:=-1*F3F111;
        SOLVE(BD,UN,JAC,FUN,DIF);
        Z[I+1,1]:=Z[I,1]+DIF[1]*WF1;
        Z[I+1,2]:=Z[I,2]+DIF[2]*WF2;
        Z[I+1,3]:=Z[I,3]+DIF[3]*WF3;
        I:=I+1;
    UNTIL MM=1;
S1000:
    WRITELN;
  END;

{**********************   AX=B SOLUTION ROUTINE   ************************}

              ( A X = B SOLUTION BY GAUSS ELIMINATION 'G-PLUS' )

PROCEDURE SOLVE(N:INTEGER;AA:ARR6;BB:ARR7;VAR XX:ARR7);
        VAR  A1:ARR6;
             B1,R:ARR7;
             I,J,K,L1:INTEGER;
             D1,D,C,M,W:REAL;
             L:ARR4;
             CH:CHAR;
  BEGIN
    A1:=AA;
    B1:=BB;
    D1:=1;
    FOR K:=1 TO N-1 DO
        BEGIN
          D:=0;
          FOR I:= K TO N DO
```

```
        BEGIN
          C:=ABS(AA[I,K]);
          IF D<C THEN
            BEGIN
              D:=C;
              L[K]:=I;
            END;
        END;
        L1:=L[K];
        IF L1 <> K THEN
            BEGIN
              D1:=-D1;
              FOR J:= K TO N DO
                  BEGIN
                    D:=AA[K,J];
                    AA[K,J]:=AA[L1,J];
                    AA[L1,J]:=D;
                  END;
            END;
        FOR I:= (K+1) TO N DO
            BEGIN
              M:= -1*AA[I,K]/AA[K,K];
              AA[I,K]:=M;
              FOR J:= (K+1) TO N DO
              AA[I,J]:=AA[I,J]+M*AA[K,J];
            END;
      END;
      FOR I:= 1 TO N DO
          D1 :=D1 * AA[I,I];
      FOR K:= 1 TO (N-1) DO
          BEGIN
                    L1:=L[K];
                    IF L1<>K THEN
                          BEGIN
                                D:=BB[K];
                                BB[K]:=BB[L1];
                                BB[L1]:=D;
                          END;
                    FOR I:= (K+1) TO N DO
                          BEGIN
                                M:= AA[I,K];
                                BB[I]:=BB[I]+ M*BB[K];
                          END;
          END;
    XX[N]:=BB[N]/AA[N,N];
    I:=N-1;
    REPEAT
      D:=BB[I];
      FOR J:= (I+1) TO N DO
          D:=D-AA[I,J]*XX[J];
      XX[I]:= D/AA[I,I];
      I:=I-1;
    UNTIL I=0;
    FOR I:= 1 TO N DO
          BEGIN
                    W:=B1[I];
                    FOR J:= 1 TO N DO
                          BEGIN
```

```
                                        W:=W - A1[I,J]*XX[J];
                                    END;
                                R[I]:=W;
                        END;
        END;

(*******************   CHECKING THE STRESSES ON THE SPRING   ***************)

PROCEDURE CHECKYIELD;
  BEGIN
        SF:=1.0;
        SEGT:=INP.YIELD/2;
        IF INP.WIDTH=0.0 THEN  CENTER:=INP.DIAM/2;
        IF INP.DIAM=0.0 THEN CENTER:=INP.HEIGTH/2;
        STRESST:=T2/INP.AREA;
        STRESSM:=M2*CENTER/INP.INR;
        STRESS:=ABS(STRESST)+ABS(STRESSM);
        SHEARSTRESS:=ABS(V2/INP.AREA);
        CX:=STRESS/2.0;
        RADIUS:=SQRT(SQR(CX)+SQR(SHEARSTRESS));
        SEGMAX:=(CX+RADIUS)*SF;
        SEGMIN:=(CX-RADIUS)*SF;
        TMAX:=0.5*(SEGMAX-SEGMIN);
        IF JYMAX=J-2 THEN
                BEGIN
                        JYLD:=20000;
                        INC(NEWPIX,5);
                        IF NEWPIX>=19 THEN NEWPIX:=4;
                END;
        IF JSMAX=J-2 THEN
                BEGIN
                        JLD:=20000;
                        IF OLDPIX=NEWPIX THEN INC(NEWPIX,5);
                END;
        IF (SEGMAX-SEGMIN) >= INP.YIELD THEN
                BEGIN
                        GOTOXY(54,2);
                        IF (JYLD>0) THEN
                                BEGIN
                                        IF JYLD>J THEN JYLD:=J;
                                        JYMAX:=J;
                                END;
                        TEXTCOLOR(140);
                        WRITELN('WARNING:');
                        TEXTCOLOR(15);
                        NEWPIX1:=NEWPIX+1;
                        GOTOXY(48,NEWPIX);
                        WRITELN('Segments ',JYLD,' through');
                        GOTOXY(48,NEWPIX1);
                        WRITELN('  ',JYMAX,' have yielded. ');
                END;
        IF TMAX >= SEGT THEN
                BEGIN
                        GOTOXY(54,2);
                        IF (JLD>0) THEN
                                BEGIN
                                        IF JLD>J THEN JLD:=J;
                                        JSMAX:=J;
```

```
                        END;
                    TEXTCOLOR(140);
                    WRITELN('WARNING:');
                    NEWPIX2:=NEWPIX+2;
                    GOTOXY(48,NEWPIX2);
                    TEXTCOLOR(15);
                    WRITELN('Segments ',JLD,' through');
                    NEWPIX3:=NEWPIX+3;
                    GOTOXY(48,NEWPIX3);
                    WRITELN('  ',JSMAX,' have sheared.');
                END;
        IF SEGMAX >= TENMAX THEN TENMAX:=SEGMAX;
        IF TMAX >= SHEARMAX THEN SHEARMAX:=TMAX;
END;

   {*********************   GEOMETRY PLOTTING PROCEDURES   ********************}

PROCEDURE PLOTMENU;
  BEGIN
       CLRSCR;
       TEXTCOLOR(WHITE);
       NPLOT:=INP.N;
       GOTOXY(1,4);
       WRITELN('                                P L O T T I N G   M E N U ');
       WRITELN('                                ~~~~~~~~~~~~~~~~~~~~~~~~~');
       WRITELN;
       TEXTCOLOR(LIGHTCYAN);
       WRITELN('                                   1. Plot geometry ');
       WRITELN('                                   2. Load plot ');
       WRITELN('                                   3. Save plot ');
       WRITELN('                                   4. Return to Main Menu');
       WRITELN;
       WRITE('                                       =====> ');
       GOON:=FALSE;
   REPEAT;
       CH := READKEY;WRITELN(CH);
       IF CH IN ['1','2','3','4'] THEN GOON := TRUE;
       IF NOT GOON THEN
       WRITELN(' Use only a number between 1 and 4.    Please try again. ');
       UNTIL  GOON;
       CASE CH OF
              '1':BEGIN
                    PLOTGEOM;
                    PLOTMENU;
                  END;
              '2':BEGIN
                    LOADPLOT;
                    PLOTMENU;
                  END;
              '3':BEGIN
                    SAVEPLOT;
                    PLOTMENU;
                  END;
              '4':MENU;
       END;
   END;

{*****************************************************************************}
```

```
{*****************************   M A I N   *****************************}
{*************************************************************************}

{************************   INITIALIZATION   ***************************}

    BEGIN
          beginning;
          OPTION:=0;
          MM:=0;
          BD.MFLAG:=0;
          BD.TFLAG:=0;
          BD.SFLAG:=0;
          MENU;
    END.
```

# Appendix B

# False Position Numerical Solver for 3 Unkowns

In order to start the segmental technique routine at any time, six values at the first node should be given. Therefore, the three unknown quantities, which are usually the moment, tension and shear, are assigned to the variables $ZZ_1$, $ZZ_2$, and $ZZ_3$ within the segmental routine. The values of these variables are fed by the solver routine. One the other hand the two initial values entered for each unknown quantity, are assigned to the first two rows of a Z matrix. For example, if the two initial values for the moment were -5.0 and -5.2, while for the initial values for the tension and shear were 1.0, 1.1, and 0.2, 0.22 respectively, then the first two rows of the Z matrix would be

$$\mathbf{Z} = = \begin{pmatrix} -5.0 & 1.0 & 0.2 \\ -5.2 & 1.1 & 0.22 \\ \vdots & \vdots & \vdots \end{pmatrix}.$$

Moreover, if the $X$ and $Y$ coordinates and the slope of the last node were 24.0, -1.0, and 0.314 respectively, then these values would be stored in a $\underline{B_S}$ vector as follows

$$\underline{B_S} = \begin{pmatrix} 24.0 \\ -1.0 \\ 0.314 \end{pmatrix} .$$

The solver, then, would work according to the following steps:

1. Set counter $k = 2$.
2. Assign
$$ZZ_1 = Z[k,1] , \quad ZZ_2 = Z[k,2] , \quad ZZ_3 = [k-1,3] .$$
3. Start the segmental routine and compute the values of the last node coordinates and slope, then assign these computed values to vector $\underline{B}$.
4. Compute the first set of differentials as,
$$\Delta F_1^{221} = B[1] - B_S[1]$$
$$\Delta F_2^{221} = B[2] - B_S[2]$$
$$\Delta F_3^{221} = B[3] - B_S[3] .$$
The superscript in the above indicate to which initial value of each unknown out of the two considered in every iteration loop was used. i.e. The 221 superscript indicates that the second initial values of the first and second unknowns were used, while the first initial value of the third unknown was used.
5. Assign
$$ZZ_1 = Z[k,1] , \quad ZZ_2 = Z[k-1,2] , \quad ZZ_3 = [k,3] .$$
6. Start the segmental routine and update the values of vector $\underline{B}$.
7. Compute the second set of differentials as,
$$\Delta F_1^{212} = B[1] - B_S[1]$$
$$\Delta F_2^{212} = B[2] - B_S[2]$$
$$\Delta F_3^{212} = B[3] - B_S[3] .$$

8. Assign

$$ZZ_1 = Z[k-1,1]., \quad ZZ_2 = Z[k,2], \quad ZZ_3 = [k,3].$$

9. Start the segmental routine and update the values of vector $\underline{B}$.

10. Compute the third set of differentials as,

$$\Delta F_1^{122} = B[1] - B_S[1]$$
$$\Delta F_2^{122} = B[2] - B_S[2]$$
$$\Delta F_3^{122} = B[3] - B_S[3].$$

11. Assign

$$ZZ_1 = Z[k,1], \quad ZZ_2 = Z[k,2], \quad ZZ_3 = [k,3].$$

12. Start the segmental routine and update the values of vector $\underline{B}$.

13. Compute the forth set of differentials as,

$$\Delta F_1^{222} = B[1] - B_S[1]$$
$$\Delta F_2^{222} = B[2] - B_S[2]$$
$$\Delta F_3^{222} = B[3] - B_S[3].$$

14. Compute the elements of the Jacobian matrix ($\mathbf{J}^{(k)}$) as follows

$$J[1,1] = (\Delta F_1^{222} - \Delta F_1^{122})/(Z[k,1] - Z[k-1,1])$$
$$J[1,2] = (\Delta F_1^{222} - \Delta F_1^{212})/(Z[k,2] - Z[k-1,2])$$
$$J[1,3] = (\Delta F_1^{222} - \Delta F_1^{221})/(Z[k,3] - Z[k-1,3])$$
$$J[2,1] = (\Delta F_2^{222} - \Delta F_2^{122})/(Z[k,1] - Z[k-1,1])$$
$$J[2,2] = (\Delta F_2^{222} - \Delta F_2^{212})/(Z[k,2] - Z[k-1,2])$$
$$J[2,3] = (\Delta F_2^{222} - \Delta F_2^{221})/(Z[k,3] - Z[k-1,3])$$
$$J[3,1] = (\Delta F_3^{222} - \Delta F_3^{122})/(Z[k,1] - Z[k-1,1])$$
$$J[3,2] = (\Delta F_3^{222} - \Delta F_3^{212})/(Z[k,2] - Z[k-1,2])$$
$$J[3,3] = (\Delta F_3^{222} - \Delta F_3^{221})/(Z[k,3] - Z[k-1,3]).$$

15. Define vector $\underline{F}^{(k)}$ such that

$$F[1] = F_1^{222}, \quad F[2] = F_2^{222}, \quad F[3] = F_3^{222}.$$

16. Solve the equation

$$\mathbf{J}^{(k)}\underline{D}^{(k)} = -\underline{F}^{(k)}$$

for $\underline{D}^{(k)}$ using a Gausian elimination routine.

17. Compute a new set of initial values for the unknowns according to the following equations

$$Z[k+1,1] = Z[k,1] + w_1 \times D[1]$$
$$Z[k+1,2] = Z[k,2] + w_2 \times D[2]$$
$$Z[k+1,3] = Z[k,1] + w_3 \times D[3]$$

where $w_1$, $w_2$, $w_3$ are relaxation factors.

18. If the difference between the computed coordinates and slope of last node and the corresponding specified values is less than the tolerance, then start the segmental routine for the last time and print the results.

19. If the difference is still higher than the tolerance value then increment counter $k$ and repeat the above steps starting from step 2.

# Appendix C

# Gauss-Quadrature Numerical Integration Routines

The following program was used to evaluate the parameter ($p$) of the elliptic integral given the integration value, which is equal to the product of the cantilever beam length and $k$ ($k = \sqrt{P/EI}$).

```
PROGRAM Find_Pramerter(INPUT,OUTPUT);
{$N+}
{          Program Uses Gauss Quadrature integration routine       }
{          to evaluate the parameter p of the first kind elliptic  }
{          inte gral knowing the integration value                 }

{             M.Sc. thesis    -      KOSAY EL-RAYES                }

USES PRINTER,DOS,CRT;
TYPE ARR1=ARRAY[1..20] OF DOUBLE;
VAR X,W:ARR1;
    N,I,J,K,L:INTEGER;
    SUM,FP,SP,INTEG,FAY,FAYT,LK,P,TOL:DOUBLE;
    CH:CHAR;

 {---------------- DEFINING THE POWER FUNCTION -------------------}
```

```
FUNCTION POW(X,R:DOUBLE):DOUBLE;
    BEGIN
      IF X=0 THEN POW:=0;
      IF X>0 THEN POW:=EXP(R*LN((X)));
      IF X<0 THEN POW:=-1*EXP(R*LN(ABS(X)));
    END;
  {---------------- DEFINING Y=X^3 * COSH(X) FUNCTION -----------------}
 FUNCTION F1(P,X:DOUBLE):DOUBLE;
     BEGIN
       F1:=1/SQRT(1-SQR(P)*SQR(SIN(X)));
     END;
 BEGIN
  {--------------     Quadrature Points     -------------------------}
    N:=6;
    X[1]:=0.238619186083197;              W[1]:= 0.467913934572691;
    X[2]:=-1*X[1];                        W[2]:= W[1];
    X[3]:=0.661209386466265;              W[3]:= 0.360761573048139;
    X[4]:=-1*X[3];                        W[4]:= W[3];
    X[5]:=0.932469514203152;              W[5]:= 0.171324492379170;
    X[6]:=-1*X[5];                        W[6]:= W[5];
   {-----------------------------------------------------------------}
   LK:=1.362010449;
   P:=0.6;
   TOL:=1.0E-9;
   L:=0;
   CLRSCR;
REPEAT
   FP:=0.0;
   L:=L+1;
   GOTOXY(70,10); WRITE(L);
   IF INTEG<LK THEN P:=P+0.00001;
   IF INTEG>LK THEN P:=P-1E-9;
   FAYT:=1/(2*P*1.362010449*1.5);
   FAY:=PI/2-ARCTAN(FAYT/SQRT(1-SQR(FAYT)));
   SP:=FAY;
   SUM:=0;
   FOR I:= 1 TO N DO
       BEGIN
         SUM:= SUM + W[I]*Fi(P,((SP-FP)*X[I]+FP+SP)/2);
       END;
   INTEG:=(SP-FP)/2*SUM;
UNTIL ABS(INTEG-LK) <= TOL;
   writeln(lst);
   WRITELN(LST,'        first elliptic integral result ');
   WRITELN(LST,' P = ',P:12:10,'   FAY = ',FAY:14:10,'   LK = ',INTEG:14:10);
 END.
```

The following program was used to evaluate an elliptic integral of the second kind. It computes, also, the $X$ and $Y$ coordinates of the fixed end of an initially curved cantilever beam deflected by a horizontal load, as well as the slope of the free end.

```
PROGRAM Elliptic_Integ2(INPUT,OUTPUT);
{$N+}
{               Program Uses Gauss Quadrature To Evaluate          }
{               Elliptic Integral of the second kind.              }
{               Also, the slope of the free end and the coordinates }
{               of the fixed end of a cantilever Beam Deflected    }
{               by a horizontal load.                              }

{               M.Sc.   thesis    -      KOSAY EL-RAYES            }

USES PRINTER,DOS,CRT;
TYPE ARR1=ARRAY[1..20] OF DOUBLE;
VAR X,W:ARR1;
    N,I,J,K,L:INTEGER;
    SUM,A,B,INTEG,FAY,FAYT,LK,P,KPAR,COGAMA,BPAR:DOUBLE;
    FpFAY,EpFAY,GAMA,CPAR,R,LENG,AEQ,BEQ,CEQ:DOUBLE;
    CH:CHAR;

 {---------------- DEFINING THE POWER FUNCTION ------------------}
FUNCTION POW(X,R:DOUBLE):DOUBLE;
    BEGIN
      IF X=0 THEN POW:=0;
      IF X>0 THEN POW:=EXP(R*LN((X)));
      IF X<0 THEN POW:=-1*EXP(R*LN(ABS(X)));
    END;
    {---------------- DEFINING                FUNCTION ----------------}
 FUNCTION F1(P,X:DOUBLE):DOUBLE;
     BEGIN
       F1:=SQRT(1-SQR(P)*SQR(SIN(X)));
     END;
 BEGIN
   {--------------------- Quadrature Points -------------------------}
    N:=6;
    X[1]:=0.238619186083197;          W[1]:= 0.467913934572691;
    X[2]:=-1*X[1];                    W[2]:= W[1];
    X[3]:=0.661209386466265;          W[3]:= 0.360761573048139;
    X[4]:=-1*X[3];                    W[4]:= W[3];
    X[5]:=0.932469514203152;          W[5]:= 0.171324493279170;
    X[6]:=-1*X[5];                    W[6]:= W[5];
   {-----------------Evaluating the integration given P,k,R,Fayt----------}
```

```
    P:=0.7056020770;        {integration parameter     }
    KPAR:=1.362010449;      {variable k =sqrt(load/EI) }
    R:=1.5;                 {Radius of curvature}
    LENG:=1.0;              {length of the beam}
    A:=0.0;
    FAYT:=1/(2*P*KPAR*R);
    FAY:=PI/2-ARCTAN(FAYT/SQRT(1-SQR(FAYT)));
    B:=FAY;
    SUM:=0;
    FOR I:= 1 TO N DO
        BEGIN
          SUM:= SUM + W[I]*F1(P,((B-A)*X[I]+A+B)/2);
        END;
    INTEG:=(B-A)/2*SUM;
  WRITELN(LST,'          second elliptic integral result ');
  WRITELN(LST,'           F[p,FAY1]= LK = ',LENG*KPAR:14:10);
  WRITELN(LST);
  WRITELN(LST,'p = ',P:12:10,'FAY1 = ',FAY:12:10,'  E[p,FAY1] = ',INTEG:14:10);
  WRITELN(LST);
  {----------------- DETERMINING THE COORDINATES ---------}
  EpFAY:=INTEG;
  FpFAY:=LENG*KPAR;
  CPAR:=(2*EpFAY-FpFAY)/KPAR;
  COGAMA:=1-2*SQR(P)+1/(2*SQR(KPAR)*SQR(R));
  GAMA:=PI/2-ARCTAN(COGAMA/SQRT(1-SQR(COGAMA)));

  AEQ:=1/(SQR(R));
  BEQ:=2/(SQR(KPAR)*R*R*R);
  CEQ:=-2*(1-COGAMA)/(SQR(KPAR)*SQR(R));

  BPAR:= (-BEQ + SQRT(SQR(BEQ)-4*AEQ*CEQ))/(2*AEQ);
  WRITELN(LST,'                    X = ',CPAR:14:10);
  WRITELN(LST);
  WRITELN(LST,'                GAMA = ',GAMA:14:10);
  WRITELN(LST);
  WRITELN(LST,'                    Y = ',BPAR:14:10);
  END.
```

# Appendix D

# Comparative Studies Data

Table D.1: Koenig et al.[24] experimental and numerical data for T-loop

| Activation | Experimental | | Numerical | |
|---|---|---|---|---|
| $(mm)$ | $M\ (N\ mm)$ | $F\ (N)$ | $M\ (N\ mm)$ | $F\ (N)$ |
| 0.0 | 0.0 | 0.0 | 0.0 | 0.0 |
| 0.25 | 1.053 | 0.255 | 1.278 | 0.286 |
| 0.50 | 2.129 | 0.525 | 2.268 | 0.607 |
| 0.75 | 3.124 | 0.788 | 3.386 | 0.875 |
| 1.00 | 4.122 | 1.022 | 4.377 | 1.142 |
| 1.25 | 5.113 | 1.251 | 5.360 | 1.420 |
| 1.50 | 6.013 | 1.492 | 6.421 | 1.710 |
| 1.75 | 7.020 | 1.715 | 7.412 | 1.970 |
| 2.00 | 7.859 | 1.933 | 8.370 | 2.160 |

(0.010" × 0.020" *stainless steel wire*)

Table D.2: Fuchshuber [20] experimental and numerical data for the T-loop

| Activation | Experimental | | Numerical | |
|---|---|---|---|---|
| $(mm)$ | $M\ (N\ mm)$ | $F\ (N)$ | $M\ (N\ mm)$ | $F\ (N)$ |
| 0.00 | 0.0 | 0.0 | 0.0 | 0.0 |
| 0.25 | 0.87 | 0.228 | 0.766 | 0.196 |
| 0.50 | 1.78 | 0.465 | 1.470 | 0.398 |
| 0.75 | 2.51 | 0.661 | 2.204 | 0.580 |
| 1.00 | 3.20 | 0.840 | 2.907 | 0.768 |
| 1.25 | 3.87 | 1.024 | 3.642 | 0.946 |
| 1.50 | 4.55 | 1.205 | 4.313 | 1.116 |
| 1.75 | 5.20 | 1.368 | 4.980 | 1.285 |
| 2.00 | 5.82 | 1.531 | 5.620 | 1.446 |

(0.010" × 0.020" *stainless steel wire*)

Table D.3: Segmental shooting technique analysis of the T-loop

| Act. $(mm)$ | $M\ (N\ mm)$ | $F\ (N)$ | $M/F\ (mm)$ |
|---|---|---|---|
| 0.00 | 0.0 | 0.0 | $\infty$ |
| 0.25 | 0.753 | 0.198 | 3.790 |
| 0.50 | 1.489 | 0.391 | 3.815 |
| 0.75 | 2.208 | 0.575 | 3.838 |
| 1.00 | 2.913 | 0.754 | 3.861 |
| 1.25 | 3.602 | 0.928 | 3.882 |
| 1.50 | 4.277 | 1.096 | 3.903 |
| 1.75 | 4.939 | 1.259 | 3.922 |
| 2.00 | 5.587 | 1.418 | 3.940 |

(0.010" × 0.020" *stainless steel wire*)

Table D.4: Experimental data for the pre-activated T-spring

| Act. (mm) | $M_l$ (N mm) | STD* | $M_r$ (N mm) | STD |
|---|---|---|---|---|
| 0.0** | 12.48 | 0.54 | 12.18 | 0.44 |
| 1.0 | 14.05 | 0.33 | 13.81 | 0.42 |
| 2.0 | 15.56 | 0.35 | 15.65 | 0.40 |
| 3.0 | 16.63 | 0.36 | 17.03 | 0.48 |
| 4.0 | 17.91 | 0.44 | 18.48 | 0.25 |
| 5.0 | 18.88 | 0.39 | 19.47 | 0.46 |

| Act. (mm) | V (N) | STD | T (N) | STD |
|---|---|---|---|---|
| 0.0 | 0.020 | 0.009 | -0.015 | 0.092 |
| 1.0 | 0.021 | 0.015 | 0.606 | 0.068 |
| 2.0 | 0.027 | 0.019 | 1.144 | 0.073 |
| 3.0 | 0.030 | 0.029 | 1.683 | 0.072 |
| 4.0 | 0.036 | 0.031 | 2.222 | 0.071 |
| 5.0 | 0.042 | 0.037 | 2.778 | 0.073 |

(0.017" × 0.025" *TMA wire*)

* *STD = standard deviation*

** *Neutral position*

Table D.5: Segmental shooting technique analysis of the pre-activated T-spring

| Act. $(mm)$ | $M_l$ $(N\ mm)$ | $M_r$ $(N\ mm)$ | $V$ $(N)$ | $T$ $(N)$ |
|---|---|---|---|---|
| 0.0 | 12.710 | 12.679 | 0.001 | 0.0 |
| 1.0 | 14.210 | 14.152 | 0.004 | 0.586 |
| 2.0 | 15.535 | 15.433 | 0.007 | 1.184 |
| 3.0 | 16.693 | 16.534 | 0.010 | 1.795 |
| 4.0 | 17.693 | 17.466 | 0.013 | 2.422 |
| 5.0 | 18.543 | 18.240 | 0.017 | 3.070 |

*(0.017" × 0.025" TMA wire)*

Table D.6: Young's modulus for different orthodontic wires

| Material | $E$ (GPa) | $STD^*$ (GPa) |
|---|---|---|
| TMA 0.017"×0.025" | 72.7 | 1.4 |
| TMA 0.016"×0.022" | 69.9 | 3.8 |
| TMA 0.018" diameter | 74.5 | 0.7 |
| TMA 0.016" diameter | 70.4 | 0.7 |
| SS 0.018"×0.025" | 173.4 | 2.6 |
| SS 0.016"×0.022" | 172.6 | 1.7 |
| SS 0.018"×0.018" | 173.8 | 1.5 |
| SS 0.018"×0.022" | 181.1 | 3.5 |
| SS 0.010"×0.020" | 172.8 | - |
| SS 0.017"×0.017" | 175.6 | - |

*(average values from tension tests)*

* *STD = standard deviation.*

*TMA = titanium molybdenum alloy , SS = stainless steel*

# Appendix E

# Stress Calculation Routine

At any point of the deformed orthodontic spring, there exists a normal force $T$, a bending moment $M$, and a shear force $V$. Both the tension and the bending moment generate normal stresses, and the total normal stress at given point would be the superposition of these stresses. This is represented by the following diagram.

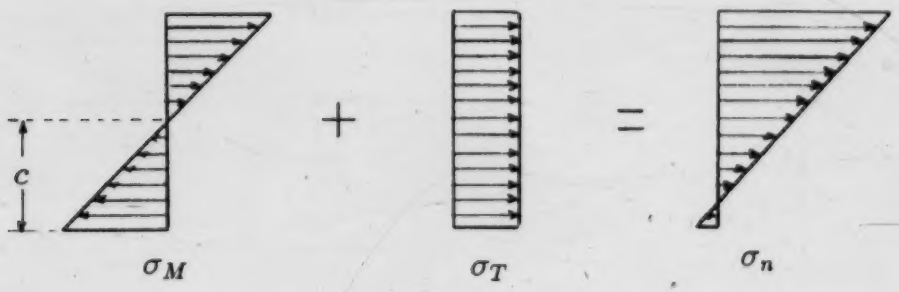


As the orthodontic wire is thin then the neutral axis, where the normal stress due the bending moment would be zero, could be assumed to be located at the mid point

of the wire cross section. Thus,

$$\sigma_M = \frac{Mc}{I}, \tag{E.1}$$

with $c$ being half the wire thickness, and $I$ is the second moment of area of the cross section.

$$\sigma_T = \frac{T}{A}, \tag{E.2}$$

where $A$ is the wire cross-sectional area. Then the maximum normal stesse would be

$$\sigma_n = \sigma_M + \sigma_T = \left|\frac{Mc}{I}\right| + \left|\frac{T}{A}\right|. \tag{E.3}$$

In addition to these normal stresses, the shear force generates a shear stress given by

$$\tau = \frac{V}{A}. \tag{E.4}$$

Therefore, the state of stress at a given point along the spring would be

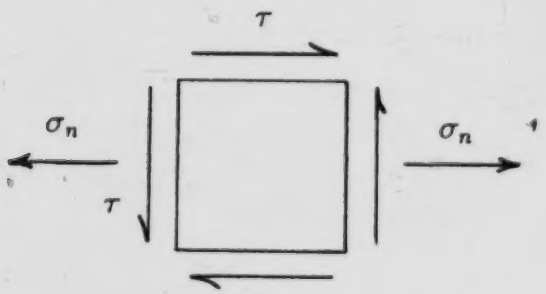


The Mohr's circle for such a state of stress is given in Figure E.1.

The following quantities could be obtained from the above Mohr's circle,

$$x_c = \frac{\sigma_n}{2} \tag{E.5}$$

$$r = \sqrt{x_c^2 + \tau^2} \tag{E.6}$$

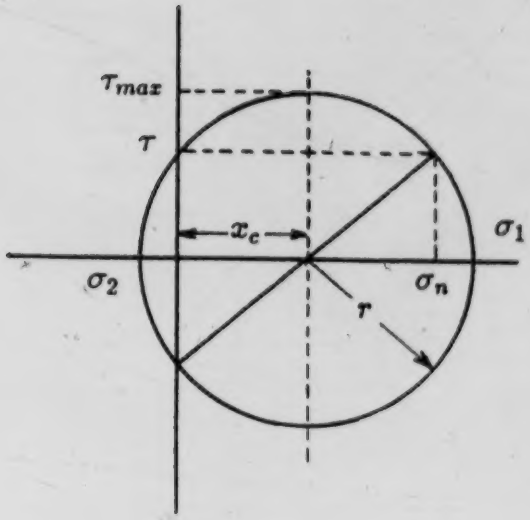


Figure E.1: Mohr's circle for an orthodontic spring element

$$\sigma_1 = x_c + r \tag{E.7}$$

$$\sigma_2 = x_c - r \tag{E.8}$$

$$\tau_{max} = \frac{1}{2}(\sigma_1 - \sigma_2) \tag{E.9}$$

If Tresca's yield criterion was followed then the orthodontic spring would yield if

$$\sigma_1 - \sigma_2 \geq \sigma_y ,$$

$$\text{or } \tau_{max} \geq \frac{\sigma_y}{2} .$$

where $\sigma_y$ is the tensile yield strength of the material.

Finally, it should be noted that the above stress calculation does not consider the residual stresses in the springs. These stresses are caused by the initial bending of the wire to form the undeformed configuration of the orthodontic spring. Therefore,

yielding might occur at a lower force and moment levels than indicated by the program.